universität wien

MASTERARBEIT | MASTER'S THESIS

Titel | Title

Developing an Integrated Data Analysis Pipeline for Clinical and Biomedical Research

verfasst von | submitted by

Philipp Trollmann BSc

angestrebter akademischer Grad | in partial fulfilment of the requirements for the degree of

Master of Science (MSc)

Wien | Vienna, 2025

Studienkennzahl lt. Studienblatt | Degree programme code as it appears on the student record sheet:	UA 066 910
Studienrichtung lt. Studienblatt | Degree programme as it appears on the student record sheet:	Masterstudium Computational Science
Betreut von | Supervisor:	Univ.-Prof. Dipl.-Ing. Dr. Jürgen Zanghellini

Acknowledgments

This thesis would not have been possible without the support of many people.

I want to thank my supervisors for giving me the opportunity to work on this amazing project, for teaching me a lot of knowledge needed for this project, and for their constant advice and encouragement. I am very proud to have worked with Daniel Wasinger, Samuel Meier-Menches, and Jürgen Zanghellini. And a big thank you to the whole group of Samuel Meier-Menches and Christopher Gerner that made this time educational and enjoyable.

My deepest gratitude goes to my family for always supporting my passion for science and for their encouragement in all situations. They awakened my curiosity and thirst for knowledge and have always supported me in my journey to achieve my goals.
And the biggest "Thank You" goes to my girlfriend Elena for always listening to all my long talks and being my safe space to calm down and be loved.

Declaration of Original Work and Ethical Conduct

I hereby declare that the research presented in this thesis was conducted solely by myself, and that the results contained herein represent my original work, carried out in strict accordance with the established principles and standards of scholarly research and writing. I have meticulously cited all sources utilized in my research endeavors. Should a source be cited immediately following a specific piece of information, it is directly pertinent to that information. Conversely, if sources are cited at the conclusion of a sentence preceding the period, they pertain only to that particular sentence. Furthermore, if these sources are cited subsequent to the period of a paragraph, they are intended to inform the entirety of the preceding section, typically encompassing the entire paragraph.
I hereby acknowledge the employment of specific tools to enhance the quality of this thesis. Specifically, I utilized ChatGPT-4o and Grammarly to refine the phrasing and facilitate a more seamless flow of the text. Additionally, DeepL and Grammarly were employed to improve grammatical accuracy and mitigate errors, while SciSpace played a crucial role in aiding the literature review and in the identification of pertinent papers. Furthermore, several individuals contributed to proofreading the document, primarily ensuring the content's clarity by correcting errors and identifying sections that were challenging to comprehend.
All assistance provided for this thesis was rendered in a supportive capacity, with all analysis, writing, and conclusions developed from my independent efforts.

Philipp Trollmann, BSc

Abstract

Despite its critical role in physiological processes, the interstitium, a fluid-filled space between cells and tissues, remains largely unmeasured in medical practice due to a lack of accessible methods. Measuring interstitial fluid via finger sweat presents a novel, non-invasive, and cost-effective solution with the potential to revolutionize clinical assessment and personal health monitoring. However, realizing this potential hinges on developing a robust normalization strategy.

Although this finger sweat-based method has effectively detected exogenous substances, accurately quantifying endogenous molecules requires a dependable approach to normalization. The complexity of sweat composition and the nuances of the sampling process introduce numerous unknown variables, posing significant challenges to establishing reliable normalization strategies.

This thesis systematically develops and evaluates normalization strategies using diverse molecules, ultimately demonstrating that no single metabolite or fixed combination provides universal normalization across finger sweat samples. The most reliable results were achieved using combinations of small, biologically relevant molecules, such as glutamic acid with, xanthine and hypoxanthine, in addition to a Median weighting strategy and VSN applied post-normalization. While these approaches improved reproducibility and robustness between studies, challenges remain due to the variable contributions of sweat and skin-derived compounds, differences in molecular linearity, and technical variations inherent to measurement methods.

Ultimately, this work highlights both the progress and complexity in normalizing finger sweat data for clinical and longitudinal studies. However, a truly universal method remains out of reach, underscoring the need for further research into the origins, dynamics, and measurement behavior of different sweat-derived features. Advancing the understanding of our sampling process and matrix will be key to realizing finger sweat as a robust matrix for personalized health diagnostics and clinical monitoring.

Zusammenfassung

Trotz seiner entscheidenden Rolle in physiologischen Prozessen bleibt das Interstitium – der flüssigkeitsgefüllter Raum zwischen Zellen und Geweben – in der medizinischen Praxis weitgehend ungenutzt, was auf das Fehlen zugänglicher Messmethoden zurückzuführen ist. Die Messung interstitieller Flüssigkeit über Fingerschweiß stellt einen neuartigen, nicht-invasiven und kostengünstigen Ansatz dar, der das Potenzial besitzt, die klinische Diagnostik und das persönliche Gesundheitsmonitoring grundlegend zu revolutionieren. Die Verwirklichung dieses Potenzials hängt jedoch maßgeblich von der Entwicklung einer robusten Normalisierungsstrategie ab.

Obwohl die auf Fingerschweiß basierende Methode bereits erfolgreich exogene Substanzen detektiert hat, ist eine zuverlässige Normalisierung notwendig, um endogene Moleküle präzise quantifizieren zu können. Die Komplexität der Schweißzusammensetzung sowie die Feinheiten im Probennahmeprozess bringen zahlreiche unbekannte Variablen mit sich und erschweren die Etablierung verlässlicher Normalisierungsstrategien.

Im Rahmen dieser Arbeit werden systematisch verschiedene Normalisierungsstrategien anhand diverser Moleküle entwickelt und evaluiert. Es konnte gezeigt werden, dass kein einzelner Metabolit oder eine festgelegte Kombination eine universelle Normalisierung für Fingerschweißproben bietet. Die zuverlässigsten Ergebnisse wurden durch die Kombination kleiner, biologisch relevanter Moleküle – wie Glutaminsäure mit Xanthin und Hypoxanthin – erzielt, ergänzt durch eine Median-Gewichtung und die Anwendung der Variance Stabilizing Normalization (VSN) nach der Normalisierung. Diese Ansätze verbesserten die Reproduzierbarkeit und Robustheit zwischen Studien, jedoch bestehen weiterhin Herausforderungen aufgrund variabler Anteile von Schweiß- und hautbürtigen Komponenten, Unterschieden in der molekularen Linearität sowie technischer Schwankungen der Messmethoden.

Insgesamt verdeutlicht diese Arbeit sowohl die erzielten Fortschritte als auch die Komplexität bei der Normalisierung von Fingerschweißdaten für klinische und longitudinale Studien. Dennoch bleibt eine wirklich universelle Methode weiterhin außer Reichweite, was den Bedarf an weiterführender Forschung zu Ursprung, Dynamik und Messverhalten schweißabgeleiteter Merkmale unterstreicht. Ein vertieftes Verständnis des Probennahmeprozesses und der Matrix ist entscheidend, um Fingerschweiß als robuste Matrix für personalisierte Gesundheitsdiagnostik und klinisches Monitoring zu etablieren.

Contents

1 | Introduction

1.1 Personalized Medicine

Personalized medicine, also known as precision or individualized medicine, has the potential to revolutionize patient treatment and become the next generation of healthcare delivery. Unlike the traditional "one-size-fits-all" approach, which applies standardized treatments to all patients with the same condition, personalized medicine assesses the unique needs of each patient and customizes medical interventions accordingly to achieve the best possible outcomes. It also transforms how treatments are developed, designed, and administered. Transitioning from universal treatments to a targeted approach can enhance treatment efficacy and minimize side effects by using the most appropriate drug at the correct dose. A wealth of information must be utilized to accomplish this, including genetics, lifestyle factors, proteomics, and the metabolic profiles of each individual. A well-known example is the use of big data analytics in genomic profiling for cancer treatment, such as in non-small cell lung cancer. High-throughput sequencing identifies mutations like EGFR or ALK, enabling clinicians to select targeted therapies that are more effective and less toxic than standard chemotherapy [1, 2]. This conceptual shift holds great promise but still encounters several challenges, such as regulatory and privacy issues, along with a lack of effective methods to measure and understand the relationship between individual changes and disease in a fast and affordable way. [3–5]

1.2 Metabolomics

Metabolomics, an interdisciplinary field that combines biology and chemistry, investigates metabolites—small molecular products of cellular processes—to provide comprehensive insights into an organism's physiological and pathological state. By simultaneously analyzing thousands of metabolites, metabolomics offers a direct snapshot of current biochemical activity, presenting a more representative measure of phenotype than genomics or proteomics alone. Even among individuals with identical genomes, metabolic profiles can differ substantially due to environmental influences, diet, microbiome composition, and disease, allowing metabolomics to capture real-time responses that genomics and proteomics may overlook. Techniques such as nuclear magnetic resonance (NMR) and mass spectrometry (MS) are utilized to analyze biological samples like blood and tissues, enabling the identification of disease biomarkers, elucidation of metabolic pathways, and improved patient stratification for targeted therapies. This establishes metabolomics as a powerful complement to genomics and proteomics in personalized medicine, despite ongoing challenges with standardization, reproducibility, and data

interpretation. [6–10]
Advanced methods such as liquid chromatography–mass spectrometry (LC-MS) have greatly expanded untargeted metabolomics, enabling the discovery of novel biomarkers across a wide range of diseases. A key challenge remains the robust annotation of detected metabolites, often requiring comprehensive reference databases like PubChem and HMDB and improved bioinformatics tools to address inconsistency and lack of standardization. While integrating metabolomics into clinical workflows currently faces barriers, including high costs, the need for specialized expertise, and data privacy concerns, these obstacles are gradually being addressed as technologies evolve and become more accessible. Continued progress in standardization and data governance will be essential for realizing the full potential of metabolomics to advance clinical diagnostics, patient stratification, and preventive care. [6–12]

1.3 Interstitium

The interstitium, once undervalued, is now recognized for its essential role in physiological processes. Situated between cells and capillaries, it facilitates the exchange of nutrients and waste, maintaining fluid balance and cellular homeostasis. Its interstitial fluid, rich in electrolytes and nutrients but lower in protein than plasma, reflects metabolic changes at the local tissue level—the site of disease or therapeutic action—rather than providing the averaged signals found in blood plasma. This makes the interstitium particularly intriguing for personalized and precision medicine, as it can reveal real-time, tissue-specific biochemical activity that may be masked in systemic circulation. Sweat, originating from the interstitial space, provides a non-invasive means to access this localized metabolic information. By analyzing sweat metabolites, which are direct reflections of interstitial fluid composition, clinicians and researchers can gain valuable insights that complement traditional blood-based analyses, further enabling individualized monitoring and targeted interventions. [13–18]

1.4 Eccrine Sweat

Eccrine sweat, especially from the fingertips, presents a novel opportunity for advancements in personalized medicine. As a hypotonic biofluid, sweat comprises not only water and electrolytes like sodium and chloride but also a diverse array of metabolites, proteins, hormones, and trace elements. [19–21]
The accessibility and richness of information contained in sweat render it an appealing choice for non-invasive health monitoring. Emerging technologies in analytical methods, such as proteomics and metabolomics, have broadened the potential applications of sweat in diagnostics. Recent studies have shown the feasibility of metabolic profiling using fingertip sweat for regular biomonitoring, offering insights into individual health status without the necessity of invasive procedures or specialized training. This promising approach addresses the compliance issues typically associated with blood sampling, paving the way for its integration into personalized medicine frameworks. [20, 22–26]
Additionally, finger sweat holds significant potential for real-time health monitoring and

tracking medication adherence. Measurements with LC-MS have already shown the utility of sweat in detecting substances like caffeine and drugs directly from fingerprints, highlighting its ability for rapid forensic and pharmacokinetic assessments. [20, 22–28]
Wearable biosensors that continuously analyze sweat composition are also being developed, incorporating sensor technology and microfluidics for real-time biochemical analysis. These advancements reinforce the role of sweat not only in traditional health diagnostics, but also in emerging areas such as therapeutic drug monitoring and even biometric identification. [25, 29–33]
As technology progresses and our understanding of sweat composition increases, finger sweat is set to become a cornerstone of personalized medicine, providing accessible, non-invasive, and comprehensive insights into individual health. [20, 22, 23]

Ongoing advancements in instrumentation and bioinformatics are crucial for overcoming challenges in sweat analysis and positioning this complex biofluid as a key resource in personalized medicine. Unlike the invasive blood collection, sweat allows for frequent, pain-free, and continuous sample collection, making it particularly attractive for real-time health monitoring outside clinical settings. Metabolomic analysis of sweat can provide dynamic insights into an individual's metabolic status, hydration, electrolyte balance, and disease markers, offering opportunities to detect early changes in health that blood tests, typically less frequent and more invasive, might miss. While promising for screening, diagnostics, and self-monitoring, these applications depend on improved methods for sweat collection, handling, and storage. Factors such as sampling sites, skin preparation, and individual physiological variability influence the accuracy and reproducibility of results. By refining analytical techniques and standard protocols, sweat metabolomics can enable affordable, on-demand health monitoring, empowering individuals and clinicians with personalized physiological data for timely interventions and lifestyle adjustments. [20, 34]

1.5 Finger Sweat Measurements

Finger sweat sampling is a specialized technique used in metabolomics studies to analyze the biochemical composition of sweat excreted through the skin. This method provides researchers valuable insights into an individual's metabolic state and physiological responses. The process includes several steps, from preparation and collection to measurement and data analysis, each contributing to the accuracy and reliability of the results (Figure 1.1). [23, 24, 35]
In the first stage, sweat is collected using pre-wetted sampling units, typically filter paper with 1 cm^2 circular areas. Subjects first clean their hands with warm water to ensure the removal of contaminants and dry them with disposable paper towels. After a brief pause of approximately 60 seconds, the sampling unit is positioned between the thumb and index finger with clean tweezers. Subjects gently hold the sampling unit for another 60 seconds, allowing sweat to be absorbed naturally without external stimulation. This method, documented in several studies [23, 24], prevents forced sweating and maintains the sample's integrity. Once collected, sampling units are carefully sealed in Eppendorf tubes and stored at low temperatures, typically around 4°C for short-term storage (several hours to days) and -20°C for long-term storage (several days to months) until sample

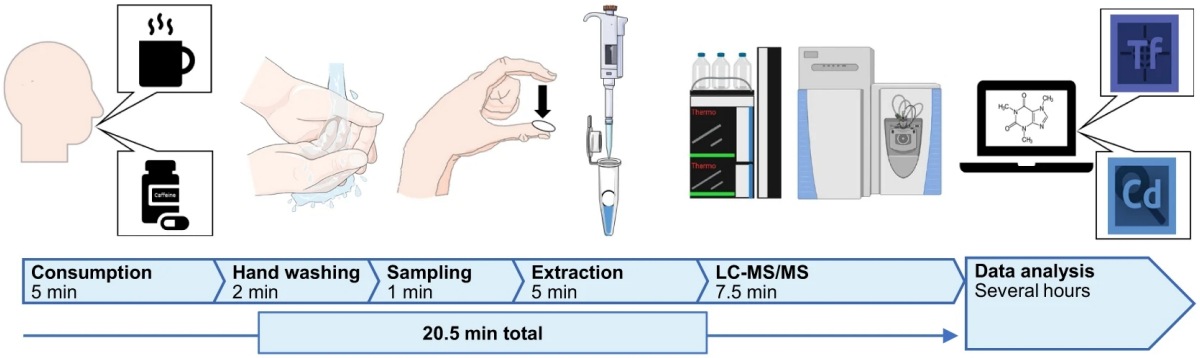

Figure 1.1 – Schematic overview of the process of finger sweat sampling and measurement. [23]

preparation. [23, 24, 35]

To extract metabolites from sweat-absorbing filters, an aqueous extraction solution containing caffeine-trimethyl-D9 and formic acid is added to the sampling unit in the Eppendorf tube. Techniques such as pipetting or ultrasonic baths are commonly used to homogenize the sample and transfer the supernatant to HPLC vials for further analysis. Some methods use filters in an additional step to remove potential fibers from the filter paper in the solution before transferring it into the vials. In these studies, unused filters, paper towels, and water blanks are processed in a similar manner to identify potential contaminants and determine background levels of metabolites. Careful preparation ensures accurate profiling of the metabolites present in sweat. [23, 24, 35]

The measurement phase involves LC-MS, typically utilizing a 'Q Exactive HF MS' paired with a 'Vanquish UHPLC' system. Chromatographic separation is conducted using a C18 column with mobile phases of water and methanol, both containing formic acid, progressing in a gradient from low to high methanol concentrations. The analysis employs an untargeted mass spectrometric approach that enables profiling of various sweat-specific features. Electrospray ionization (ESI) is conducted in positive and negative modes, covering a wide mass-to-charge ratio (m/z) scan range. This advanced setup ensures high-resolution detection and precise identification of metabolites. [23, 24, 35]

The final step is a thorough analysis of the acquired data. Software such as *Compound Discoverer* is utilized to identify and verify compounds by comparing MS/MS spectra with reference databases like *mzcloud* and *PubChem*. Feature annotation and statistical evaluations are performed using tools such as *MZmine*, *SIRIUS*, and *Perseus* to facilitate comprehensive data processing. This step includes data transformation, filtering, and normalization to extract meaningful insights from the obtained metabolomic profiles. [23, 24, 35]

1.6 Data Processing

In the rapidly advancing field of metabolomics, data analysis has become critical. In recent years, the massive data generation from cutting-edge analysis methods, such as LC-MS, has necessitated the development of robust data processing and analysis pipelines. These pipelines are essential for transforming raw data sets into meaningful insights across

multiple data types, unlocking a systematic understanding of biological systems. The effective integration and analysis of these complex data types require a structured workflow that emphasizes best practices to avoid common pitfalls, such as data inconsistency or loss of critical context. [36–40]

Automated analysis of LC-MS data is a challenging yet crucial task. LC-MS data's complexity and sheer volume necessitate sophisticated bioinformatics tools designed to interpret and extract valuable biological information. These tools are often open source, making them available for broad application without the limitations of proprietary software, thus promoting standardization and collaboration across different research initiatives. The common workflow for this task can be divided into several key steps: data preprocessing, feature extraction, statistical analysis, and, optionally, pathway mapping. [39–43]

Data processing converts raw data into an analyzable format through standardization and harmonization, ensuring compatibility across omics technologies. Creating comprehensive metadata captures essential details of datasets for widespread and effective use. Using open-source software and documenting processing steps enhances transparency, reusability, and collaboration, thereby boosting scientific confidence. [38, 43, 44]

The process begins by converting raw data into user-friendly formats, using tools such as *ProteoWizard's MSConvert* [45] to create .mzML files with centroid peaks, a standard for MS data. *MSConvert* is a versatile, open-source tool that ensures cross-platform accessibility and enables researchers to perform filtering and transformation tasks during conversion. Its integration aids in managing multiple vendor formats, facilitating broader data sharing and analysis. [23, 45, 46]

After conversion, extensive processing with software such as *MZmine* or *XCMS* is employed to extract, align, and annotate features. *MZmine* [47], a robust platform for processing LC-MS data, offers tools for non-targeted feature detection, chromatographic analysis, and metabolite identification. Its community-driven evolution highlights its versatility and adaptability to new data processing challenges. Feature annotation is crucial and can be improved by tools such as *SIRIUS* [48, 49], which specializes in molecular structure elucidation from high-resolution LC-MS/MS data. *SIRIUS* incorporates advanced algorithms for isotope pattern analysis and fragmentation tree construction, enabling accurate identification of unknown compounds even when they are not present in existing spectral libraries. Unlike traditional spectral library matching, which can only identify compounds with previously acquired reference spectra, SIRIUS uses computational methods to infer molecular structures based on fragmentation patterns, allowing for the detection and annotation of novel or rare metabolites. [23, 43, 50–52]

After feature extraction, robust statistical analyses are conducted using programming languages like *R* or *Python*. Users can leverage extensive package ecosystems to implement custom workflows that address specific analytical needs, with packages such as *LIMMA* (Linear Models for Microarray and Omics Data) [53, 54] enabling thorough statistical testing to derive valuable biological insights, such as metabolite regulation. Throughout this pipeline, striking a balance between throughput efficiency and data accuracy is crucial, as excessive speed or annotation errors can threaten data integrity and analysis. [23, 24, 35]

Data analysis pipelines should be set up and run according to certain practices that are followed for optimal results. Preprocessing steps should be employed to minimize instrument artifacts and irrelevant variability, thus improving the signal-to-noise ratio. Novel methods for data imputation, missing value handling, and outlier detection should be considered to improve data quality. However, even when best practices are followed, random error is inevitably introduced during data acquisition—so how can we choose appropriate normalization techniques that correct for these uncertainties and ensure reliable results? [41, 55, 56]

1.7 Normalization

Normalization is an important preprocessing step in both targeted and untargeted metabolomics, especially when dealing with biological samples such as finger sweat in LC-MS studies. The primary goal of normalization is to reduce systematic variability that can obscure true biological signals. In metabolomics experiments, factors such as variations in instrumental sensitivity, differences in sample preparation, and inherent variations in sample volume present significant challenges to data consistency and reliability. Eliminating or reducing these variabilities is the primary goal, but this is not always achievable. Therefore, an appropriate normalization strategy is necessary to minimize variance and experimental artifacts, ensuring accurate conclusions in all circumstances. [23, 28, 41, 42, 57, 58]

Normalization in metabolomics is commonly classified as either pre-acquisition or post-acquisition. Pre-acquisition normalization involves adjusting sample volume or concentration before data collection, often using reference measures like creatinine in urine or cell count in cell extracts. While this approach helps control for differences in sample amount, it is often limited by the availability of reliable reference markers, particularly for complex matrices such as sweat, where sample composition and volume can vary greatly between individuals and conditions. [42, 59]

When pre-acquisition normalization is not feasible, post-acquisition normalization methods are used to adjust for differences in total metabolite amount after data collection. Using various statistical techniques applied after data acquisition to correct sample-to-sample variations. Total Sum Normalization (TSN) is one method, where all measurements in a sample are scaled relative to that sample's total signal intensity, effectively standardizing the data to a common baseline. Probabilistic Quotient Normalization (PQN) is a crucial technique for normalizing sample intensities in contexts with uncertain sample volumes, such as sweat metabolomics. Unlike integral normalization, which assumes that the total signal integral reflects dilution, PQN assumes that most signal intensities are dependent on dilution. It calculates a "most likely quotient" from the distribution of signal quotients between a sample and a reference spectrum to normalize the data. This process involves initial integral normalization, selecting a reference spectrum, such as a median spectrum of all samples, calculating signal quotients, and normalizing by the median of these quotients. [41, 42, 57–63]

Table 1.1 – Overview of major post-acquisition normalization methods for omics data [58–61]

Method	**Purpose/Definition**
Total Signal (Sum, TIC)	Scale each sample by its total signal (e.g., sum of intensities)
Mean/Median Normalization	Scale features so that each sample has a common mean or median
Log Transformation	Reduces skew/heteroscedasticity, approximates normality
Quantile Normalization	Forces feature distributions to be the same across samples
Probabilistic Quotient (PQN)	Corrects for dilution using a reference sample's distribution
Variance Stabilizing Normalization (VSN)	Transforms data so variance is approximately constant
Internal Standards	Normalize using known spikes or endogenous standards
QC-based Correction (e.g., QC-RLSC, LOESS)	Use quality control samples to correct instrument drift or batch effects
Batch/Hidden Effect Correction (ComBat, RUV, SVA, EigenMS)	Adjusts to remove technical batch and hidden sample effects
ANOVA/ANCOVA	Adjust data for known confounding variables

The PQN formula (Equation (1.1)) [57, 58, 60, 61, 63] can be expressed as:

$$x'_{ij} = \frac{x_{ij}}{\text{median}\left(\frac{x_{ij}}{r_j}\right)} \tag{1.1}$$

where x'_{ij} represents the normalized intensity of the i-th metabolite in the j-th sample, x_{ij} denotes the raw intensity, and $\frac{x_{ij}}{r_j}$ indicates the ratio of the raw intensity to the reference spectrum intensity. The median of these ratios is utilized for normalization, ensuring that the normalized data reflects dilution effects. PQN's strength lies in its ability to underscore relative changes without requiring calibration curves or prior knowledge of metabolites. While it assumes average metabolite stability over time, which may limit its application in dynamic conditions, PQN remains valuable for its robustness and adaptability, remaining largely unaffected by the choice of the reference spectrum. [41, 42, 57, 58, 60, 61, 63]
Variance Stabilization Normalization (VSN) offers another level of refinement by applying transformations that stabilize the variance across different intensity ranges [41]. It transforms data using functions like logarithmic or inverse hyperbolic sine to handle heteroscedastic distributions, thus making the data more amenable to statistical analysis and enhancing the detection of subtle biological differences. The strategy involves calibrating the data, quantifying differential expression, and stabilizing variance over the intensity range. [64–66]

The VSN transformation (Equation (1.2)) [64] can be expressed mathematically as:

$$x'_{ij} = \text{arsinh}(a + b \cdot (o_i + s_i \cdot x_{ij})) \tag{1.2}$$

In this equation, x'_{ij} represents the normalized intensity for the i-th metabolite in the j-th sample, x_{ij} signifies the raw intensity and o_i and s_i are the offsets and scaling factors used to calibrate the data. The parameters a and b are estimated to minimize variance dependence on mean intensity, assuring consistent variance across the transformed dataset. This stability is essential for reliably comparing data across different conditions, as it diminishes technical variability and emphasizes insights into genuine biological differences. VSN is particularly advantageous because it does not require extensive prior calibration or specific knowledge about the data, like PQN, allowing for broad applicability across various experimental conditions. The transformation is effective due to its smooth transition across intensity ranges, which differs from PQN and offers greater reliability in detecting subtle variations without introducing significant bias from heteroscedasticity. [64–66]

Feature-based normalization strategies utilizing specific metabolite signals, combined with statistical weighting methods such as z-score normalization, rank-based scaling, and median or mean scaling, can be employed for integrative analyses. These approaches ensure that each feature contributes equally to the normalization strategy or statistical analysis, minimizing the biasing effects of extreme values or outliers and allowing for a more nuanced interpretation of the data. [67]

These normalization strategies are particularly advantageous in the context of time-course measurements, where metabolite levels can fluctuate rapidly. Techniques like PQN and VSN can be enhanced by combining them with comprehensive feature scaling to manage temporal data variability effectively. This approach increases sensitivity in detecting significant biological changes while reducing the confounding effects of technical noise. [23, 57]

The selection of a normalization strategy should align with the study's specific objectives and the characteristics of the analyzed samples. In sweat metabolomics, where sample sizes can be unpredictable and variability is significant, combining PQN or VSN alongside feature-based normalization may provide a strong and adaptable framework to improve data integrity, ensuring that technical artifacts do not mask biological insights. [42, 57].

1.8 Bateman Function

The Bateman function is a vital mathematical model frequently employed in pharmacokinetics to illustrate the concentration-time profile of a drug following administration. This model is crucial due to its simplicity and effective approximation. It adheres to the concept of a bi-exponential function, which is especially useful when assessing drug administration, where the intricate processes of absorption, distribution, and elimination converge. [68–70]

Despite its utility, the model is based on two primary assumptions: instant peak absorption following administration and immediate uniform distribution throughout the body in a one-compartment system. These simplifications may result in inaccurate

predictions of drug behavior due to their non-physiological representations. Nevertheless, the Bateman function remains a favored tool for fitting oral and intravenous (IV) concentration-time data. [68, 71]
Pharmacokinetics is vital in drug development and therapeutics, concentrating on how drugs are absorbed, distributed, metabolized, and excreted in the body. To ensure effective and safe dosing regimens, it is essential to anticipate how a drug behaves in the body over time, using compartmental models for this purpose (Figure 1.2). [68, 72]

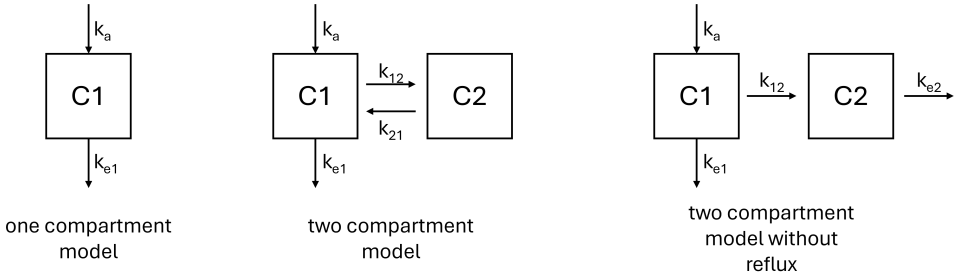

Figure 1.2 – Overview of various pharmacokinetic compartment models. [72]

Despite the limitations, the primary goal of using these prediction models is to inform dosage decisions and achieve the desired therapeutic effects without causing toxicity. The simplicity of the Bateman function highlights its ongoing relevance, enabling initial pharmacokinetic approximations and acting as a standard from which more precise techniques, like time-dependent fractional absorption models, are created. [69, 72]
However, they can also model predicted metabolism rates to establish a ground truth that aids in developing normalization strategies, because known parameters and assumptions define the simulated concentration-time profiles produced by these models. This creates a reliable reference standard against which new analytical methods can be objectively assessed. In situations where true metabolic rates or drug concentrations are unknown in experimental data, model-generated data allow researchers to evaluate how accurately normalization techniques recover the correct values rigorously. Thus, the use of pharmacokinetic models is essential not only for understanding drug behavior, but also for developing and validating computational approaches that require a trustworthy benchmark for comparison. [23, 57, 68, 72]

$$C(t) = \frac{D \cdot BA \cdot k_a}{V_d \cdot (k_a - k_e)} \cdot \left(e^{-k_e \cdot t} - e^{-k_a \cdot t}\right) \tag{1.3}$$

The one-compartment model predicts the drug concentration $C(t)$ at time t in a single homogeneous compartment (Equation (1.3)). In this context, D represents the administered dose, BA represents the bioavailability of the drug, V_d denotes the volume of distribution, k_a refers to the absorption rate constant, and k_e signifies the elimination rate constant. Although this model is straightforward, it does not consider varying distribution rates across different body regions. [57, 71, 72]

$$\begin{aligned} C_1(t) &= \frac{D \cdot BA \cdot k_a}{V_1} \left(\frac{k_{21}}{k_e - k_{21}} \left(e^{-k_{21} \cdot t} - e^{-k_e \cdot t}\right) + \frac{1}{k_a - k_e} \left(e^{-k_e \cdot t} - e^{-k_a \cdot t}\right) \right) \\ C_2(t) &= \frac{C_1(t) \cdot k_{12}}{k_{12} - k_{21}} \cdot \left(e^{-k_{21} \cdot t} - e^{-k_{12} \cdot t}\right) \end{aligned} \tag{1.4}$$

The two-compartment model is utilized in scenarios requiring a more nuanced representation of drug distribution (Equation (1.4)). This model takes into account the central compartment (bloodstream and rapidly distributed organs) and the peripheral compartment (slower equilibrating tissues and interstitum), with differential equations formulated for inputs and outputs. It builds upon the single-compartment model by accounting for the central and peripheral compartment distribution. It reflects the interplay between absorption (k_a) and elimination (k_e), adjusted by the inter-compartmental exchange rates k_{21} and k_{12}. The concentration in the peripheral compartment, $C_2(t)$, relies on $C_1(t)$ and considers the transfer rate k_{12} and the elimination rate k_{21} to and from the peripheral area. This added complexity models drug distribution dynamics more accurately across various body regions. [72, 73]

$$\begin{aligned} C_1(t) &= \frac{D \cdot BA \cdot k_a}{V_1 \cdot (k_a - k_{e1})} \left(e^{-(k_{e1}+k_{12})\cdot t} - e^{-k_a \cdot t}\right) \\ C_2(t) &= \frac{C_1(t) \cdot k_{12}}{k_{12} - k_{21}} \cdot \left(e^{-k_{21}\cdot t} - e^{-k_{12}\cdot t}\right) \end{aligned} \tag{1.5}$$

The two-compartment model can be modified and simplified to simulate the blood and interstitial compartments based on the assumption that flow between compartment 1 (blood+interstitium) and compartment 2 (finger sweat as proxy for interstitium) is unidirectional (Equation (1.5)). This assumption is justified when considering that the flow from the sweat back into the interstitium is almost non-existent and thus can be neglected for simplification purposes in short-term predictions [74].

1.9 Bayesian Optimization

Bayesian optimization is a robust model-based method for efficiently locating the global minimum of a complex, computationally expensive function, particularly when these functions exhibit noise or are stochastic. This technique proves especially beneficial in situations where assessing the objective function may take minutes, hours, or even longer, making it essential to minimize the number of evaluations required to achieve an optimal solution. Its applications extend across various fields, including machine learning, pharmacokinetics, and accelerator physics, among others. [75–78]

The process of Bayesian optimization utilizes a surrogate model, typically a Gaussian process (GP), to approximate the objective function. This surrogate model offers predictions of the function's values and an estimate of the uncertainty related to those predictions. This dual output enables Bayesian optimization to navigate the search space strategically, balancing exploration with exploitation, respectively balancing the investigation of areas of high uncertainty with the focus on areas predicted to yield high values. [75–77]

Acquisition functions play a crucial role in Bayesian optimization. These functions determine the next sampling point by assessing the trade-off between exploration and exploitation. Common acquisition functions include Expected Improvement (EI), Probability of Improvement (PI), and Upper Confidence Bound (UCB). Specifically, the Expected Improvement function is favored for its balance of usability and effectiveness in various scenarios, as it optimizes both the potential for improvement and the certainty of

known measurements. [75–77]
Bayesian optimization can easily be used to address real-world problems, using tools such as the ‘bayesOpt‘ function in *R* [79]. This function offers extensive customization options, facilitating improvements in machine learning algorithms and highlighting the adaptability and wide-ranging applications of Bayesian optimization [75, 76].

2 | Aim of Thesis

This thesis aims to develop a robust normalization method for measuring finger sweat, which has the potential to be applied in various fields of personalized medicine. Currently, there is no straightforward way to monitor interstitial fluids for a better understanding of medical treatments. The existing standard method of blood sampling only provides insights into the body's transport medium, representing just one compartment and missing critical information from interstitial fluids, which are essential for understanding diseases and drug efficacy. Blood sampling is also invasive, raising ethical concerns when performed frequently, as it can cause discomfort and harm, and requires trained personnel. In contrast, the finger sweat method is non-invasive and can be used as a proxy for the interstitial compartment, revealing new insights into disease progression and treatment effects. This method promises a rapid and cost-effective tool that enables patients to take samples themselves over extended periods. This could enhance our understanding of the impacts of individual medications and disease states [22–24, 28]. However, this method is still under development, and this work aims to further its advancement.

A proper normalization strategy is crucial for obtaining valid results from clinical data. The sampling method poses a challenge because the exact volume of finger sweat cannot be determined, leading to an inevitable error in sample amount. Various techniques exist in the literature for metabolomic studies, including 'total sum normalization', 'probabilistic quotient normalization' (PQN), 'quantile normalization' [41], internal standards, and machine learning approaches [80]. Some researchers attempt to utilize specific proteins [81], which can increase median variance; others concentrate on single molecules like creatinine [28, 82], which also encounter issues such as variations from matrix suppression [83] or fluctuating concentrations due to illnesses [84]. Additionally, some explore mathematical models to adjust for sample size errors using caffeine metabolism curves [23]. Each method presents distinct challenges that render them inadequate for addressing sample size errors. While mathematical modeling of caffeine seems to be the most effective approach, it requires caffeine ingestion before measurement and demands time series samples, making it impractical. Alternatively, using a relatively stable metabolite such as creatinine for normalization could be promising. However, relying on a single molecule can result in methods that are less stable and robust, as fluctuations in its levels may not accurately reflect true variations in the sample. Therefore, a different strategy needs to be developed, potentially involving a combination of several relatively well-regulated metabolites to correct for sample size error.

The overarching aim of this thesis is to develop and validate a robust, universal normalization strategy for finger sweat metabolomics—using a combination of biologically relevant endogenous molecules—to enable reliable intra- and inter-individual comparison of sweat samples, thereby enhancing the methodological robustness and interpretability of non-invasive sweat-based biofluid analysis. To achieve this, the thesis pursues three specific objectives: (i) developing and assessing normalization approaches that correct for unknown sweat volumes to improve data comparability and pharmacokinetic curve fitting, (ii) validating the robustness and transferability of the proposed normalization strategy across multiple studies and diverse subject populations, and (iii) getting a better understanding of the composition and origin of the human fingertip sweat metabolome. Collectively, these efforts are directed toward establishing a standardized and reliable methodological framework for non-invasive metabolomic monitoring via finger sweat sampling.

3 | Methods

3.1 Data Processing

The LC-MS raw data files generated in *ThermoFisher* .raw format were converted to centroided .mzML files using *MSConvert* (version 3.0.24123) from *ProteoWizard*. This conversion was necessary as downstream processing in *MZmine* requires centroided data, and the standardized .mzML format facilitates cross-platform analysis and data sharing. Following conversion, all .mzML files for each experiment were loaded into *MZmine* (version 4.3.0) for further processing. A batch file tailored to the LC-MS methods used during acquisition was applied to carry out the processing steps, which included feature extraction, retention time alignment, and blank background correction to enhance data accuracy. The merged and cleaned features were then exported as a .csv file for subsequent analysis in *R*.
Additionally, a .mgf file was exported from *MZmine* and transferred to *SIRIUS* (version 5.8.6) to assist with feature annotation. *SIRIUS* facilitated the prediction of molecular structures by comparing MS/MS data with databases and assigning annotations along with confidence scores, helping to identify unknown compounds.
Skyline (version 23.1.0.455) was utilized for the manual inspection of the raw data and verification of specific features.
In *RStudio* using *R* (version 4.4.0), the data exported from *MZmine* and *SIRIUS* were compiled into a coherent data matrix for statistical analysis. This included data cleaning, such as identifying and removing outlier samples and eliminating potentially noisy features. The final dataset of m/z values, retention times, feature IDs, annotations, and areas under the curve (AUCs) was prepared for rigorous statistical evaluation.

3.2 Normalization Approach

The finger sweat sampling method presents a significant challenge due to the unknown volume of sweat collected. This variability can complicate comparisons between different samples and necessitates a robust normalization method to adjust for the differences in sweat volume (Figure 3.1).
Potential molecules suitable for a normalization strategy were first identified. These molecules should be stable, biologically relevant, and regulated within the interstitium. Furthermore, they must be consistently present and detectable in all samples, with minimal matrix suppression effects. Literature reviews were conducted to identify such molecules, followed by confirmation using *Skyline* to ensure consistently defined and present molecules across samples. Attention was also given to potential sources of

contamination, including skin care products, and any contaminated candidates were excluded.
Potential weighting strategies were explored to address the scaling differences of various features in the normalization strategies. Established variance stabilization methods were also assessed to determine their effectiveness in enhancing the normalization process.
The overall strategy for testing normalization combinations was iteratively refined in response to preliminary findings. Details of specific approaches and improvements are outlined in the Results and Discussion section.
Various different approaches and methods were tested on the journey throughout this thesis. But all of them used one or more aspects of the method described in Figure 3.1. To rank the normalization methods, Bateman functions were fitted to pharmacokinetic data points for ingested metabolites with known metabolic time curves. The experimental data was scaled between 0 and 1 to be able to always fit with the same Bateman parameters. One- or two-compartment models were applied, with the quality of the curve fits serving as a scoring criterion for normalization effectiveness.
Additional evaluation methods involved clustering of dataset features and calculating silhouette scores to assess cluster density and separation. A correction factor (F.corr, Equation (3.1)) was calculated by dividing the measured abundance by the predicted abundance from the Bateman function. The consistency of F.corr across pharmacokinetic curves for different molecules from the same sample was used to measure how well sweat volume could be predicted and corrected. In the last calculations, an additional evaluation was performed that tested if more significant features could be found in data sets expected to have differential regulation after normalization than from the raw data, which was tested with *LIMMA* for the time series data.

$$F.corr = \frac{AUC_{measured}}{AUC_{predicted}} \tag{3.1}$$

Initially, a brute-force method was employed to test all possible combinations. However, as the complexity of the dataset increased, necessitating more tests and computational resources, a Bayesian optimization approach was adopted to streamline the testing process. This advanced technique proved to be more efficient as the datasets expanded and additional dimensions needed exploration, facilitating comprehensive testing of normalization strategies. Yet, this optimization algorithm was not perfectly suitable for the problem at hand and for some parts a brute-force calculation was used again to calculate normalization combinations with a combinatory approach.

All calculations were performed on a server with 32 cores (64 threads) and 264 GB of RAM to run extensive calculations in a reasonable time by executing them in parallel.

The data analysis and calculation pipeline developed for this project is available at:
https://github.com/FilyCode/Fingersweat-Normalization-Approach.

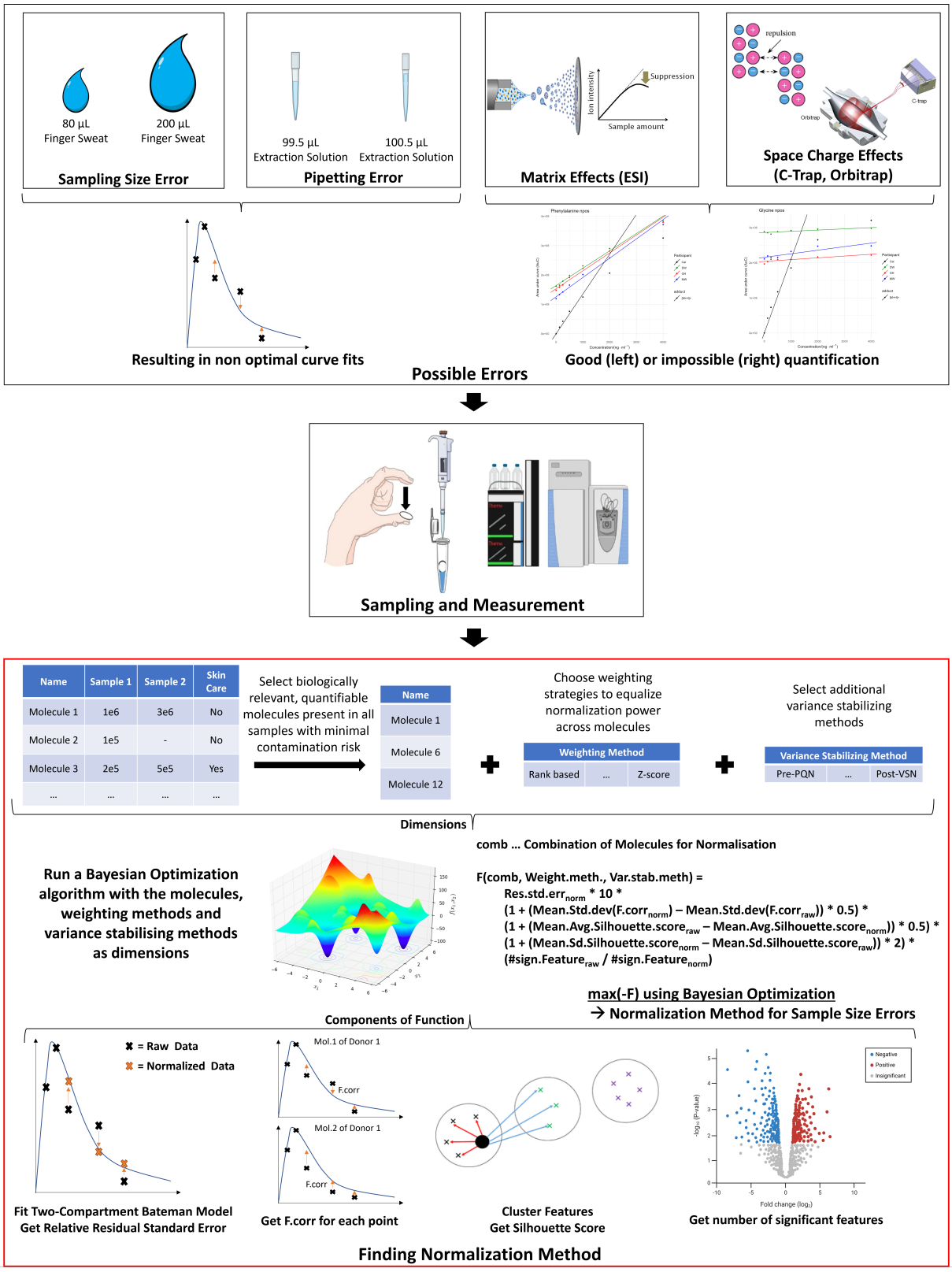

Figure 3.1 – Schematic overview of the potential errors and the approach for finding a normalization method to correct for the sample size error. The section outlined in red is the part worked on in this thesis, the rest is for context and better understanding of the circumstances.

This thesis draws upon a diverse array of finger sweat LC-MS metabolomics datasets, originating from multiple studies designed to investigate a range of physiological and experimental conditions. The primary datasets for this work stem from four caffeine intervention studies, as well as a set of wine intervention experiments. An assortment of supplementary datasets derived from additional studies further enriches the analyses presented.

The central focus has been on four core caffeine studies conducted in distinct experimental settings. The first caffeine study involved the collection of 28 finger sweat samples from a single donor, employing both Kimtech (Kim) and chromatography (Chrom) sampling papers. Samples were taken from both hands over the course of two consecutive days. Each day, sweat was collected once before coffee consumption and five more times at 45-minute intervals following ingestion, thereby permitting detailed intra-individual and methodological comparisons. The second caffeine study expanded the scale, encompassing 240 samples from six different donors. In this experiment, two pre-wetting protocols, using either water (H_2O) or isopropanol (IPA), were applied to the sampling paper to gauge their effects on metabolite recovery. Donors refrained from caffeine for 48 hours before ingesting a standardized caffeine pill, and sweat samples were then collected hourly from both hands over a nine-hour period.

Increasing further in complexity, the third caffeine study included 391 samples from 25 donors [23]. Participants underwent between 12 and 72 hours of caffeine abstinence prior to consuming a caffeine pill. Sampling was intensive, with each participant contributing 15 to 24 samples over a duration of 24 to 27 hours, thus capturing rich longitudinal metabolomic data. The fourth caffeine study analyzed 215 samples from six donors, each of whom abstained from caffeine for 48 hours and subsequently participated in two interventions: matcha tea on one day, and coffee on another, with a 48-hour interval between the two. Across each intervention, donors performed 18 sampling points over the course of 24 hours.

In addition to the caffeine-related investigations, two wine studies were analyzed to explore dietary and metabolic effects. The preliminary wine study collected 36 samples from four donors, with three baseline samplings prior to the body weight-normalized wine ingestion, and three subsequent samples at hourly intervals. Sampling was again performed on both hands utilizing Kimtech and chromatography papers. The main wine study broadened the scale, comprising 144 samples from 18 donors. Sampling was conducted at eight hourly time points: three before any intervention, followed by an ingestion of baked potatoes with olive oil, and then a body weight-adjusted quantity of wine. Four additional post-wine samples completed this sequence, providing insights into the metabolomic dynamics associated with controlled food and alcohol intake.

A set of additional datasets further broadened the scope of this thesis, providing valuable data under diverse conditions and, in most cases, without strictly defined time-course sampling. The linear feature study contributed 105 samples from eight donors, focusing on the evaluation of different matrix dilutions. In contrast, the sweat feature (AluDeo) study comprised 36 samples from six donors, with samples collected at three different time points and from both hands, where each hand received a distinct deodorant

application. The AttZol study included 180 samples from 60 donors, each of whom was sampled three times over an eight-hour period. The Long Covid study consisted of 34 samples from various donors, collected at multiple time points spanning several weeks or months. The methotrexate (MTX) study involved 158 samples from 14 donors who received methotrexate and then provided between nine and twenty finger sweat samples each, collected over periods ranging from 48 hours up to seven days, thereby enabling detailed pharmacokinetic analysis. Additional datasets included the Granat study, which contributed 19 samples from six donors collected at three defined time points following pomegranate juice ingestion, and the Kepler study, which consisted of two samples from a single donor.

4 | Results and Discussion

The search for a normalization method that reduced the variance from the sampling process focused on normalizing sweat volume to enable a more robust and consistent interpretation and comparison of finger sweat samples. This journey is explored in the following pages, detailing the many different approaches tested, with each result leading to new discoveries and adjustments for the next attempt.

4.1 Molecule Selection

Initially, potential molecules for a normalization approach were identified. An extensive literature review focused on sweat and interstitial molecules, as well as various well-known molecules from metabolic pathways, yielded a list of 66 different molecules (Table 4.1).

Table 4.1 – List of 66 bioactive molecules potentially usable for a normalization strategy.

Molecule Name	Molecule Name	Molecule Name
DL-Tyrosine	DL-Tryptophan	5-Hydroxytryptophan
Hippuric acid	Urocanic acid	Niacinamide
Succinic acid	Oleamide	Glutaric Acid
Creatinine	Carnitine	Uric Acid
Uracil	Hypoxanthine	Serine
Glutamic acid	Iso/Leucine	DL-Phenylalanine
Suberic acid	Carnosine	Homocysteine
Retinoic acid	Lumazine	Lumichrome
Pyridoxal	4-Pyridoxic acid	Ascorbic acid
Ergocalciferol	7-Dehydrocholesterol	Uridine
Xanthine	Myristic acid	Palmitoleic acid
Stearic acid	Cholic acid	Adenosine
Adenosine Triphosphate	Pyruvate	Acetyl-CoA
NADH	FADH2	Riboflavin
Glycerol	Lactate	Glutathione
α-Ketoglutarate	Succinyl-CoA	Ornithine
Citrulline	Phosphoenolpyruvate	Dihydroxyacetone Phosphate
Oxaloacetate	Glutamine	Asparagine
Aspartate	Histidine	Arginine
Alanine	Glycine	Betaine
Phosphatidylserine	Ubiquinol	Allantoin
N-Acetyl Glucosamine	Biliverdin	Bilirubin

Next, these molecules were checked in *Skyline* to see if they were consistently present in finger sweat. If not, they are unsuitable for a normalization approach. Over 672 finger sweat samples and 14 processing blanks (ProcBlanks) from 8 experiments were analyzed, including samples from all genders, ages, and healthy and sick individuals. Only 32 of the 66 molecules were found consistently across all samples (Table 4.2). The next step was to check for potential contamination from daily care products. Molecules with more than 10 occurrences of hand lotions were later removed from the list, which reduced the list to 24 molecules. Additionally, cis- and trans-urocanic acid were considered for summation, given that both isomers are synthesized in the skin and play crucial roles in skin physiology, immune modulation, and disease processes [85].

Table 4.2 – Filtered list of molecules with the LC-MS properties and how often they appear in cosmetics and hand lotion ([86] researched on 24.06.2024).

Molecule Name	**Molecular Formula**	**Precursor Adduct**	**Explicit Retention Time**	**# Cosmetics**	**# Hand Lotions**
DL-Tyrosine	$C_9H_{11}NO_3$	[M+H]+	0.88	162	2
DL-Tryptophan	$C_{11}H_{12}N_2O_2$	[M+H]+	2.36	77	1
Hippuric acid	$C_9H_9NO_3$	[M-H]-	2.97	0	0
trans-Urocanic acid	$C_6H_6N_2O_2$	[M-H]-	0.54	0	0
cis-Urocanic acid	$C_6H_6N_2O_2$	[M-H]-	0.66	0	0
Niacinamide	$C_6H_6N_2O$	[M+H]+	0.63	2149	46
Succinic acid	$C_4H_6O_4$	[M-H]-	0.93	22	2
Glutaric Acid	$C_5H_8O_4$	[M-H]-	1.5	0	0
Creatinine	$C_4H_7N_3O$	[M+H]+	0.44	21	1
Carnitine	$C_7H_{15}NO_3$	[M+H]+	0.43	157	1
Uric Acid	$C_5H_4N_4O_3$	[M+H]+	0.77	1	0
Uracil	$C_4H_4N_2O_2$	[M+H]+	0.98	11	1
Hypoxanthine	$C_5H_4N_4O$	[M+H]+	0.79	0	0
Serine	$C_3H_7NO_3$	[M+H]+	0.44	825	16
Glutamic acid	$C_5H_9NO_4$	[M+H]+	0.45	365	6
Iso-Leucine	$C_6H_{13}NO_2$	[M+H]+	0.85	200	2
Suberic acid	$C_8H_{14}O_4$	[M+H]+	3.76	0	0
DL-Phenylalanine	$C_9H_{11}NO_2$	[M+H]+	1.6	198	3
Carnosine	$C_9H_{14}N_4O_3$	[M+H]+	4.32	290	0
Xanthine	$C_5H_4N_4O_2$	[M+H]+	0.94	34	1
Adenosine	$C_{10}H_{13}N_5O_4$	[M+H]+	1.1	466	4
Citrulline	$C_6H_{13}N_3O_3$	[M+H]+	0.45	106	2
Glutamine	$C_5H_{10}N_2O_3$	[M+H]+	0.44	156	3
Asparagine	$C_4H_8N_2O_3$	[M+H]+	0.44	12	0
Aspartate	$C_4H_7NO_4$	[M+H]+	0.44	349	2
Histidine	$C_6H_9N_3O_2$	[M+H]+	0.44	218	3
Arginine	$C_6H_{14}N_4O_2$	[M+H]+	0.44	1830	28
Alanine	$C_3H_7NO_2$	[M+H]+	0.44	517	7
Glycine	$C_2H_5NO_2$	[M+H]+	0.44	5440	241
Betaine1	$C_5H_{11}NO_2$	[M+H]+	0.46	7021	59
Betaine2	$C_5H_{11}NO_2$	[M+H]+	0.55	7021	59
Allantoin	$C_4H_6N_4O_3$	[M-H]-	0.48	5192	306

4.2 Molecule Evaluation and General Data Overview

The next step was to better understand the selected molecules and their behavior in various finger sweat samples across different experiments. To achieve this, the abundance values of molecules were normalized against the internal caffeine-D9 standard and plotted across multiple studies. These values were compared with other molecules, and the relative standard deviation of the molecules was examined between different individuals and studies (Figure 4.1). The full data can be accessed in the Appendix (Appendix Figure 5.1 - Figure 5.4).
It can be concluded that there is a discrepancy in abundance among different molecules, with some showing higher abundance than others. This should be considered when using a combination of these molecules as a normalization factor, which requires weighting the various molecules to ensure they all have a similar influence on the overall factor. The molecules demonstrate a comparable abundance distribution across the studies, indicating their biological significance and stability. There are distinct differences in the relative standard deviation (RSD) for some molecules in certain studies, as well as individual discrepancies.

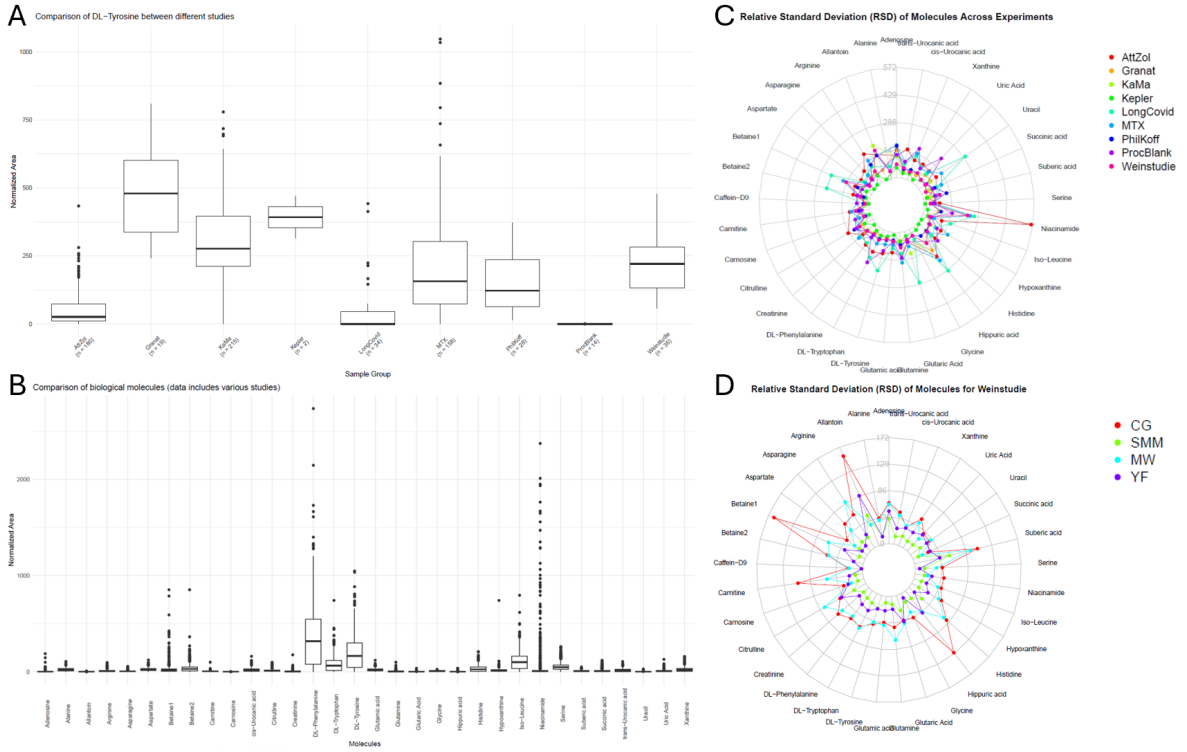

Figure 4.1 – Overview over different performed evaluation tests. A) Boxplot overview of caffeine-d9 normalized tyrosine abundance over various experiments, B) Comparison of the selected molecules over all experiments, C) RSD of the selected molecules for various experiments, D) RSD of the selected molecules for different individuals of a study.

Now that the molecules and their presence in finger sweat have been examined in various studies, the next step is to test how these molecules influence the data, improve group distinction, and assess how effectively they can normalize the pharmacokinetic curves. For

this purpose, data from two different unpublished caffeine studies by the Gerner group, with samples collected over several hours, were used, hereafter referred to as caffeine study 1 and caffeine study 2.

It was tested to determine how molecules could normalize data and whether they could account for the sampling paper used. The data from the caffeine study 1, which utilized two different types of sampling paper, Kimtech (Kim) and Chromatography (Chrom) paper, was compared using PCA and RSD and normalized for each individual molecule. Some molecules, such as amino acids, brought the two groups together, rendering them indistinguishable. Other molecules, including succinic acid and uric acid, maintained separation between the groups. The collapse of the groups can mean that the information is lost, but it can also indicate that the normalization removes the differences between the papers, showing that the overall sample is the same despite the different types of sampling paper, as the same person was sampled. The overall RSD increases for most normalizing molecules, some keep it at a level similar to the raw RSD values, but none reduce it. A higher RSD could mean that the normalization introduces random variance or that the interesting and important features can better demonstrate their changes after normalization, which would aid in establishing their statistical significance (Figure 4.2, Appendix Figure 5.7 & Figure 5.8).

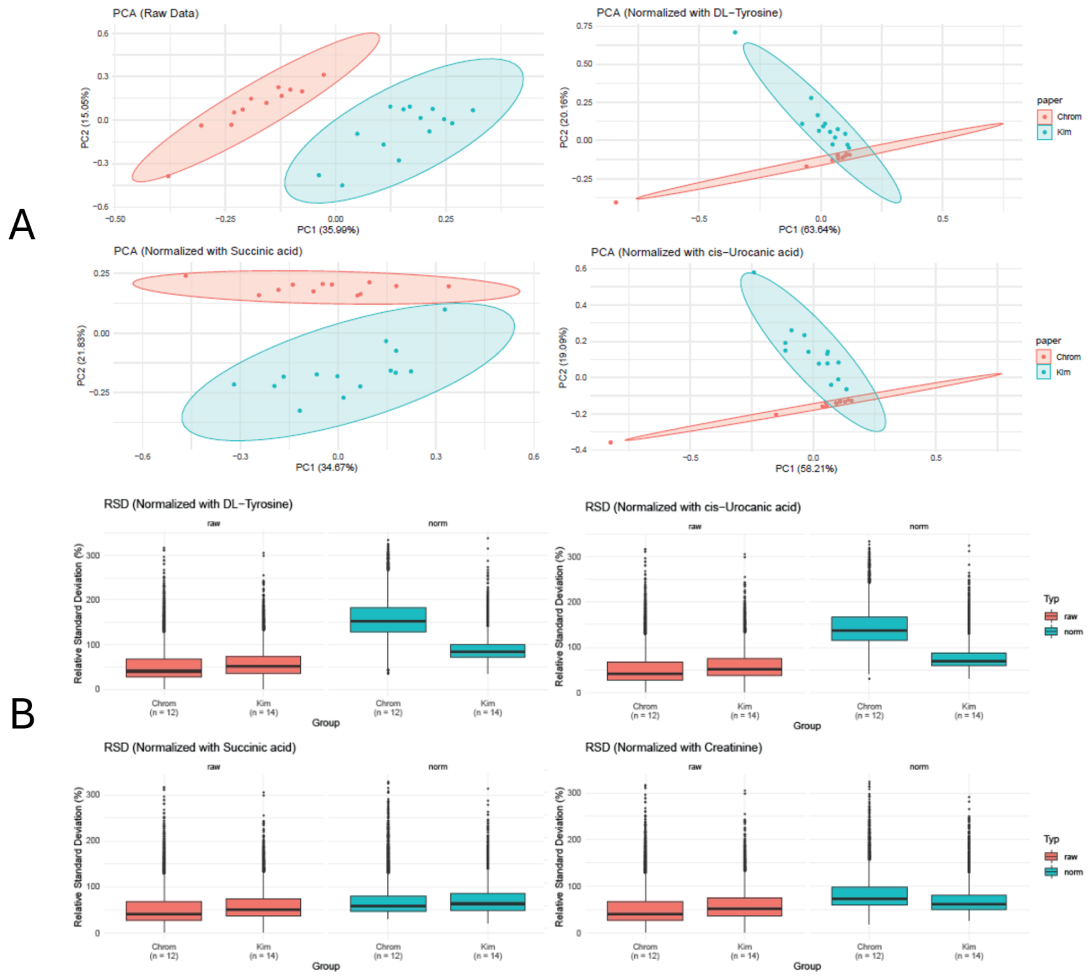

Figure 4.2 – The effect of different normalization molecules on a feature base of the caffeine study 1. A) PCA, B) RSD.

Then, the normalization effect of various selected molecules for the caffeine curves was tested. Some molecules, such as tyrosine, smooth the curve well but occasionally produce outliers that differ significantly from the pharmacokinetic curve, which was predicted using a one-compartment Bateman function. Others, like niacinamide, demonstrate variation between sampling days, while hippuric acid simply flattens the entire curve, and citrulline exhibits effective smoothing without outliers (Appendix Figure 5.9 & Figure 5.10). The curve fit for the raw data already is quite good, indicating that most points from the raw data are already fitting to the predicted curve.

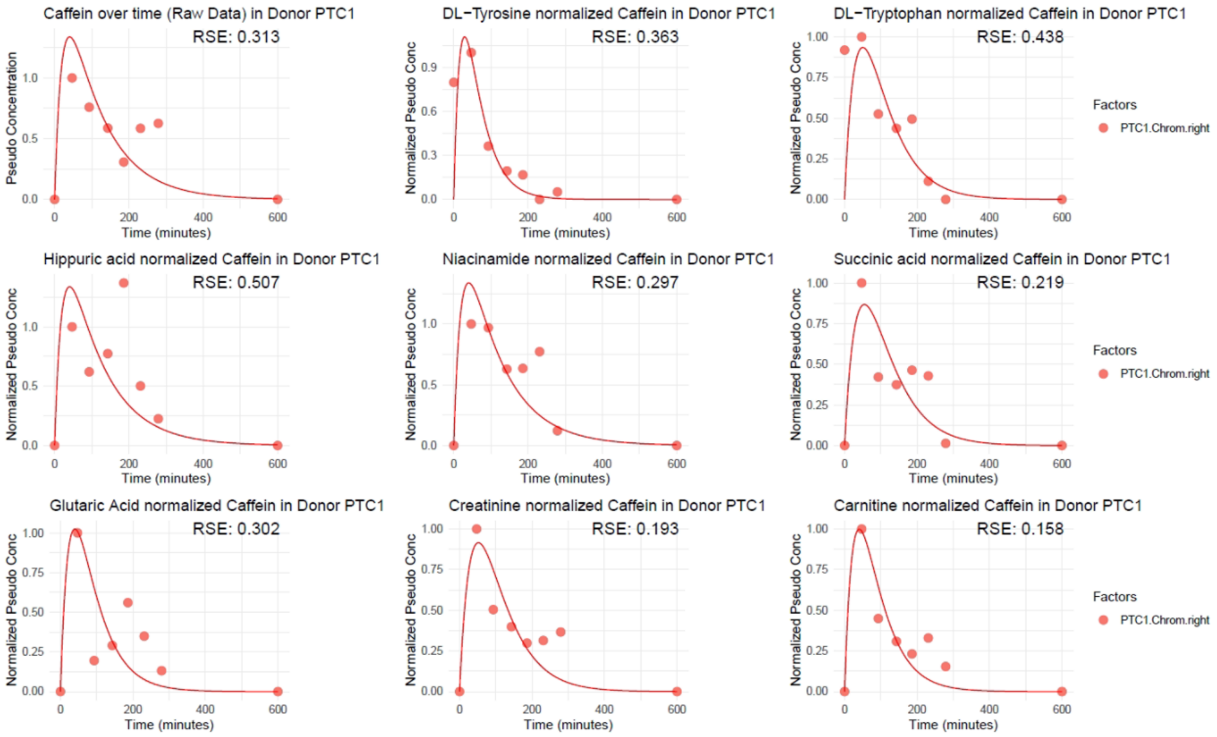

Figure 4.3 – Different normalization molecules and their effect on a pharmacokinetic caffeine curve with a fitted one-compartment Bateman function.

It is important to keep in mind the underlying pharmacokinetic profile expected for caffeine in this context. The signal should be low or close to zero at baseline, increase following ingestion, and then gradually decline. Therefore, while global measures such as RSE and PCA differences are useful for assessing model performance, a critical evaluation of the curve shape is needed. For instance, if certain normalizations result in a higher apparent caffeine signal at t0 compared to t1, this not only lacks biological plausibility but indicates a failure in capturing the true underlying kinetics. This disconnect between statistical improvement and pharmacological plausibility is particularly evident in some normalization approaches.

However, the mathematical model may not be complex enough to accurately predict the true pharmacokinetics since the finger sweat compartment is not yet fully understood, and there are some outliers from the predicted curve. Some molecules, such as tyrosine, appeared to have a good curve fit visually, but resulted in a higher relative standard error (RSE) than other molecules, like glutaric acid, which had a less visually appealing fit. Overall, most molecules show a certain degree of improvement either in optical curve fit or RSE, yet they all have their own problems and the normalization is not consistently

good over all experiments. It is hoped that the normalized data can be fit even better and more robust to the predicted curve with an appropriate normalization approach (Figure 4.3).

It can be concluded that the molecules exhibit a normalization trend in the right direction. However, it is also suggested that a single molecule alone is insufficient to establish a robust normalization strategy applicable to all cases. Therefore, the next steps involve finding combinations of molecules that fulfill this need. Nevertheless, as previously observed, the molecules have varying degrees of abundance. Thus, a weighting strategy is necessary to ensure that each molecule in the combination possesses equal normalization power.

Different weighting strategies were evaluated using the sum of all selected normalization molecules. These were compared to normalization methods that used only tyrosine, a total sum normalization (TSN), and a simple non-weighted sum of the normalization molecules. Various weighting approaches for normalization were examined, such as compressing all values by taking the square root of the abundance (Sqrt) or the logarithm of 2 (Log2), which decreases the abundance of larger values more than that of smaller ones. Another approach involved multiplying the abundance by the rank (Rank) or the rank squared (Rank2) of the sorted abundances, which enhanced the smaller features more than the larger ones. Other tested methods included dividing the normalization features by their mean (Mean) or median (Median) values, and a Z-score stabilization was used (Med.Std.dev).
The tyrosine normalization, as shown previously (Figure 4.2 & Figure 4.3), pushes the different paper groups closer together in the PCA, increases the RSD slightly, and smooths the caffeine curves, but has some outliers. The TSN maintains the PCA and RSD values similar to the raw data while smoothing the curves slightly. The non-weighted sum of the selected normalization molecules falls between tyrosine and TSN, indicating that the most abundant amino acids have a significant impact and that weighting is necessary. The various weighting strategies do not exhibit significant differences from each other in the PCA and RSD compared to each other. They mostly keep the groups separated and display a similar, slightly higher RSD than the raw data. Additionally, the curves appear similar with only slight variations, which require further testing to draw stronger conclusions about which method may be superior (Figure 4.4, Appendix Figure 5.11 & Figure 5.12).

Now the sum of all selected molecules was tested with various weighting strategies but it is not known if some molecules are better or worse at normalization than others. So it needs to be tested if certain combinations of molecules perform better than others.

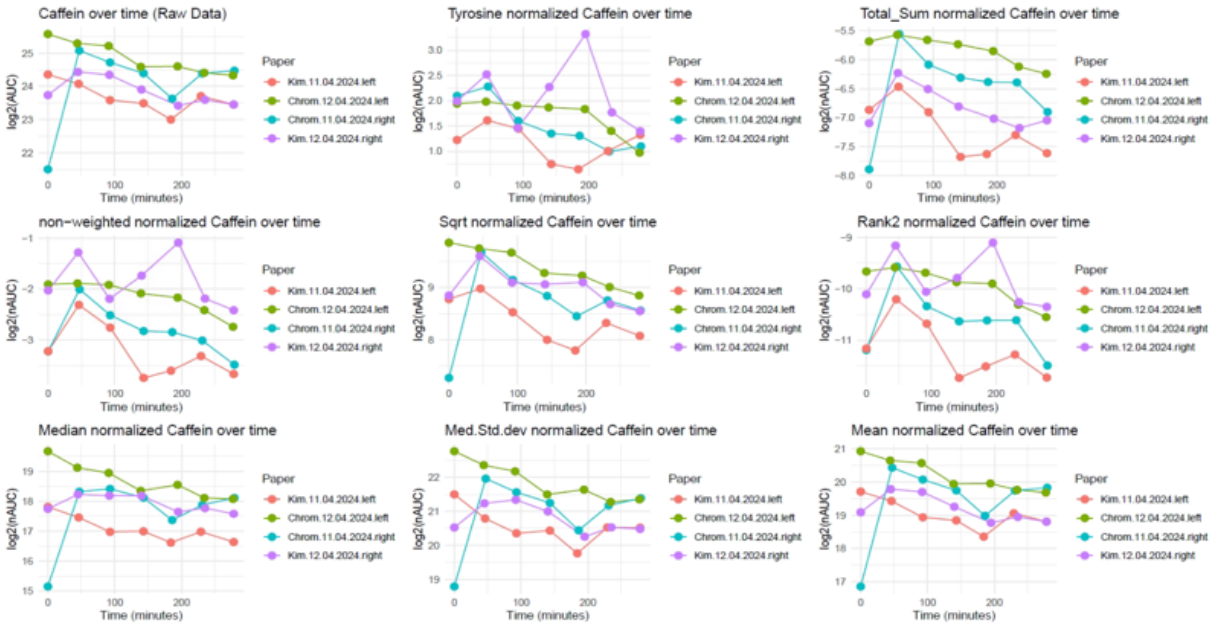

Figure 4.4 – Comparison of weighting strategies for the molecule combinations used to normalize pharmacokinetic caffeine curves with selected biological molecules on caffeine study 1.

In the next parts, all permutations of the normalization molecules were planned for testing. Therefore, the total number of molecules needed to be reduced from the original 32. Otherwise, the number of combinations would be too extensive to calculate. Molecules that appeared more than 10 times in hand lotions were removed to avoid potential contamination. Additionally, various sampling and measuring methods were employed across the different studies, with some molecules being too small to measure or later determined to be less effective for normalization, leading to their exclusion from the relevant normalization tests in subsequent combination tests. The tables of the normalization molecules utilized in each study can be found in the Appendix.

4.3 Search for Normalization Combination

4.3.1 Testing Individual Caffeine Datasets

The results indicated that specific biologically relevant molecules provided a meaningful normalization strategy. However, these molecules varied in abundance, which necessitated a weighting strategy. Additionally, each molecule alone was not robust enough, so combinations of several were required to achieve the desired effect. The task then became to identify such combinations and the optimal weighting methods. Variance-stabilizing methods like PQN and VSN, commonly used to manage samples with varying variance, were also tested during the search for an effective normalization method for finger sweat samples.

The question is how to find the best combination and measure it. To achieve this, all possible combinations of molecules (Appendix Table 5.1) and weighting methods were calculated on the caffeine study 2 dataset, where the caffeine data were fitted with a one-compartment Bateman function. The scoring was done using the residuals from the points to the predicted curve, which was fitted separately for each normalization combination. This resulted in several million calculated combinations through a brute-force approach. The results were filtered to identify the best combinations for each donor. The variance-stabilizing methods PQN and VSN did not improve the curve fit, they merely rescaled the points. The leading combinations yielded a good fit, good RSE respectively, but the highest scores were achieved by pushing the data points to zero to minimize the residuals (Figure 4.5). This led to the implementation of a self-calculated relative residual calculation for future calculations to prevent this from occurring. For this amount of calculations, it is also possible to find random combinations that happen to fit this person's curve but may not transfer to other individuals or studies.

Some combinations appear to work well. However, they were tested individually on each donor. Therefore, it needs to be determined whether they also work for the other donors in the same study. Thus, the top combinations from each donor were selected and tested on all donors, and the residuals of the samples for the fitted Bateman function were plotted. It can be observed that the residuals remain similar for most donors and do not improve significantly. Yet, some combinations cannot achieve normalization for all donors (Figure 4.6, Appendix Figure 5.14).

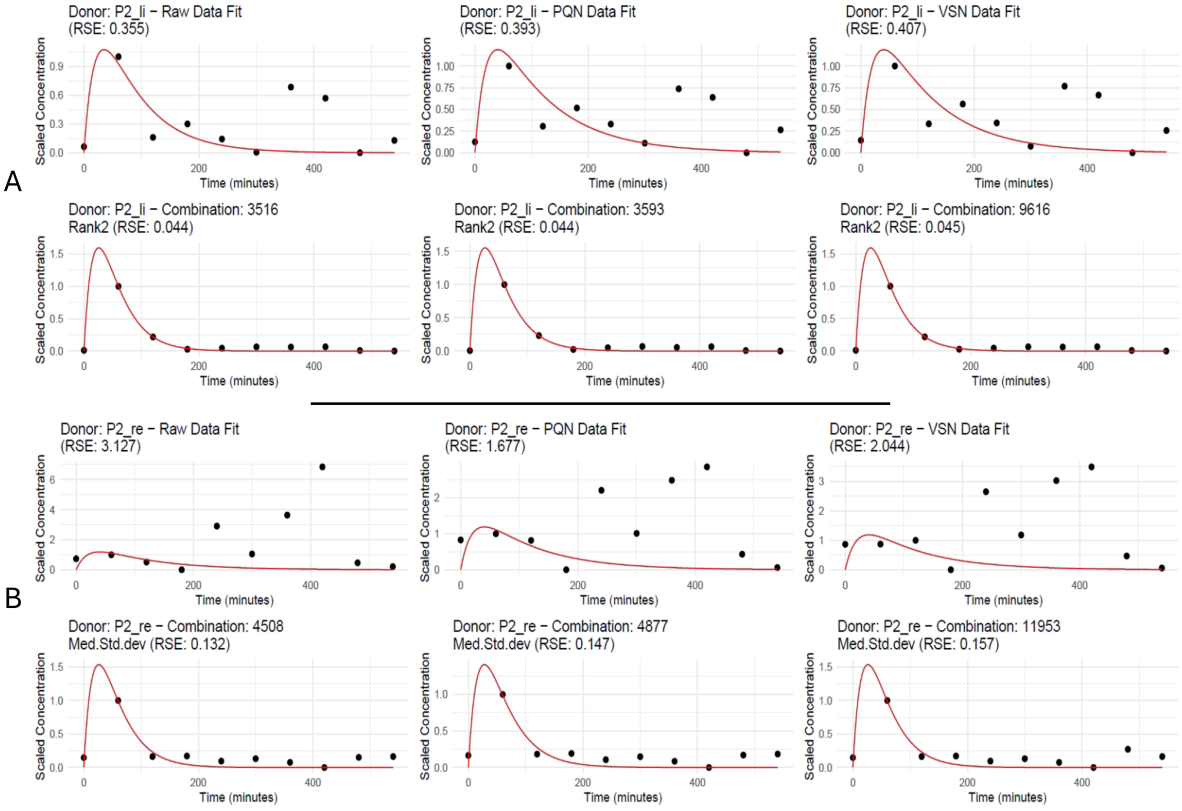

Figure 4.5 – Comparison of found top normalization combinations and the raw data, as well as the PQN and VSN stabilized data. A) Top hits for donor P2 left hand, B) Top hits for donor P2 right hand.

Figure 4.6 – Comparison of the residuals for each sample regarding the top normalization combinations in the caffeine study 2, tested on all donors alongside the raw data and the PQN and VSN stabilized data for comparison.

These calculations for various normalization combinations were also conducted using PQN or VSN stabilized data to determine if variance-stabilized data improved curve fitting. However, merely examining the top few combinations from millions of calculations does not provide a complete picture, making comparison difficult. Therefore, the standard deviation (SD) of the residuals for each combination across all donors was analyzed using a boxplot. The top 10000 combinations were filtered for those that could normalize at least 6 of the 12 different donors in the study (Figure 4.7, Appendix Figure 5.15). Normalizing the raw data directly yielded the lowest variance in the calculated combinations' SD but could not achieve the same minimum SD values as the combinations with PQN or VSN. Additionally, only 67 combinations for the raw data met the filtering criteria, compared to 1055 for the PQN and 1512 for the VSN stabilized datasets. This indicates that fewer combinations could fit more than 6 donors for the raw dataset. Also, no raw combination could fit all 12 donors. The combinations of the PQN and VSN stabilized datasets appeared similar. Yet, the VSN combinations had even more combinations that fit the criteria and reached lower SD values than the PQN combinations.

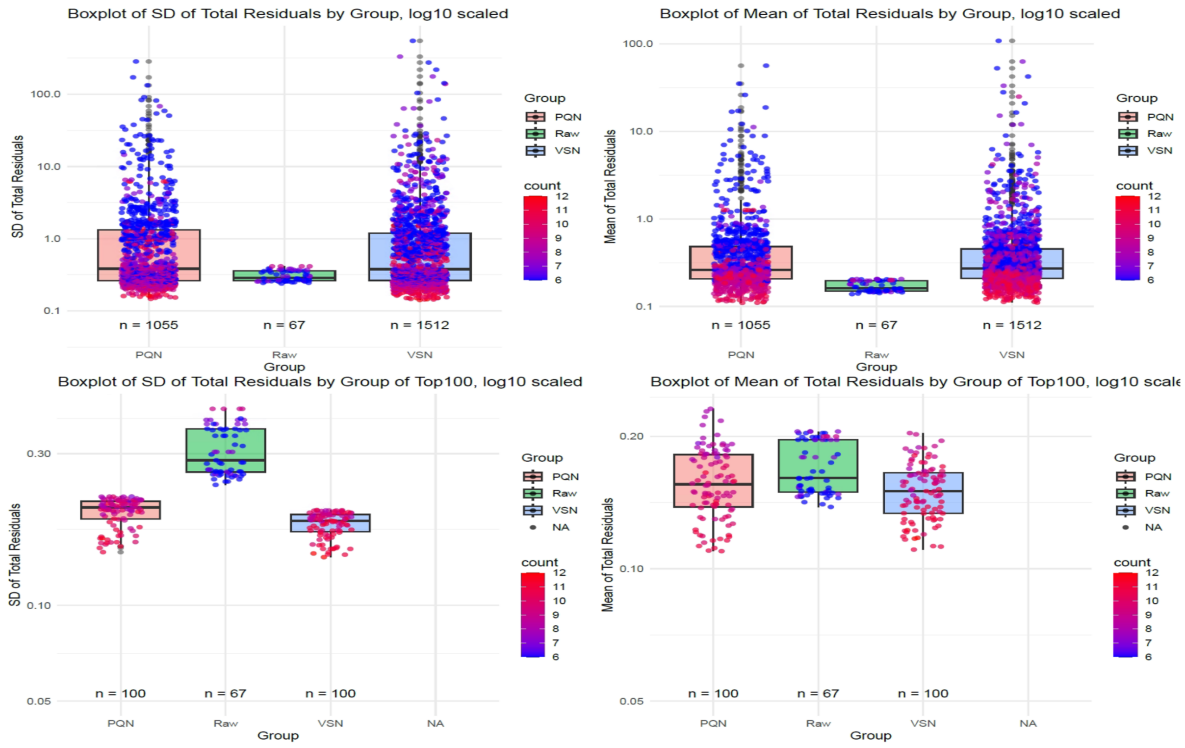

Figure 4.7 – Overview of the standard deviation of the residuals for all donors concerning the top 10000 normalization combinations that can normalize 6 or more of the 12 different donors in the caffeine study 2, using boxplots.

Some combinations enhance the theoretical pharmacokinetic caffeine curves, while others detract from them. Variance stabilizing could potentially improve the data, but it may also worsen it for many combinations and seems to depend on the donors. Additionally, the raw data mostly already displays strong pharmacokinetic curves, indicating that the finger sweat method functions quite well. However, a strategy is needed to enhance its robustness (Figure 4.7 & Figure 4.8).

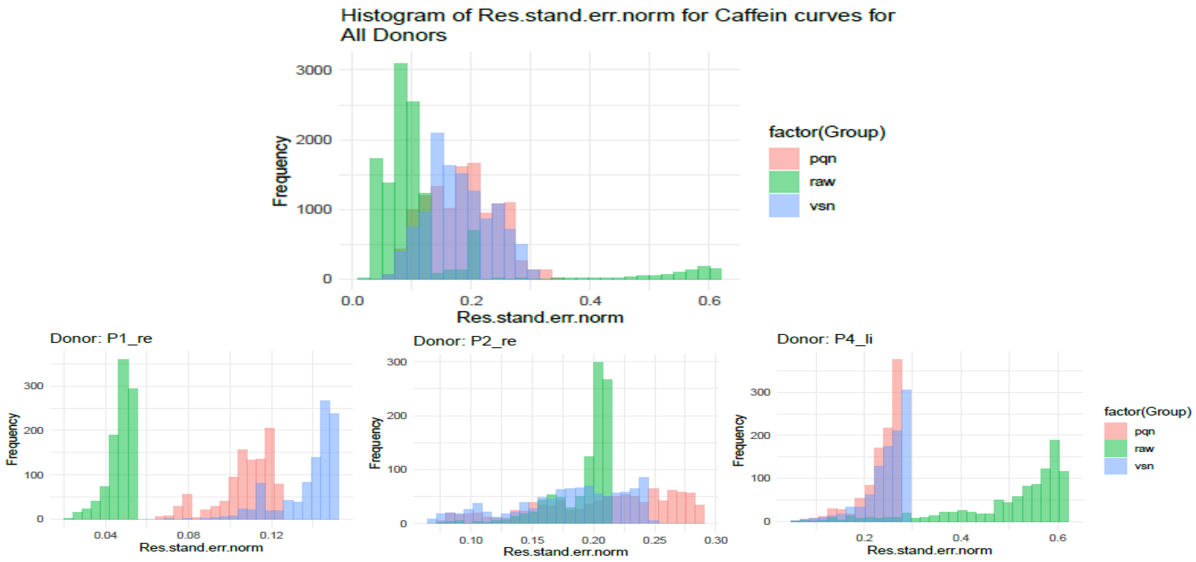

Figure 4.8 – Histograms residual standard error (Res.std.err) of normalized caffeine curves from caffeine study 2 for raw, PQN, and VSN datasets as a comparison of stabilization.

Table 4.3 – Comparison of the counts how often the normalization molecules happen to be in the top 10 or 20 methods of the top 10000 combinations and are top combinations for at least 6 different donors. Comparing raw and variance stabilised datasets. Missing entries are indicated by '-'.

norm. molecule	Raw Top 10	Raw Top 20	PQN Top 10	PQN Top 20	VSN Top 10	VSN Top 20
Citrulline	10	20	10	20	10	20
Hypoxanthine	10	20	10	20	10	20
Xanthine	10	20	10	20	10	20
Urocanic acid sum	10	20	-	-	-	-
Glutamic acid	6	9	10	20	10	20
Creatinine	5	9	5	13	2	3
DL-Phenylalanine	5	8	5	11	6	12
DL-Tyrosine	5	7	8	12	4	8
DL-Tryptophan	1	4	6	10	7	10
Iso-Leucine1	2	2	7	12	7	13
Iso-Leucine2	5	12	9	-	-	-
Succinic acid	6	10	-	-	-	-
Uric Acid	5	10	-	4	2	8
Uracil	5	10	-	-	-	-
Adenosine	5	6	5	-	-	3
Hippuric acid	2	5	-	-	-	-
Carnitine	-	2	-	-	-	-

The frequency with which the normalization molecules appear among the top 10 or 20 methods of the top 10000 combinations of at least 6 different donors was analyzed to determine if certain molecules are present in all the top combinations. This was tested us-

ing raw and variance-stabilized data (Table 4.3). The molecules citrulline, hypoxanthine, and xanthine appeared in every top combination. In contrast, others, like glutamic acid, appeared only in the variance-stabilized datasets in all top combinations, while urocanic acid was present only in the raw dataset. Also, only the weighting method 'Rank2' was found in all these top combinations.

Certain patterns emerge regarding the normalization effectiveness of specific molecules. Additionally, the Rank2 weighting stands out as the most effective. It can also be inferred that PQN and VSN normalization, as a preliminary step, aid in size-error normalization for biological molecules, although this is dependent on particular combinations. While it does not universally enhance performance, the right subsequent normalization choice can lead to data improvements.

Now, it needed to be determined whether the methods identified in the caffeine study 2 were transferable to other studies. Therefore, they were tested on the caffeine study 1. It was found that the top combinations showed RSE improvement. However, proving that this normalized data reflects the true values is difficult, as there are no ground truth values. Additionally, it is evident that the combinations affect different donors in various ways, and the top combination for one donor is not always transferable to another Figure 4.9, Appendix Figure 5.16).

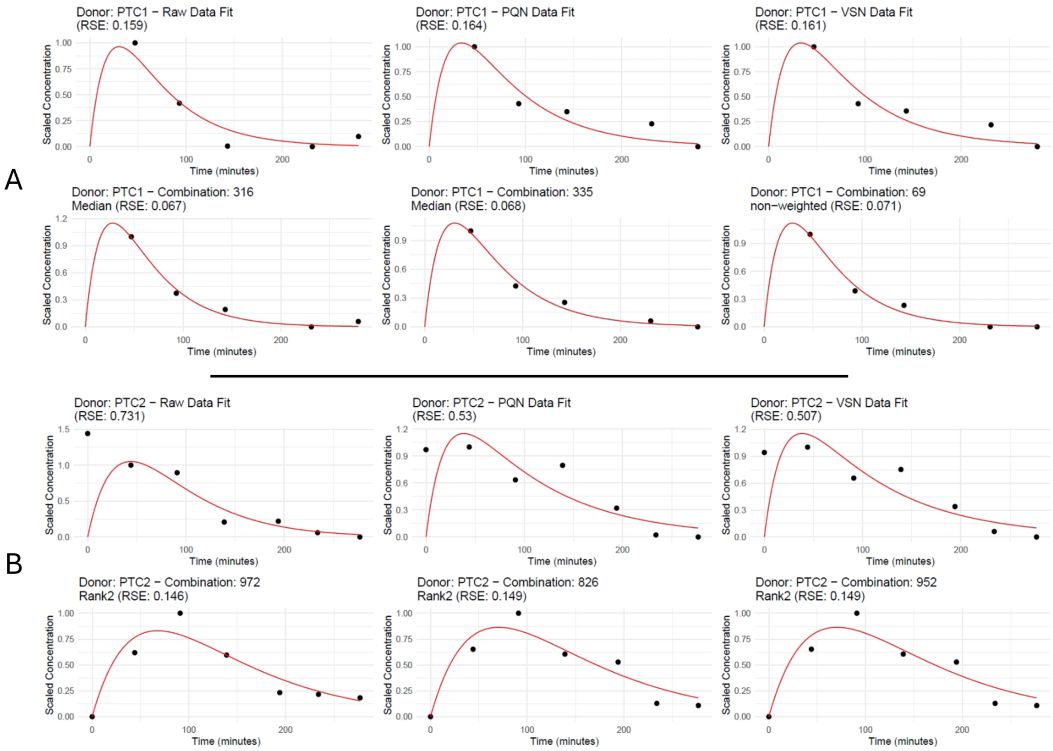

Figure 4.9 – Comparison of found top normalization combinations from the filtered combinations from the caffeine study 2 dataset, the raw data, as well as the PQN and VSN stabilized data. A) Top hits for donor PT day one with chromatography paper, B) Top hits for donor PT day two with chromatography paper.

The CVs in the caffeine study 1 were analyzed. First, the CVs of all untargeted features in each sample were calculated, the overall CVs of each sample were compared with one another, and plotted as boxplots for each donor. The CVs of all samples were in a similar range. However, the donors sampled with Kimtech paper (PTK1 and PTK2) exhibited a lower overall CV than those sampled with chromatography paper (PTC1 and PTC2). Next, the CVs over all untargeted features were analyzed over all samples based on the variance stabilization and a normalization strategy using tyrosine. These were also tested in a different order to determine if the sequence of stabilization and normalization affected the outcome. Applying PQN and VSN slightly reduces the overall CV compared to the raw values. VSN appears to reduce CV a bit more than PQN, although it is difficult to conclude definitively. Notably, applying tyrosine normalization increases the overall CV, whether used alone or following variance stabilization. Nevertheless, applying tyrosine normalization first and then executing variance stabilization results in the smallest CVs (Figure 4.10).

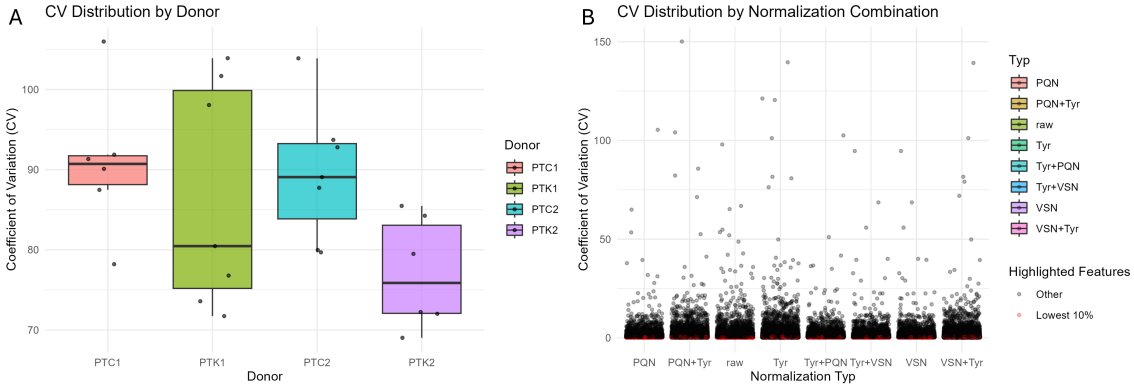

Figure 4.10 – Comparison of CV values for the caffeine study 1. A) CV comparison of all features in the samples of different donors. B) CV comparison for all features over all samples, comparing different stabilization and normalization strategies and their sequence of them.

The caffeine study 1, which used the latest sampling and measuring methods, was also tested on its own with different normalization molecules (Appendix Table 5.2), yet this study was limited by the number of samples it had and the limited variance of donors.

Other caffeine datasets were also tested, including one caffeine study testing coffee and matcha (hereafter referred to as caffeine study 4), which indicated that sample quality is the most crucial factor. If a mostly functioning pharmacokinetic curve characteristic is not already present, it becomes significantly more challenging to improve it (Appendix Figure 5.17).

The largest tested caffeine study was conducted by Julia Brunmair, hereafter referred to as caffeine study 3 [23]. This study demonstrated a pharmacokinetic caffeine curve. However, the points were also noisy and did not conform to a smooth curve fit. Although these datasets were generated using earlier methodologies, with different sampling techniques and LC-MS protocols, the underlying sample matrix remained the same. This allowed for assessing whether the promising normalization combinations would still be

applicable despite analytical differences. By applying these strategies to an older dataset, it was possible to evaluate whether normalization performance depended on the biological origin of the analytes rather than the specific analytical methods used. An improvement could be found, yet the top combinations tended to compress the data points, which reduced the error but did not yield a representative and good fit (Figure 4.11).

So, it can be concluded that some molecules have the potential to improve the curve fit and reduce variance. Also, variance stabilization methods can potentially enhance data quality, and weighting methods are needed to allow effective normalization combinations. However, it is challenging to find normalization combinations that are universally effective, transferable not just between donors but also across experiments. Calculating millions of combinations for each study does not yield satisfactory results, as identifying combinations that transfer well between studies from such a vast amount of combinations is difficult. Thus, a different approach is required, one that not only returns the residual error of each combination for each donor but also adopts a more comprehensive strategy. This would involve providing a score for each combination that reflects the fit across all donors from several studies in order to attain a more complete picture and hopefully derive universal normalization combinations.

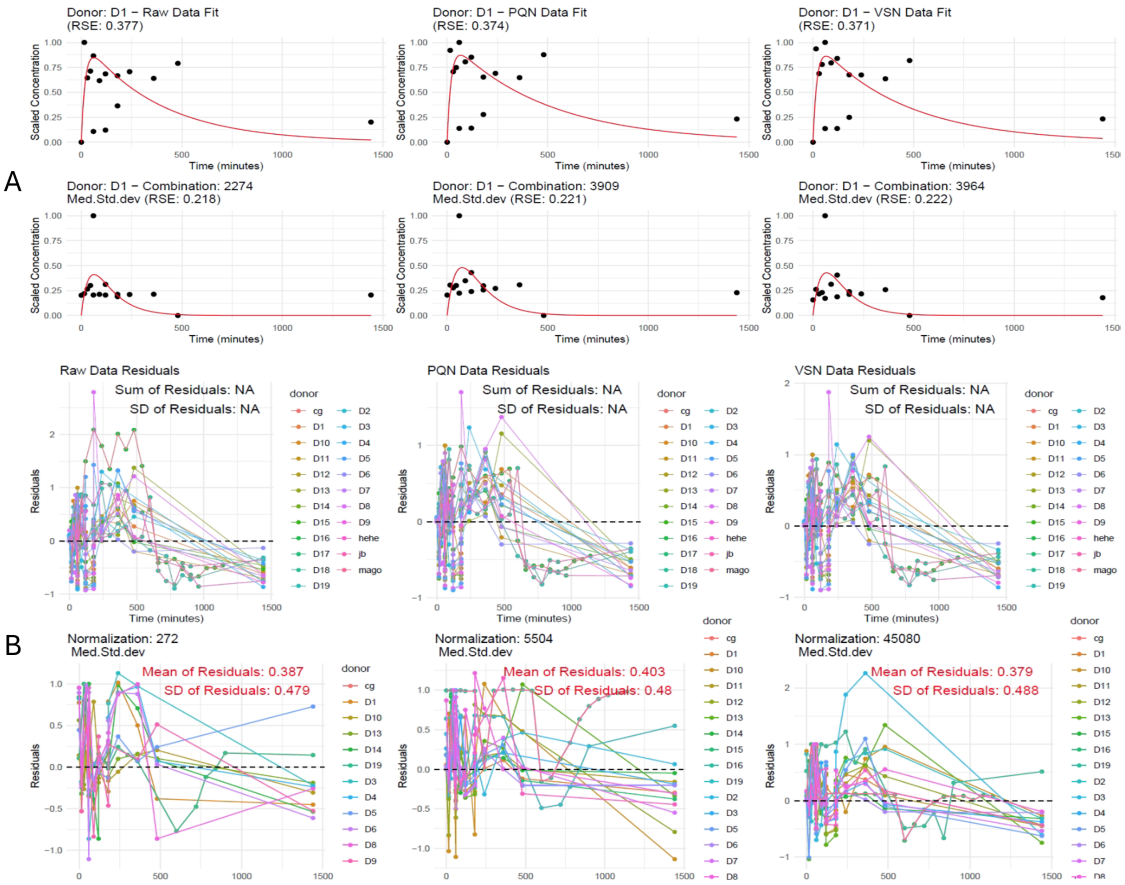

Figure 4.11 – Comparison of found top normalization combinations from the caffeine study 3 dataset, the raw data, as well as the PQN and VSN stabilized data. A) Top normalized curves for donor D1, B) Comparison of residuals for each sample to the fitted curve for all donors for the top normalization combinations.

4.3.2 Testing Combined Caffeine Datasets using Bayesian Optimization Algorithm

The next step was to combine the caffeine datasets from caffeine study 1, caffeine study 2, and caffeine study 3 to derive more universal normalization methods, utilizing hundreds of data points from dozens of donors. While the studies employed different measurement methods, which initially required alignment, this combined dataset represents the largest, most comprehensive, and comparable resource available at the time for this analysis. Other datasets did not offer sufficiently controlled pharmacokinetic curve data, making this the optimal choice for developing and evaluating normalization approaches.
Given the increase in dataset size, exhaustive testing of millions of normalization combinations was no longer computationally feasible. To address this, an optimization algorithm was employed to efficiently search the multidimensional parameter space. Specifically, Bayesian optimization was selected due to its ability to identify local optima across complex parameter landscapes. In this framework, different weighting and variance stabilizing methods were considered as distinct dimensions, with each normalization molecule representing its own additional parameter. The optimization objective was defined as minimizing the sum of the relative residuals across all fitted curves. This process was implemented using the bayesOpt function in *R*.

Listing 4.1 – Bayesian Optimization Code Snippet

```
opt_res <- bayesOpt(
  FUN = function(method, pqn_vsn, m1, m2, m3, m4, m5, m6, m7, m8, m9, m10, m11) {
    weights <- c(m1, m2, m3, m4, m5, m6, m7, m8, m9, m10, m11)
    # Decode method from integer to string
    method_decoded <- norm_methods[floor(method)]
    pqn_vsn_none <- ifelse(pqn_vsn <= 1, NA, ifelse(pqn_vsn <= 2, "PQN", "VSN"))
    # Evaluate the combination
    score <- evaluate_combination(method_decoded, weights, pqn_vsn_none)
    return(list(Score = score, pqn_vsn_used = toString(pqn_vsn_none),
                method_name = toString(method_decoded),
                comb = toString(norm_feature_list$Molecule.Name[weights > 0.5])))
  },
  bounds = search_space,
  initPoints = 60,  # Initial random evaluations
  iters.n = 12000,  # Number of maximal iterations
  iters.k = 120,    # Number of times to sample FUN at each optimization step
  acq = "ei",       # Acquisition function
  eps = -0.03,      # Parameter to focus a little more on exploration
  convThresh = 1e+07, # Stricter convergence
  acqThresh = 0.6,  # Allow local optima with reasonable utility
  otherHalting = list(timeLimit = 86400, minUtility = 1e-2), # Stop criteria
  parallel = TRUE,  # Parallel execution
  plotProgress = TRUE
)
```

The initial optimization calculations utilized a one-compartment model to fit the caffeine curve across the data points, incorporating 11 normalization molecules (Appendix Table 5.4). Cis and trans-urocanic acid were combined to obtain the total abundance. Weighting methods such as Rank2, Median, and Med.Std.dev were employed, alongside PQN and VSN as variance stabilization methods. PQN and VSN were pre-calculated and provided as factors for each sample to the function. This precalculated VSN factors represent a simplified version of VSN, as VSN first stabilizes various intensity ranges of the data differently before condensing into a single factor for each sample, effectively rendering it an intensity-weighted PQN stabilization, this was done as at this point in the thesis a single factor was needed for the optimized function and therefore the normal VSN was not usable.

The optimization was run for a maximum of 24 hours, during which it completed 16 epochs, with 120 samplings of the search space each, while attempting to find the optimal combination for the normalization across all the donors. It must be noted that the optimization approach is not ideal for this problem, as it performs best with continuous values. However, here we have a continuous search space that is mapped to discrete dimensions, whether to include a molecule in the combination or to use which weighting or variance stabilization method. The optimization algorithm still operates effectively but may produce duplicates of the same combinations, even while exploring different regions of its search space, which can also slow down the discovery of the optimal solutions. Therefore, the algorithm was adjusted to prioritize exploration over exploitation since delving deeper into the maximum would yield more duplicates. It is important to test as many combinations as possible to increase the chances of finding the best one. Additionally, we can utilize those duplicates to identify which local optima were discovered, as they tend to be sampled more frequently.

The sampling results of the BayesOpt algorithm indicate that each molecule and combination have been tested a similar number of times. This is evident in the network of all combinations without duplicates. This consistency is crucial, as statistically, finding random favorable results for a certain molecule that was sampled more frequently would be more likely. Additionally, some molecules perform better than others, such as succinic acid and uric acid, which have been sampled more often and rank highly among the top combinations (Figure 4.12).

In the top combinations, PQN performs best for variance stabilization, while the Median excels in the weighting methods. The non-stabilized and non-weighted combinations do not appear at all in the top combinations.

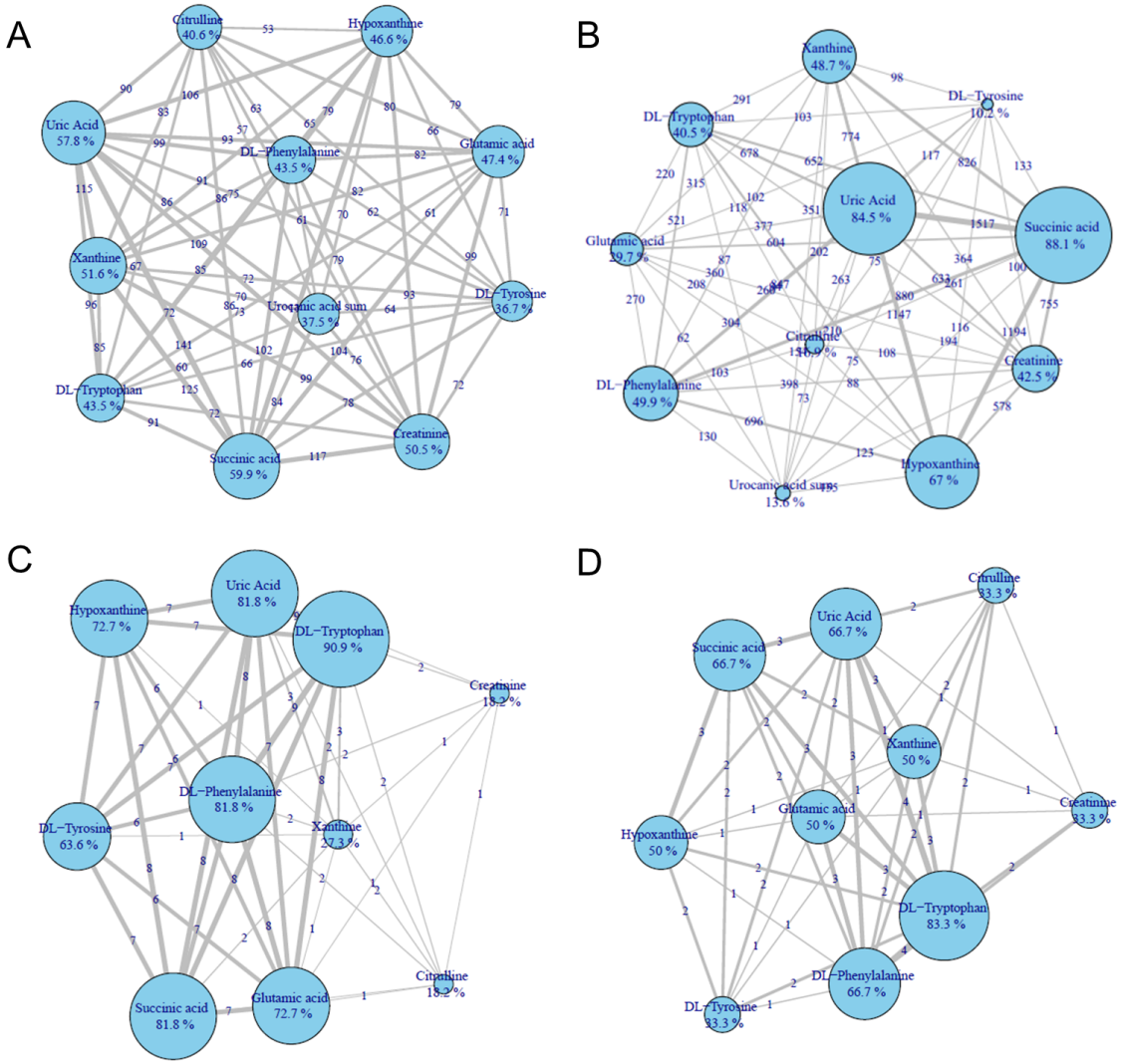

Figure 4.12 – Co-occurence networks of the sampled molecules exploring the best normalization combinations of the combined caffeine studies using the BayesOpt algorithm, displaying the percentage of each molecule in the combination and how frequently they co-occur with other molecules in the sampled combinations. A) All sampled combinations without duplicates, B) All sampled combinations with duplicates, C) Top combinations with a score only 20% bigger than the best found combination with duplicates, D) Top combinations with a score only 20% bigger than the best found combination without duplicates.

4.3.3 Testing the Wine Study Dataset using Bayesian Optimization Algorithm

The caffeine studies used up to this point were from different studies, using various and mostly outdated methods, and were therefore not fully optimal for the search of the normalization method. A new study utilized the latest methods, involving 14 participants who drank wine under standardized conditions and sampled finger sweat over several hours. All participants consumed the same meal, baked potatoes with only olive oil and salt, and received a body-weight standardized amount of wine. This study produced pharmacokinetic curves for various wine and potato-related molecules, which could be used to fit modeled curves and determine normalization combinations using the method established in previous datasets. The Bayesian optimization method was employed to fit curves for all donors for five wine molecules and two potato-related molecules (Appendix Table 5.5).

For the optimization calculation using the wine study, the normalization molecules were further filtered based on the previous calculations of the caffeine study. Early retention time molecules, such as citrulline and trans-urocanic acid, were removed since they elute in the injection peak and have a larger variance. However, glutamic acid was retained due to its significant abundance. Glutaric acid and succinic acid were found in high abundance in the processing blank samples, which tested only the paper itself. Some other molecules were added, including uracil, propionylcarnitine, glycerophosphocholine, and N-acetylneuraminic acid. For the pharmacokinetic curves, all time points preceding the ingestion of wine were excluded from the analysis. The T0 time point, corresponding to the moment immediately prior to wine intake, was set to an abundance of zero to reflect baseline conditions. Additionally, an artificial zero endpoint was introduced at eight hours post-ingestion to ensure the curve returned to baseline by the end of the observation period.
Seven molecules (five from wine and two from potatoes) were selected for curve fitting using a one-compartment model similar to the caffeine study. Fifteen dimensions were defined for the search space, incorporating weighting methods such as Rank2, Median, and Med.Std.dev, along with strategies like PQN/VSN or None, and 13 molecules (Appendix Table 5.6) were examined.
The optimization algorithm ran again for 24 hours and 15 epochs, demonstrating a good exploration of the search space and that most tested combinations performed well. Some molecules are found much more frequently in the top combinations than others. For example, N-acetylneuraminic acid, glycerophosphocholine, propionylcarnitine, and creatinine. Tyrosine and uracil also performed well, as they are found in many top combinations (Figure 4.13).
In the top combinations, the non-stabilized combinations appeared most frequently, which differs from the results of the caffeine studies, while the Median excelled in the weighting methods, mirroring the caffeine studies.

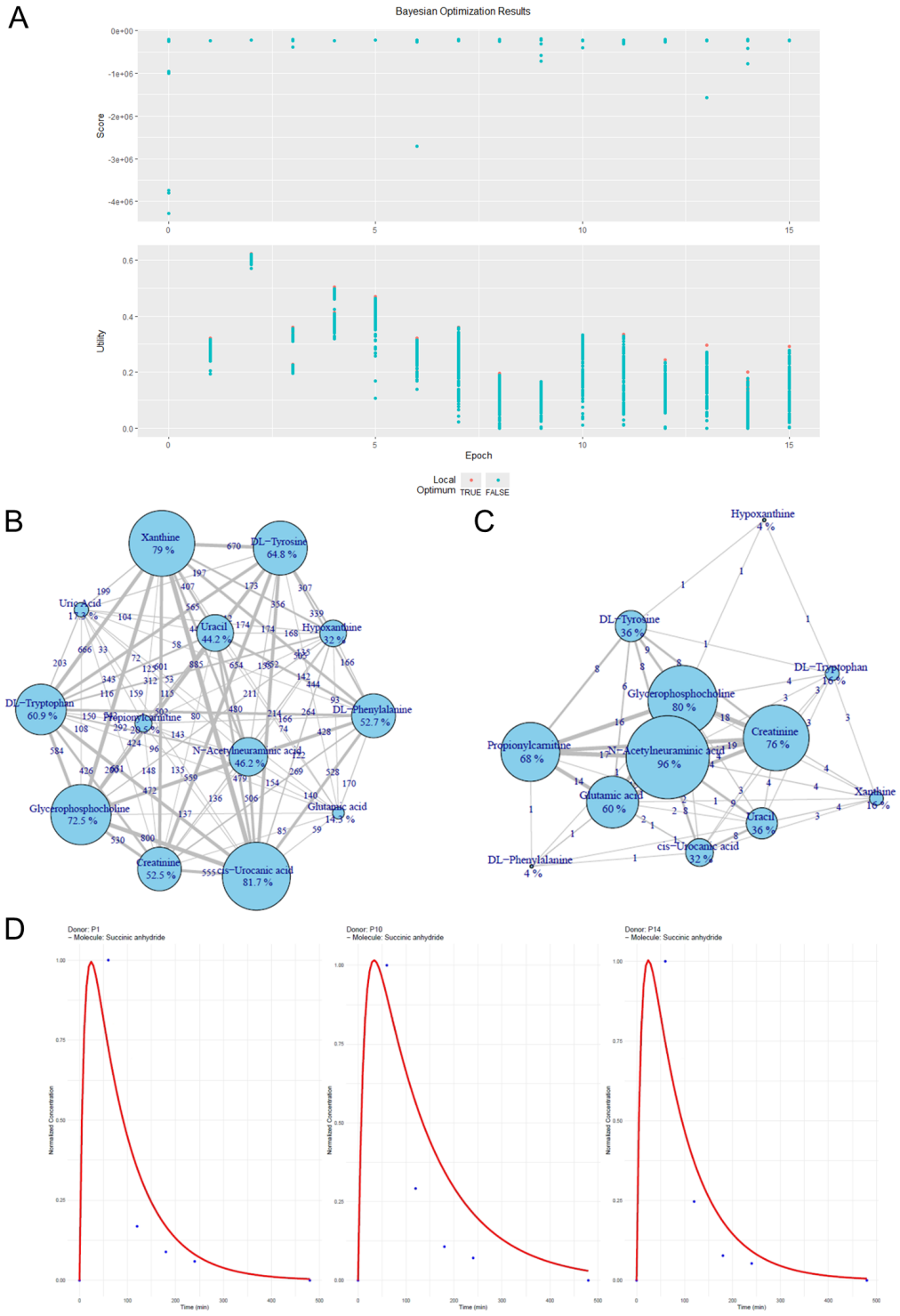

Figure 4.13 – Co-occurence networks of the sampled molecules exploring the best normalization combinations of the wine study using the BayesOpt algorithm, displaying the percentage of each molecule in the combination and how frequently they co-occur with other molecules in the sampled combinations A) Overview of the sampled combinations over the epochs during the bayesOpt calculation, B) Top combinations with a score only 20% bigger than the best found combination with duplicates, C) Top combinations with a score only 10% bigger than the best found combination with duplicates, D) Fitted functions over normalized data for several donors.

The fitted curves for the wine and potato molecules generally appear satisfactory. However, two molecules (Tetraethyl pyrophosphite and 3,7-Dihydro-1-butyl-7-(5,6-dihydroxyhexyl)-3-methyl-1H-purine-2,6-dione) have data points that cannot be fitted to the curve at all (Appendix Figure 5.19). After investigating the data, it was determined that these molecules are near the limit of detection (LOD), and at times, noise overlaps with those peaks, leading to incorrect abundance values and distorting the normalization approach. Therefore, these two molecules were excluded from further calculations, and gallic acid was added as an additional pharmacokinetic molecule (Appendix Table 5.7). Additionally, citrate and fumarate were included in the normalization molecules, bringing the total to 15 molecules (Appendix Table 5.8). Moreover, it was observed that the fitted curves do not fully represent the actual metabolic processes when using the one-compartment Bateman function, as the data points seem to have a different kinetic than the predicting one-compartment model. Consequently, the model was adjusted to a two-compartment Bateman function to better predict the metabolic processes. The scoring was modified so that the normalized curve fitting was compared to the raw fit, and if the residuals were more than 10% worse, it received an additional penalty to the score.

The optimization calculation with the adjusted parameters revealed a group of molecules (propionylcarnitine, creatinine, cis-urocanic acid, DL-tryptophan, glycerophosphocholine, fumarate, hypoxanthine, DL-tyrosine) that are frequently utilized in the top combinations. In the top combinations, PQN and non-stabilized combinations performs best for variance stabilization, while the Med.Std.dev excels in the weighting methods. The fitted curves from the two-compartment model fit better than those from the one-compartment model. It is also evident that the raw data already exhibit a good curve fit, and normalization only slightly alters this. Sometimes, the fitted curve remains unchanged even when the data points shift marginally (Figure 4.14, Appendix Figure 5.20).

Therefore, it can be concluded that the two-compartment Bateman function models the metabolic processes more effectively. The raw data already exhibit an almost perfect curve fit, needing only slight stabilization to ensure the method's robustness. However, this only applies to molecules that possess well-defined peak shapes, are sufficiently abundant, and are not close to the LOD. This limitation also restricts the potential for identifying the best normalization combination solely based on the fitted curves. Additional parameters must be tested and incorporated into the scoring.

With this knowledge, the next optimization run was adjusted accordingly. It still utilized a two-compartment model, but the search space comprised 17 dimensions, incorporating various weighting methods (non-weighted, Rank2, Median, Sqrt, Log2), normalization techniques (PQN, VSN, or none), and 15 distinct molecules. The Med.Std.dev can perform well but may also return negative normalization factors, making it a non-robust method and was consequently excluded. Instead, Sqrt and Log were included. Experimental curves needed to include a minimum of four points, with changes to the point at T0 now set at 300, given that the lowest measured value is 370. Correction factors (corr_factor) were introduced to compare the predicted sweat volume ($\frac{Area_{measured}}{Area_{predicted}}$)

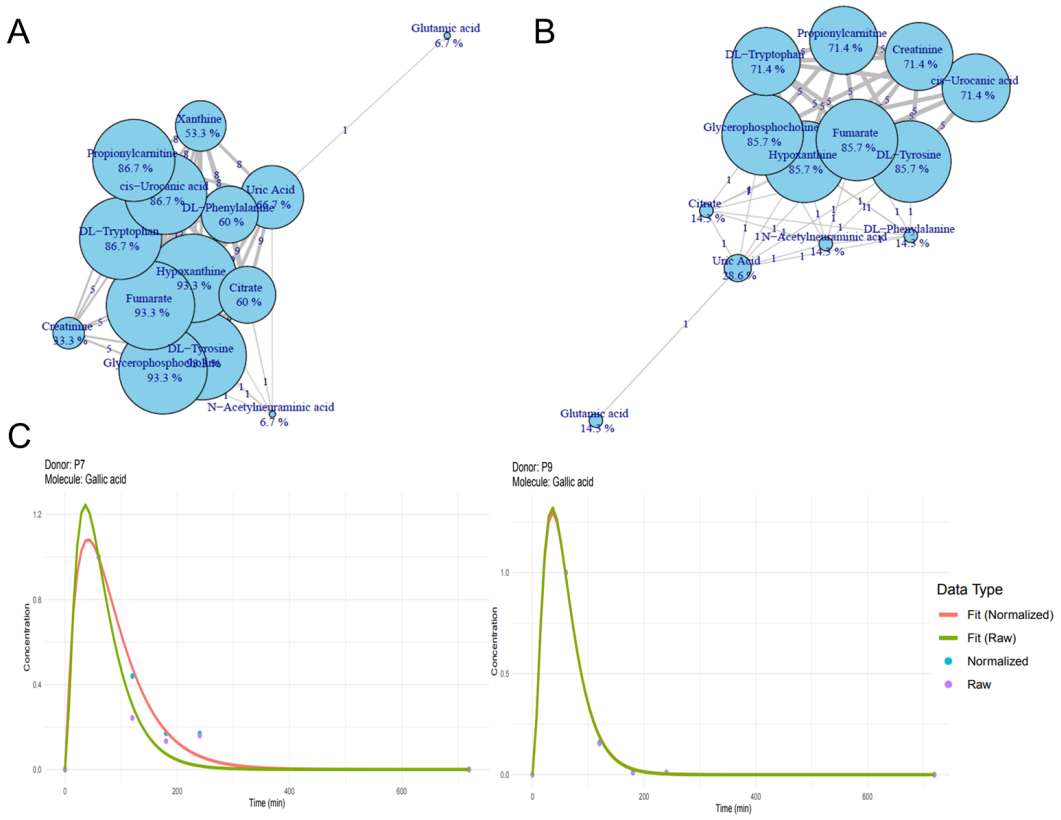

Figure 4.14 – Co-occurence networks of the sampled molecules exploring the best normalization combinations of the wine study using the BayesOpt algorithm, displaying the percentage of each molecule in the combination and how frequently they co-occur with other molecules in the sampled combinations A) Top combinations with a score only 20% bigger than the best found combination with duplicates, B) Top combinations with a score only 10% bigger than the best found combination with duplicates, C) Fitted functions over normalized and raw data for several donors.

between different molecules for the same sample. Correction factors for abundance values below 3000 were excluded, maximizing accuracy by excluding high-variance data close to the LOD. The standard deviation of the corr_factor of all molecules from the same sample was calculated and compared between normalized and raw data to determine if the predicted sweat volume becomes more similar for different molecules for the same sample. Clustering of potato and wine features was analyzed using hierarchical clustering, which automatically choose the number of clusters resulting in the lowest mean silhouette score, leveraging average silhouette scores for cluster separation and the standard deviation of silhouette scores for cluster density. Rewards and punishments were applied based on corr_factor and clustering performance, ensuring enhanced normalization calculations.

For the calculation including all those new parameters the convergence started to take longer to calculate so the exploration was increased even further and the calculations are starting to take longer reducing the amount of epochs run in 24 hours to around 7.
The top combinations often included hypoxanthine, fumarate, DL-phenylalanine, glutamic acid, cis-urocanic acid, uracil, and N-acetylneuraminic acid, which are primarily

also found in the leading combinations of previous calculations (Figure 4.15).
The clustering and corr_factors altered the situation, resulting in non-variance-stabilized combinations predominantly appearing among the top combinations, along with Log2 as the weighting method. The hierarchical clustering shows improved clusters for the normalized data compared to the raw data. Notably, hierarchical clustering revealed better cluster separation for the normalized data compared to the raw data. Normalization influenced not only the silhouette scores but also the optimal cluster size, suggesting that normalization may help reduce the impact of spurious outliers and yield more robust clusters.

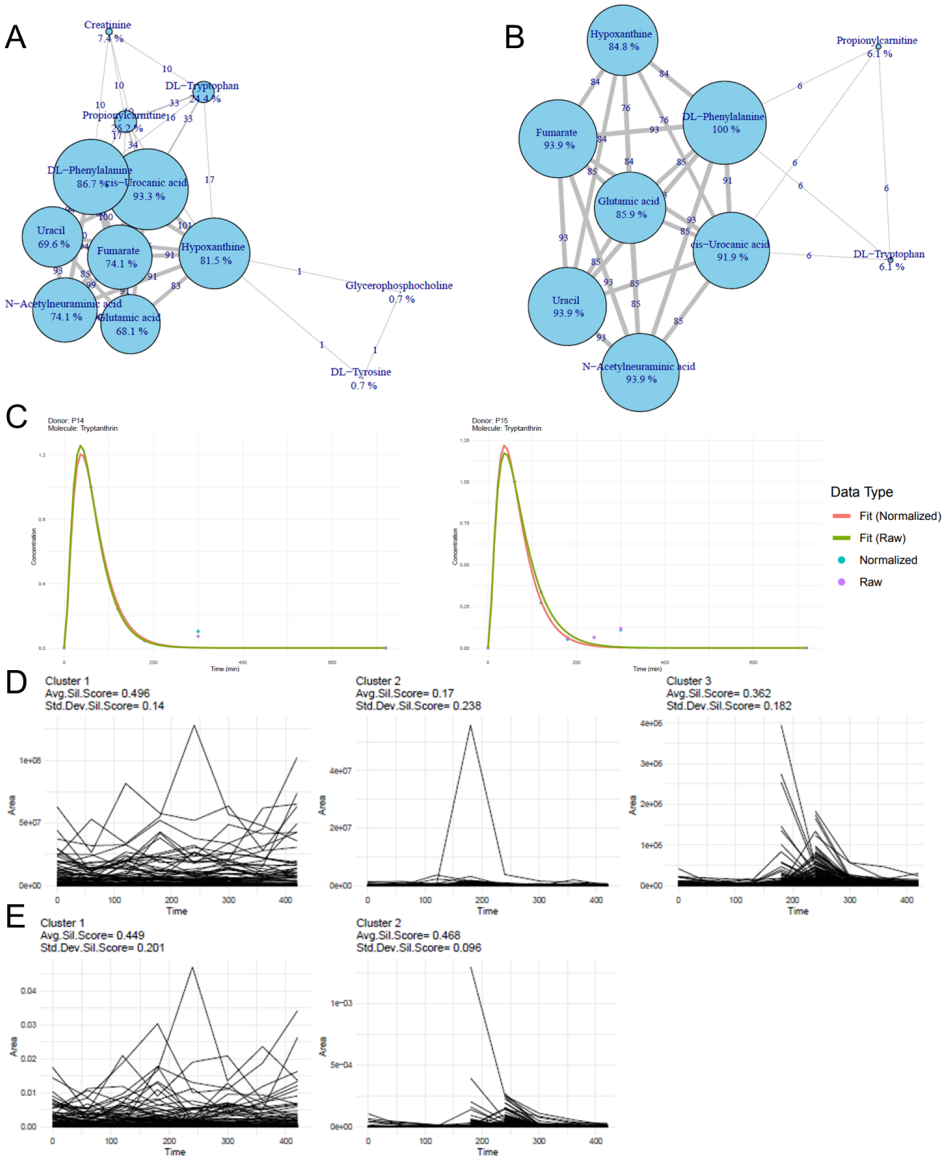

Figure 4.15 – Co-occurence networks of the sampled molecules exploring the best normalization combinations of the wine study using the BayesOpt algorithm. A) Top combinations with a score only 50% bigger than the best found combination with duplicates, B) Top combinations with a score only 10% bigger than the best found combination with duplicates, C) Fitted functions over normalized and raw data for several donors, D) Automatic hierachical Clustering of raw data, E) Automatic hierachical Clustering of normalized data.

For the following calculations, several adjustments were made through various test runs. The calculation continued on the wine study dataset, and the two-compartment model remained unchanged. To address convergence issues, exploration levels were further increased (Listing 4.2). Citrate was excluded due to its consistently poor performance in prior calculations and potential confounding effects related to skin care products. An omission of variance stabilization in previous clustering analyses was identified and corrected. A significant methodological update involved introducing the option to apply variance stabilization—specifically PQN or VSN—not just before normalization but also after normalization. Previously, stabilization was performed solely prior to normalization; now, both pre- and post-normalization stabilization are possible, allowing a more comprehensive evaluation of the impact of stabilization order. Additionally, full VSN (fullVSN) was integrated as a stabilization option rather than relying only on the former VSN factor. While this addition complicated the calculations, it offers a more complete overview of the effects of different variance stabilization approaches. The search space for optimizations thus expanded to 16 dimensions, including various weighting methods (non-weighted, Rank2, Median, Sqrt, Log2), variance stabilization methods (PQN, VSN, fullVSN, post-PQN, post-VSN, post-fullVSN, None), and 14 normalization molecules. The scoring system was also refined to account for different testing parameters, now reducing clustering weights, converting fixed penalties to percentage weights, and amplifying the curve error by a factor of 10 to better highlight differences between combinations.

Listing 4.2 – Adjusted Bayesian Optimization Code Snippet

```
opt_res <- bayesOpt(
  FUN = function(method, pqn_vsn, m1, m2, m3, m4, m5, m6, m7, m8, m9, m10, m11, m12, m13,
       m14) {
    weights <- c(m1, m2, m3, m4, m5, m6, m7, m8, m9, m10, m11, m12, m13, m14)
    # Decode method from integer to string
    method_decoded <- norm_methods[floor(method)]
    pqn_vsn_none <- pqn_vsn_methods[floor(pqn_vsn)]
    # Evaluate the combination
    score <- evaluate_combination(method_decoded, weights, pqn_vsn_none)
    return(list(Score = score, pqn_vsn_used = toString(pqn_vsn_none),
                method_name = toString(method_decoded),
                comb = toString(norm_feature_list$Molecule.Name[weights > 0.5])))
  },
  bounds = search_space,
  initPoints = 60,  # Initial random evaluations
  iters.n = 1680,   # Number of iterations (14 epochs = 1680)
  iters.k = 120,    # Number of times to sample FUN at each optimization step
  acq = "ei",       # Acquisition function
  eps = -0.1,       # Parameter to focus a little more on exploration
  convThresh = 5e+07, # Stricter convergence
  acqThresh = 0.6,  # Allow local optima with reasonable utility
  otherHalting = list(timeLimit = 86400, minUtility = 1e-2), # Stop criteria
  parallel = TRUE,  # Parallel execution
  plotProgress = TRUE
)
```

With all the adjustments made to the scoring function, it was run again, revealing that a well-defined optimum can be identified. The top normalization combinations consistently include cis-urocanic acid and glycerophosphocholine, and may include uracil. Weighting occurs with Rank2 and is stabilized with VSN (Figure 4.16).

However, it is nearly impossible to prove that this is the best possible combination. Simply extending the algorithm's search duration is inefficient, as each new epoch requires more time to find the next optimal step. Nevertheless, the optimization algorithm can be executed multiple times, and since it selects random starting parameters in the search space, it has the potential to discover different minima. Thus, to sample the search space more comprehensively, the same function was run 10 additional times to obtain results from 11 runs, each conducted for 24 hours across as many epochs as possible, averaging 8 epochs per run.
After the 11 runs, the top minima resembled only the first run. They were still weighted with Rank 2 and stabilized with VSN. The most frequently used molecules remained cis-urocanic acid, glycerophosphocholine, and uracil, but they also included other molecules to varying degrees (Figure 4.16).

For now, it can be concluded that some molecules, like cis-urocanic acid, glycerophosphocholine, and uracil, with the weighting method Rank2 and the stabilization of VSN, can robustly improve the data quality of finger sweat samples.

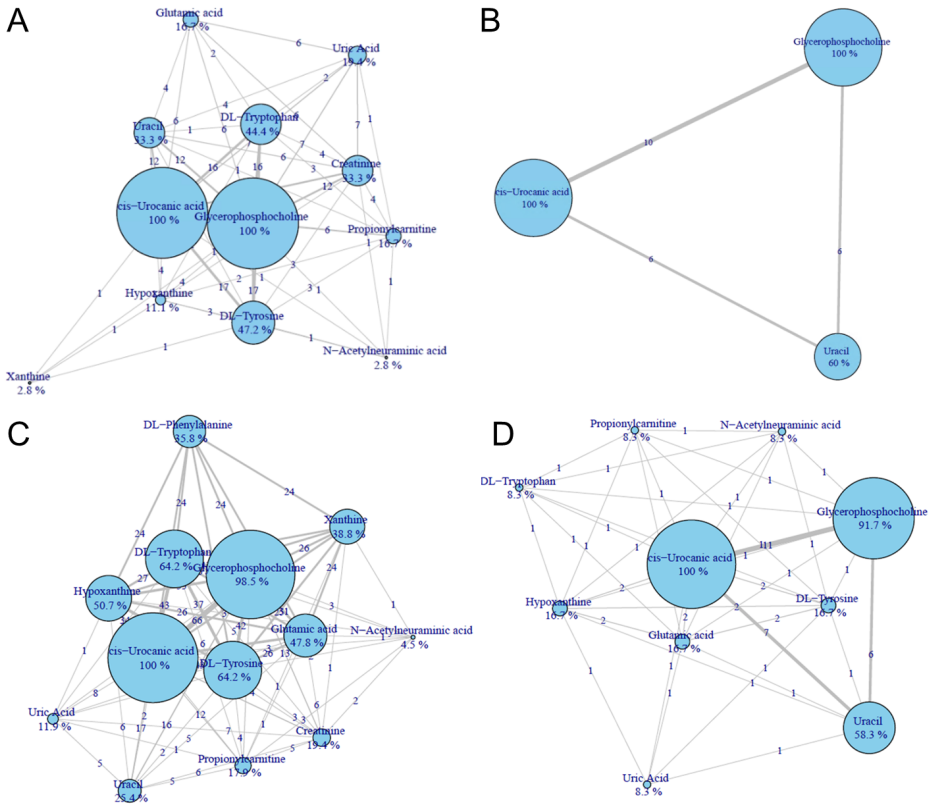

Figure 4.16 – Co-occurence networks of the sampled molecules exploring the best normalization combinations of the wine study using the BayesOpt algorithm of 1 and 11 runs of the same scoring function. A) Top combinations with a score only 20% bigger than the best found combination with duplicates, B) Top combinations with a score only 10% bigger than the best found combination with duplicates, C) Top combinations of 11 runs with a score only 20% bigger than the best found combination with duplicates, D) Top combinations of 11 runs with a score only 10% bigger than the best found combination with duplicates.

However, the data analysis conducted so far has focused only on the top few combinations, which does not provide a comprehensive view of all tested combinations. To address this limitation, all tested combinations—calculated over 11 runs using the latest evaluation function—were visualized as boxplots for direct side-by-side comparison. It is important to note that, for this analysis, lower scores indicate better results, indicating an improved performance, and the higher the score that worse the combination of normalization molecules perform.
The different weighting methods appear comparable to each other. Log2 seems to produce the worst scores, but overall is similar to the other methods. Sqrt seems to be slightly better, but this is probably due to a lack of data, as pick rate by the optimization algorithm was low. However, the non-weighted methods seem to perform worse than the weighted ones, indicating that the weighting improves normalization (Figure 4.17).
The different variance stabilization methods appear to be partially comparable to one another. Log2 seems capable of producing both the worst and the best scores. The fullVSN methods do not exhibit as high a variance as the others but are overall significantly worse than the other methods. The post stabilization seems slightly better than its pre counterpart in all cases. However, the non-stabilized combinations perform similarly, perhaps even better, than the stabilized ones. Thus, the chosen stabilization methods do not improve the normalization (Figure 4.17).
All the different molecules behave very similarly, none better than the others. Only cis-urocanic acid performs better than the rest. Additionally, all the least effective combinations appear from the Log2 and VSN combinations. Furthermore, most tested and effective combinations are below 10 molecules, primarily below 6 (Figure 4.17).

The optimization calculation appears capable of identifying good combinations when focusing solely on the top scores. However, there isn't a significant difference between the molecules, weighting, and stabilization methods overall. Additionally, it remains unproven whether the best combinations have truly been discovered. The optimization algorithm, applied over 11 runs with an average of 8 epochs and 120 samplings each, yielded slightly over 10,000 calculated combinations. Yet, only slightly more than 4,000 of these are unique, as good combinations tended to be sampled multiple times. The total number of possible combinations for the molecules is 16,383, and when factoring in the 5 different weighting methods and 7 different variance stabilizing methods, this results in 573,405 unique combinations. Thus, less than 0.7% of the possible combinations were tested using the optimization approach. To determine if other combinations might be even better and to ensure that some minima are not overlooked, it would be necessary to calculate all possible combinations.

$$\begin{aligned} C(n,r) &= \binom{n}{r} = \frac{n!}{r!(n-r)!} \\ \sum_{r=1}^{14} \binom{14}{r} &= \sum_{r=1}^{14} \frac{14!}{r!(14-r)!} = 2^{14} - 1 = 16,383 \end{aligned} \tag{4.1}$$

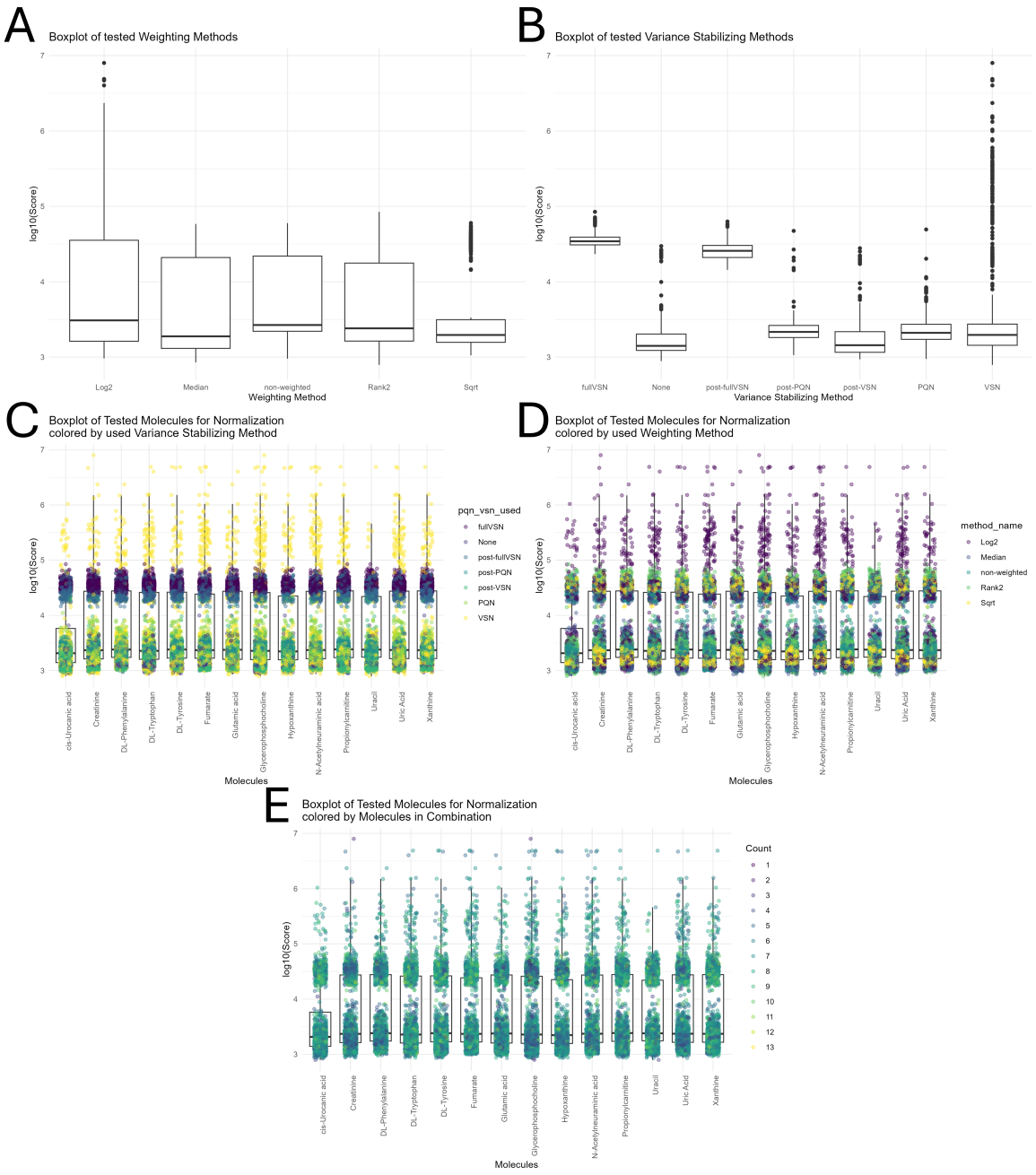

Figure 4.17 – Complete overview of all sampled combinations of the BayesOpt algorithm from the wine study, illustrated using boxplots. A) Overview of tested weighting methods, B) Overview of tested variance-stabilizing methods, C) Overview of tested normalization molecules, colored by variance-stabilizing methods, D) Overview of tested normalization molecules, colored by weighting methods, E) Overview of tested normalization molecules, colored by the count of the molecules used combination.

4.3.4 Testing the Wine Study Dataset using a Combinatorial Bruteforce Approach

The previous optimization approach reveals that the top combinations exhibit a certain pattern, but the overall picture remains unclear. Additionally, only a small fraction of the total possible combinations was calculated, making it uncertain whether the best combination was found. Therefore, a brute-force approach was the next step to calculate all possible combinations.

The calculation continued with the wine study dataset, and the two-compartment model remained unchanged. New results from the Gerner group indicated that not all molecules in finger sweat exhibit a linear relationship between the measured abundance and their concentration, primarily due to ion suppression effects in the ESI. The molecules used demonstrated sufficient linearity, but additional molecules were incorporated based on these new findings. The ion mode for phenylalanine and xanthine was adjusted as they showed improved linearity in the negative ESI mode. Propionylcarnitine was removed because its peak shape sometimes resulted in inconsistent integration. Five other molecules that displayed good linearity were added, along with two control molecules (glycine, serine) that exhibited no linearity, bringing the total to 20 molecules (Appendix Table 5.9).
Additionally, a LIMMA test was included to assist with the scoring by checking the number of significantly regulated features over the study period. The fullVSN stabilization was removed again because it required substantial computation time and consistently yielded poor scores in the last approach, thereby reducing the number of calculations and the calculation time needed.

Yet, the combinations of all molecules multiplied by the different weighting and stabilization methods would be far too many with the 20 molecules, resulting in 26,214,375 calculations (1,048,575 × 25). However, as noted with the optimization, the most effective combinations are up to 6 molecules each. Using combinatorial methods to draw 1 to 6 molecules from the total makes the calculation feasible with only 1,511,475 (60,459 × 25). Running it in parallel on 60 threads, a calculation speed of around 4,500 combinations per hour could be achieved, requiring 14 days to complete all calculations, a similar duration to the 11 runs of the optimization approach, yet processing 360 times more combinations.

$$
\begin{aligned}
C(n,r) &= \binom{n}{r} = \frac{n!}{r!(n-r)!} \\
\sum_{r=1}^{20} \binom{20}{r} &= \sum_{r=1}^{20} \frac{20!}{r!(20-r)!} = 2^{20} - 1 = 1,048,575 \\
\sum_{r=1}^{6} \binom{20}{r} &= \sum_{r=1}^{6} \frac{20!}{r!(20-r)!} = 60,459
\end{aligned}
\tag{4.2}
$$

All 1.5 million combinations were calculated to obtain a more comprehensive result regarding the combinations and their normalization effect.

Once again, the various weighting methods seem comparable to one another. Log2 yields both the lowest and the highest scores, while overall remaining similar to the other methods. Sqrt performs slightly better on average. Rank2 shows the same performance as the non-weighted method, and both methods rank the lowest, suggesting that weighting enhances normalization and that the Rank2 method performs the same as doing no weighting at all (Figure 4.17).
The various variance stabilization methods seem to be partially comparable to one another. VSN yields both the best and worst results, and post-VSN is similar to the non-stabilized method, with both performing better than the others, indicating that stabilization is not necessary for these molecules (Figure 4.17).
All the different molecules behave very similarly, with none performing better than the others. Only cis-urocanic acid shows slight improvement over the rest. Additionally, the control molecules, serine and glycine, did not perform worse, contrary to expectations. However, if their abundance remains constant and does not change with increasing concentration, they likely have little impact on the normalization process and may only contribute minor additional stabilization. Moreover, all the least effective combinations arise from the Log2 and VSN combinations again (Figure 4.17).

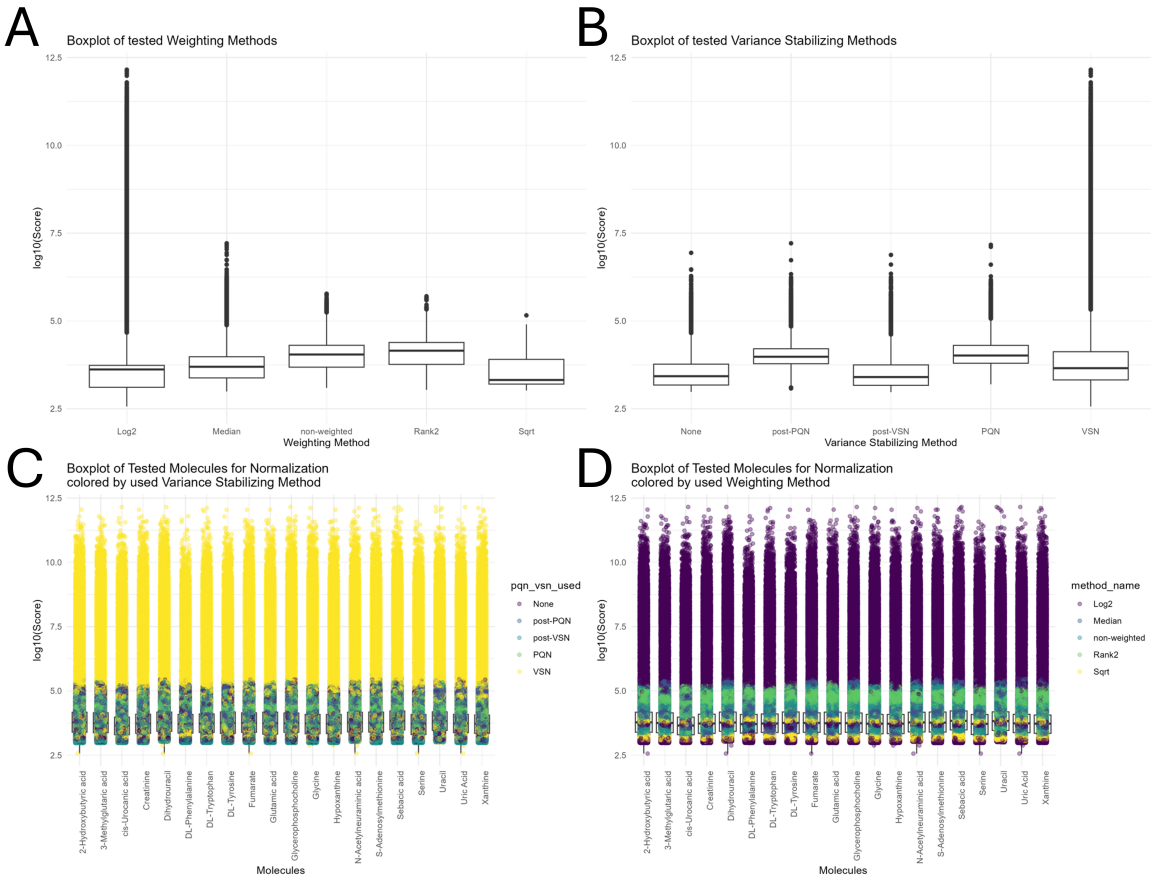

Figure 4.18 – Complete overview of all combinatorial combinations (1-6 out of 20) from the wine study, illustrated using boxplots. A) Overview of tested weighting methods, B) Overview of tested variance-stabilizing methods, C) Overview of tested normalization molecules, colored by variance-stabilizing methods, D) Overview of tested normalization molecules, colored by weighting methods.

All the chosen molecules have undergone several evaluation steps and filters. They all show relatively similar performance, and the variance stabilization methods do not seem necessary. However, some weighting methods improve the normalization. The question now is whether the selection of the molecules has been biased in any way. The raw curves themselves already appear quite good, and the current normalization methods seem to stabilize them rather than truly normalize the data. This is not bad *per se*, but it does not achieve the intended effect.

The next step involved selecting random molecules from the available dataset with qualities similar to those of the currently selected molecules. After processing the data, it was found that 2,999 of the 6,796 total features contained a SIRIUS annotation, which signifies the presence of MS/MS (MS2) spectra for these features. By design, the method used for acquiring MS2 data tends to select only the most highly abundant features for fragmentation and annotation. Consequently, these 2,999 features should represent the most abundant metabolites in the dataset, making them less susceptible to random fluctuations. From this set, 15 features were randomly selected using the *sample* function in *R*, with the seed set to 456 (Appendix Table 5.10).

These 15 randomly chosen molecules were used to run the next calculation round. Again, this was a brute-force approach with the same calculation setting as the previous run with the 20 selected and filtered down molecules, and it also used a combinatorial approach by taking all possible combinations with 1 to 6 molecules.

Log2 yields the best results for the weighting methods, with Sqrt performing similarly but slightly worse on average. Rank2 and Median demonstrate performance comparable to the non-weighted method, with Median exhibiting the best minimum of all. This suggests that weighting enhances normalization and that the Rank2 method performs similarly to using no weighting, thus supporting the previous calculations. Compared to the selected molecule calculations, the variance for the Median, Rank2, and non-weighting increased, remained similar for Rank2, and improved for Log2 (Figure 4.21).

The different variance stabilization methods appear somewhat comparable to each other once more. VSN and post-VSN are akin to the non-stabilized technique, outperforming the PQN variants. However, VSN exhibits the poorest combinations, while PQN shows the best minima. This further suggests that stabilization does not enhance the curve fits for the finger sweat method. Compared to the selected molecule calculations, the variance increased for all methods (Figure 4.21).

All the different molecules behave very similarly, only one molecule has significantly higher scores. Compared to the selected molecule calculations, the variance increased for all molecules, the average scores are similar, and the best and worst scores are better for the random molecules. The biggest difference is that the worst combinations are not driven by a VSN+Log2 combination (Figure 4.21).

New results from the Gerner group show that certain molecules exhibit good linearity between their concentration in finger sweat samples and their abundance. Others show no change in response, while most fall somewhere in between. Additional findings indicate that the measured molecules are not solely derived from sweat. Some originate from the skin, and many exist on a spectrum in between. The currently selected molecules do not

seem to originate from sweat but are rather eluted from skin cells. This could lead to a stabilization of the results with a consistent background. However, the goal of normalizing for sweat volume can not be achieved with the current molecules.
The data from the linearity and feature origin experiments (not included in full in this thesis) have been analyzed, and the intersection of these two experiments has been further refined. The linearity experiment produced linearity data for 8576 features, with 1285 showing excellent linearity, while the feature origin experiment identified 259 features that mainly originate from sweat. The log2 abundances before and after stopping sweating with a deodorant containing aluminum were subtracted and referred to here as the mean sweat change. The lower the mean sweat change, the more strictly it originates from sweat. Neither the features demonstrating good linearity nor those primarily originating from sweat showed a significant correlation with retention time, as they are distributed throughout the entire duration of the measurement. The intersection of these two datasets consists of 85 features, which can be identified in both lists. These features already had an excellent linearity with an R^2 greater than 0.99. They were further filtered to include only those strictly originating from sweat, with an annotation confidence greater than 0.2. This resulted in 23 features, which were manually checked in *Skyline* for the wine study dataset and were further reduced to 15 consistently found features with well-defined peak shapes and not filtered out by *mzMine*. The filtered intersecting features are distributed over the whole retention time range and have an R^2 above 0.994 (Figure 4.19, Appendix Table 5.11).

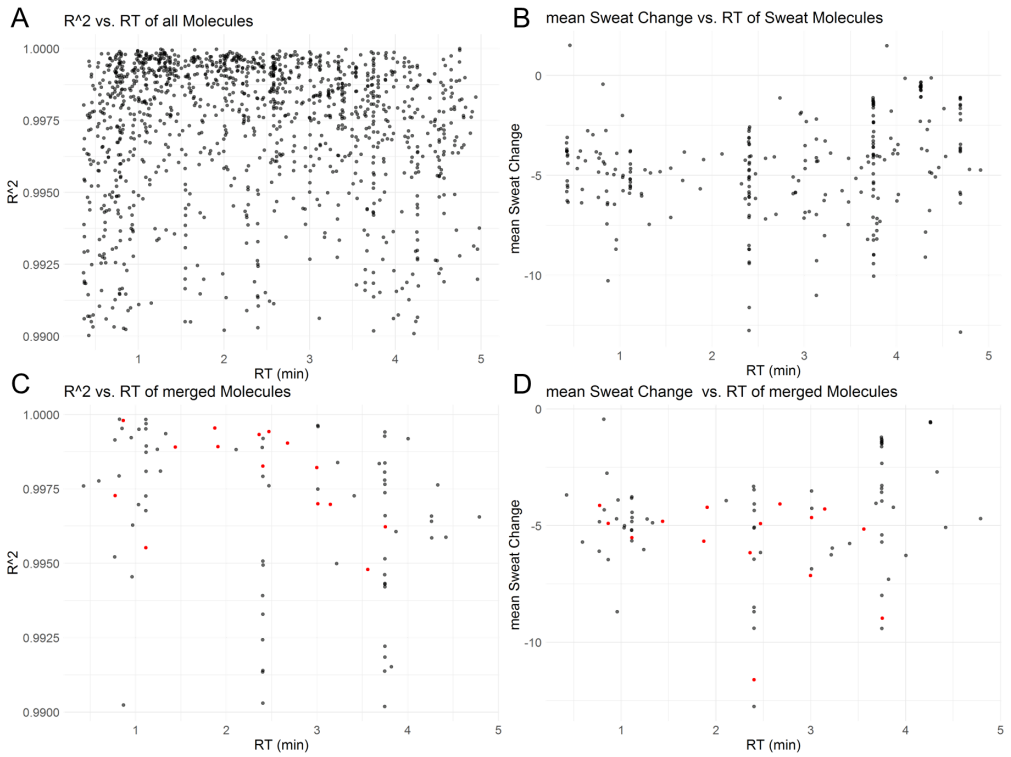

Figure 4.19 – Overview of the linearity and origin datasets and the 85 intersecting features. The features marked in red are the 15 remaining features after filtering. A) Distribution of the features with good linearity, B) Distribution of the features mostly originating from sweat, C) Distribution of the merged features, D) Distribution of the merged features.

To include a negative control for the scoring calculation common contamination's were tested. For this a similar filtering process to the linear sweat features was applied. The linear feature dataset was used again, with a slightly less stringent dataset of 1463 features showing excellent linearity. The deadorant experiment also identified 542 common features mainly originating from contamination occurring during sample preparation. For the features mainly derived from contamination, a group of only 25 molecules has a retention time smaller than 1 minute. Most contamination features elute relatively late, with 407 out of the 542 features eluting after 3 minutes. The intersection of these two datasets consists of 48 features, which can be identified in both lists. These features already had an excellent linearity with an R^2 greater than 0.99. They were further filtered to include only those mainly originating as contamination and needed a logFC greater than 8, an adjusted p-value less than 0.01, and an annotation confidence of more than 0.2. This resulted in 23 features, which were manually checked in Skyline for the wine study dataset and were further reduced to 11 consistently found features with well-defined peak shapes and not filtered out by mzMine. The filtered intersecting features all have a retention time exceeding 3.3 minutes. The filtered contamination features also include some in-source fragments of the same molecule and show rather similar properties (Figure 4.20, Appendix Table 5.12).

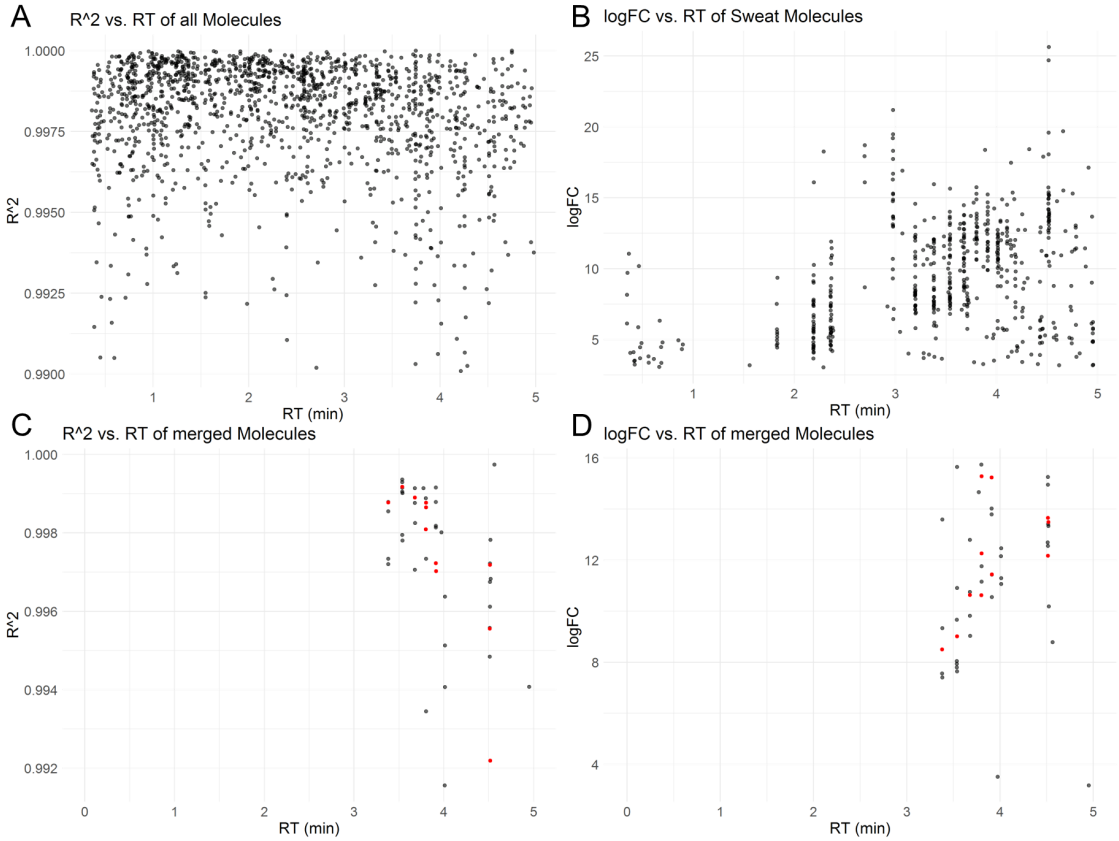

Figure 4.20 – Overview of the linearity and contamination datasets and the 48 intersecting features. The features marked in red are the 11 remaining features after filtering. A) Distribution of the features with good linearity, B) Distribution of the features mostly originating from contamination, C) Distribution of the merged features and the 11 filtered ones in red, D) Distribution of the merged features and the 11 filtered ones in red.

The average scores for the linear sweat features were found to be similar to those of both the selected and random feature sets. Among the weighting methods tested, Log2 and Sqrt transformations produced the most favorable outcomes. The Rank2 and Median weighting approaches demonstrated performances comparable to the non-weighted method, with Median showing a slight advantage. These findings are consistent with previous calculations. When compared to the selected molecule and random molecule results, most weighting methods yielded slightly lower scores for the linear sweat features, with only Log2 and Rank2 showing improved average performance (Figure 4.21).

Application of various variance stabilization methods tended to result in slightly poorer results on average than when using unstabilized data. In particular, VSN produced the weakest combinations, while post-VSN combinations provided the best minima. These observations further support earlier results, indicating that stabilization does not enhance curve fitting for the finger sweat method. The observed variance for linear sweat features was consistent with that of the random features across all methods (Figure 4.21).

The behavior of different linear sweat molecules resembled that of the random molecules, with both generally performing slightly worse than the selected molecules. For linear sweat molecules, increased variance and lower average scores were observed compared to the selected molecules. However, the best scores were similar across groups. Notably, the worst-case results for the sweat features remained better than those of the selected molecules, and the previously noted tendency for the VSN+Log2 combination to produce the lowest scores did not reappear (Figure 4.21).

For linear contamination features, higher average scores were observed compared to the other feature sets, with Log2 and Sqrt transformations again producing the best results among the weighting methods. The Rank2 and Median approaches performed similarly to the non-weighted method. Compared to all other tested molecules, worse scores were found with the contamination features, which is considered a positive indication. Since contamination should not directly correlate with sweat volume or sample amount, the poorer results help to confirm that the method appropriately identifies effective normalization combinations (Figure 4.21).

The results for the linear contamination features have a higher average score overall than the other tested features, with Log2 and Sqrt yielding the best results for the weighting methods on average. Rank2 and Median demonstrate performance comparable to the non-weighted method. Compared to all other tested molecule calculations, the results for all weighting methods worsened. This is excellent, as it shows that contamination, which should have no direct correlation to sweat volume and sample amount, therefore produces worse scores, highlighting the effectiveness of the method in identifying true normalization combinations (4.21).

Variance stabilization techniques for contamination features offered no improvements. On average, these methods performed worse than previous calculations and were associated with increased variance (Figure 4.21).

All linear contamination molecules displayed similar behavior and, overall, performed worse than any other tested group of molecules. Only one random molecule performed comparably, possibly related to contamination, suggesting that biological features from sweat, skin, or external sources can be distinguished. For the contamination molecules,

increased variance and higher average scores were observed in comparison to prior calculations. However, the best scores were similar, and the worst scores were, in fact, better than those recorded for the selected molecules. The highest scores for contamination features occurred mainly with the VSN+Log2 method (Figure 4.21).

The most recent results are consistent with earlier findings. Both Log2 and Sqrt weighting methods continue to show potential for improving normalization, while Median weighting provides more modest benefits. Stabilization methods produce results similar to those obtained without stabilization, and the PQN approaches are generally found to underperform compared to the non-stabilized combinations. Across all tested groups, individual molecules exhibit comparable performance within their respective categories.
As anticipated, the linear contamination features display substantially poorer outcomes than any other group. Also, the linear sweat features yield slightly higher average scores than the selected molecules, which was not expected. It had been hypothesized that sweat-derived features would offer better curve fits. This unexpected trend may result from several factors: improved clustering or the use of significant features may have artificially raised the scores for the selected group, stabilization may be more effective for these particular curves than projected, or the two-compartment Bateman function may inadequately represent the finger sweat compartment, influencing the results in favor of the selected features.
Furthermore, the data suggest that bioactive features can be reliably distinguished from contaminants, and, to a lesser extent, features originating from sweat can be separated from those derived from skin by their overall scores. However, numerous aspects of the normalization process remain poorly understood, making it difficult to establish a definitive normalization strategy that performs optimally across all experimental conditions and studies.

At the very least, the bias in the score composition can be verified to some extent by using the individual parameters to score only the curve fit, relying solely on the curve fitting error of the normalized curve and the correction factor.
Implementing and plotting the new curve score reveals no significant difference between the total score and the curve score. The results exhibit only slight variations in scale, but the overall conclusion remains unchanged. Therefore, the scoring bias can be disproven (Figure 4.22).

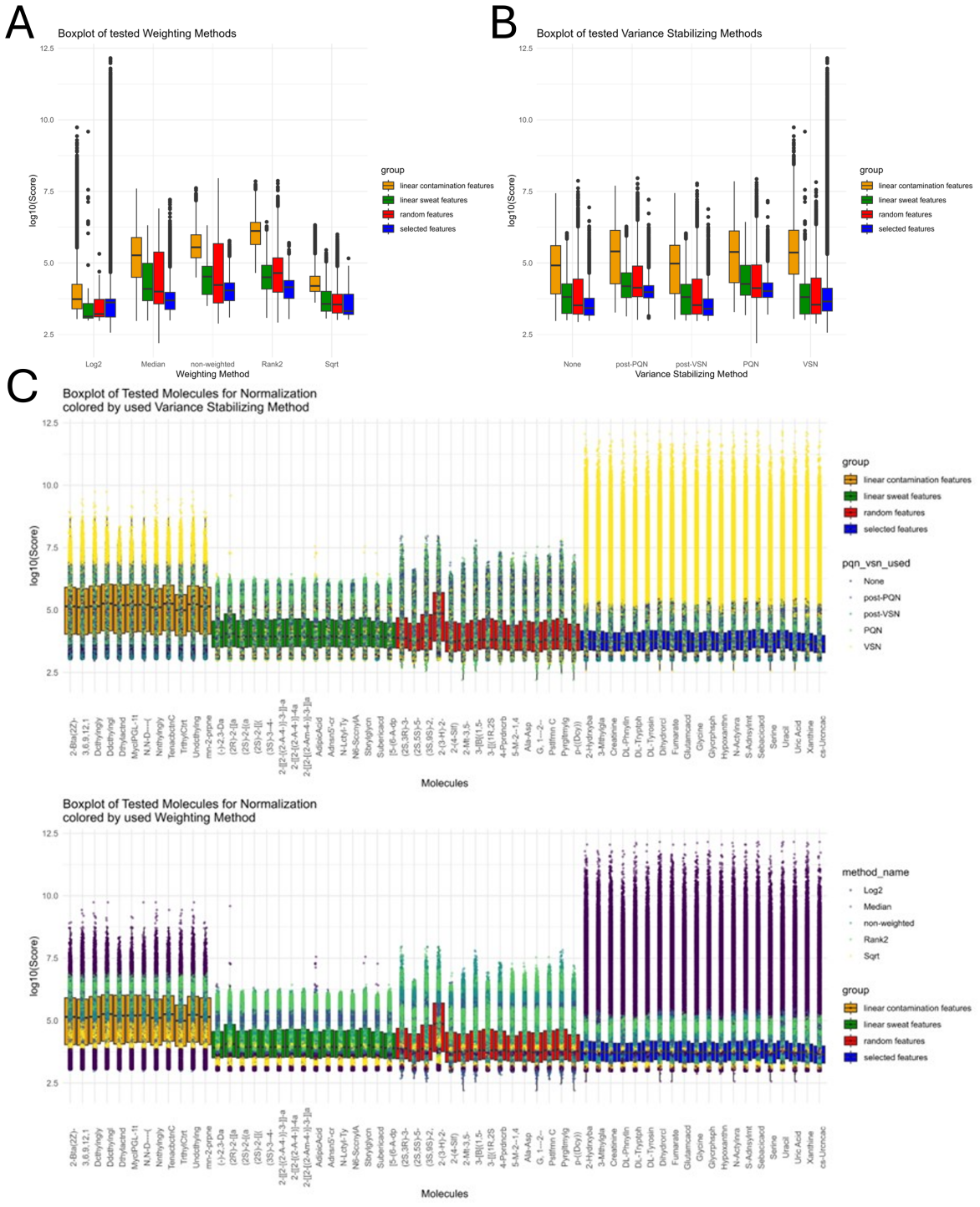

Figure 4.21 – Complete overview of all combinatorial combinations for all the different performed calculations from the wine study, illustrated using boxplots. The 20 selected molecules are in blue (selected features), the 15 random molecules are in red (random features), the 15 linear sweat features are in green (linear sweat features), and the 11 linear common contamination samples are in orange (linear contamination features). A) Overview of tested weighting methods, B) Overview of tested variance-stabilizing methods, C) Overview of tested normalization molecules, colored by variance-stabilizing methods, D) Overview of tested normalization molecules, colored by weighting methods.

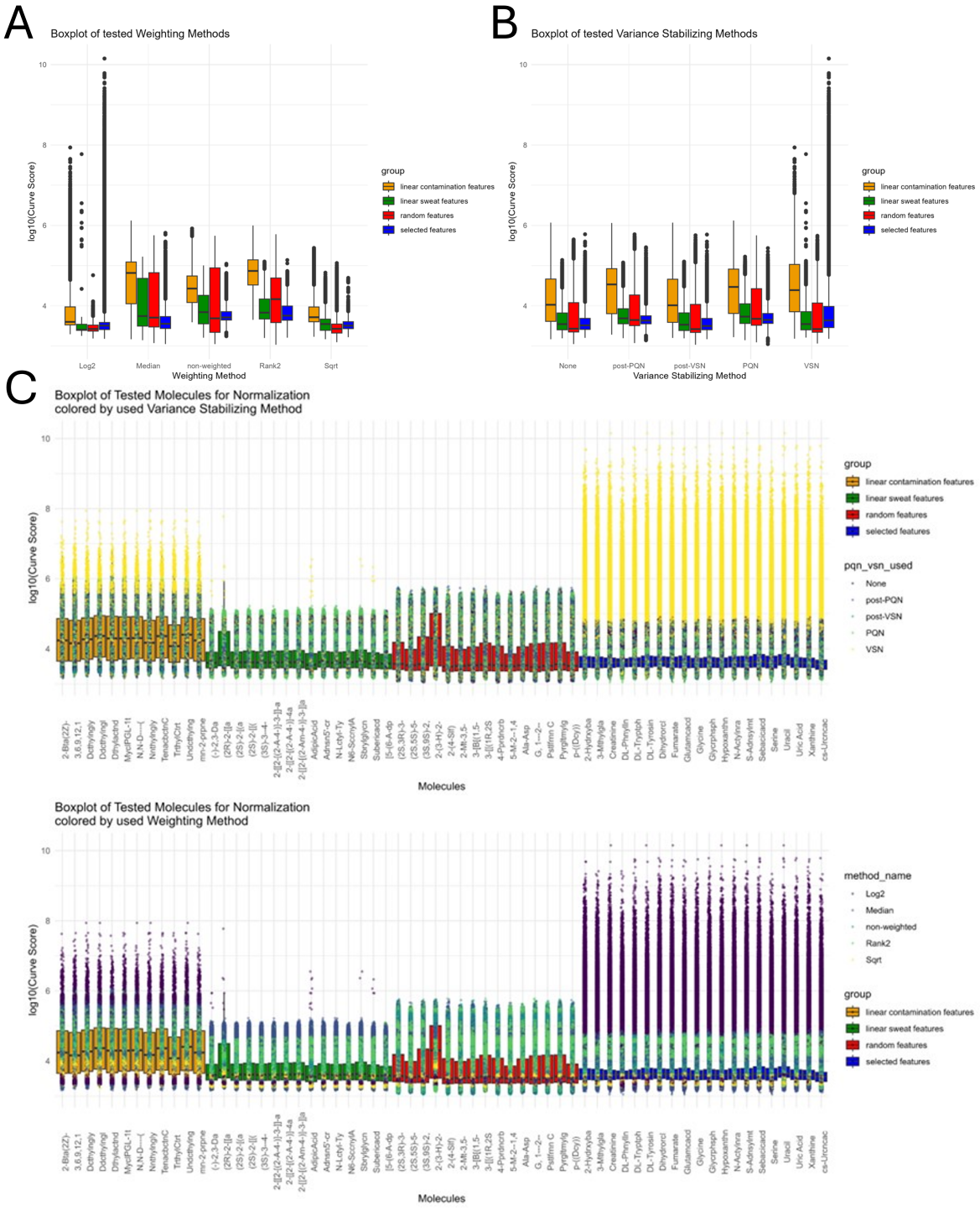

Figure 4.22 – Complete overview of all combinatorial combinations for all the different performed calculations from the wine study, compared by curve score, illustrated using boxplots. The 20 selected molecules are in blue (selected features), the 15 random molecules are in red (random features), the 15 linear sweat features are in green (linear sweat features), and the 11 linear common contamination samples are in orange (linear contamination features). A) Overview of tested weighting methods, B) Overview of tested variance-stabilizing methods, C) Overview of tested normalization molecules, colored by variance-stabilizing methods, D) Overview of tested normalization molecules, colored by weighting methods.

The previous tests first selected molecules based on various calculations and parameters. Then, random molecules from the dataset were chosen for comparison to assess differences, which were expected to perform worse. Lastly, features that elute from sweat itself and exhibit good linearity in the measurements were also tested, with an expectation of better performance than the others. As well as linear common contamination's, which performed worse in average to the others. However, all these molecules behaved quite similarly, and it was difficult to determine which results were mere coincidences and random occurrences of statistical probability resulting from multitesting.
To evaluate the performance of pure random values in the calculation, 15 imaginary features were created, and random values ranging from 10^3 to 10^8 were generated for all samples, as this range is expected for the abundance values in the dataset.

The results for the pure random features look quite different from the previous calculations, with only Log2 performing similarly and showing good results. All the other weighting methods perform significantly worse compared to the true features. This indicates that while Log2 provides effective weighting, it might be too effective, removing valuable information yet still yielding good scores. The curve fit does not deteriorate, and since the raw curve is already quite good, the loss of information results in a decent score. This suggests that Log2 is unsuitable for use in a normalization combination. Also, for Sqrt the best pure random combinations perform better than all others, even if on average it performs worse, indication that it is unsuitable as well (Figure 4.23). The molecules were plotted against the pure curve scores to test for potential bias in the scoring. The average of the true features (selected, sweat, and random) improved slightly. In contrast, the random values remained the same (Appendix Figure 5.21).
All variance stabilization methods performed significantly worse when applied to purely random values, as expected, since these approaches are not intended to operate effectively on randomly distributed data. The stabilized results are nearly indistinguishable from those obtained without stabilization. Although variance stabilization has not yielded notable improvements in overall scores, it may still contribute to greater robustness of the normalization process by decreasing sensitivity to outliers or technical variation—effects that are not reflected in the scoring metric (Figure 4.23).
All the different random values behave very similarly, as expected, and are on average significantly worse than all the other tested features before. Compared to the other calculations, the variance increased, yet was comparable to the linear contamination features (Figure 4.23).

The conclusions can now be adapted because Log2 and Sqrt are clearly unsuitable as a weighting method. The variance stabilization does not improve the scores, but could still help in enhance the method's robustness, which is not reflected in the scores and would need testing over diverse datasets. Additionally, it can be demonstrated that features selected using different criteria can indeed improve the scores. Nevertheless, the raw data itself is already better than expected, and sometimes the wrong combinations can worsen the score. On the other hand, the right combination of methods could aid in improving the analysis of finger sweat data and make it more robust.

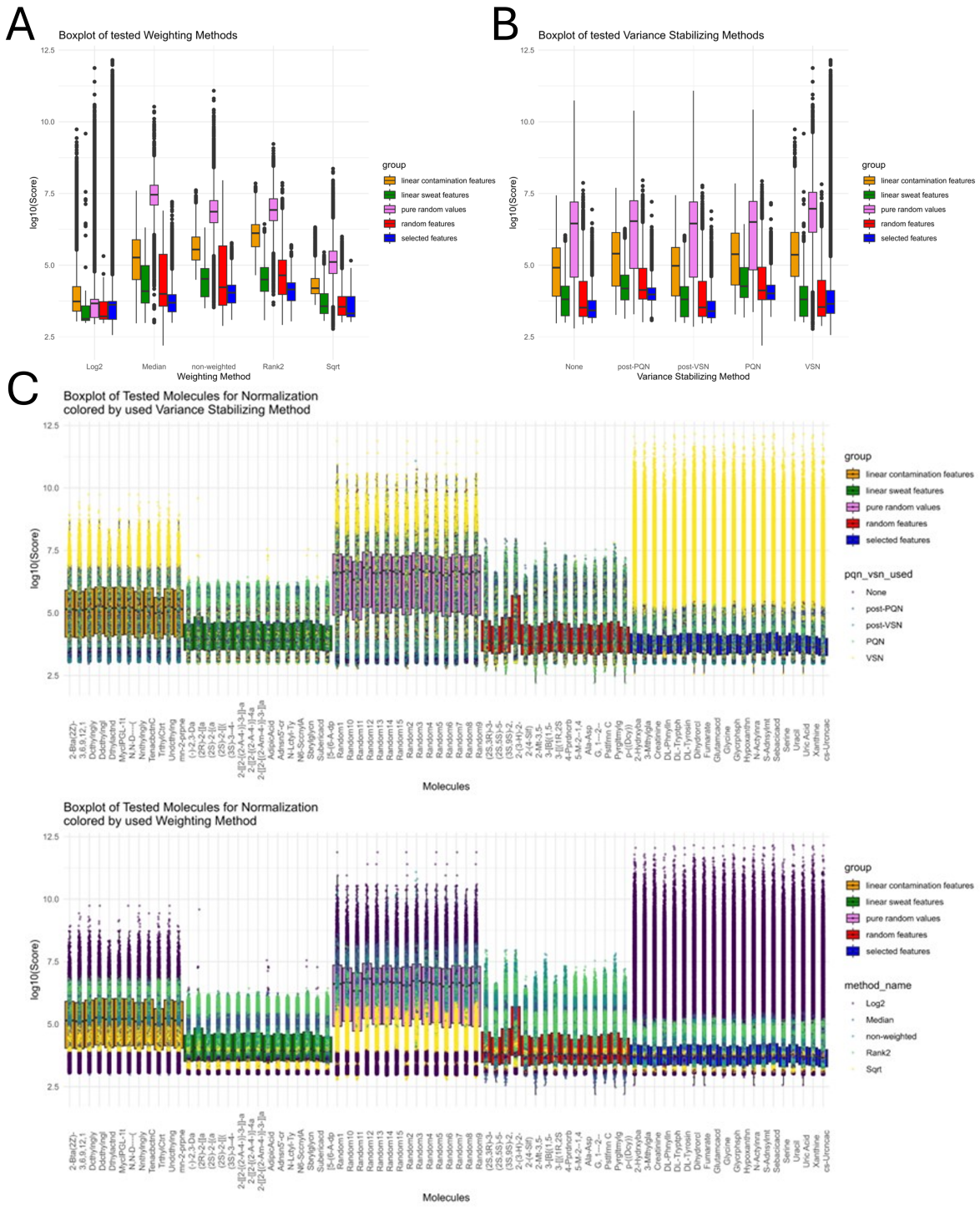

Figure 4.23 – Complete overview of all combinatorial combinations for all the different performed calculations from the wine study, illustrated using boxplots. The 20 selected molecules are in blue (selected features), the 15 random molecules are in red (random features), the 15 linear sweat features are in green (linear sweat features), and the 11 linear common contamination samples are in orange (linear contamination features), and the 15 purely random values are in violet (pure random values). A) Overview of tested weighting methods, B) Overview of tested variance-stabilizing methods, C) Overview of tested normalization molecules, colored by variance-stabilizing methods, D) Overview of tested normalization molecules, colored by weighting methods.

So to get a more correct view of the normalization properties of the different molecules the unsuitable methods need to be filtered out. So Log2 and Sqrt get removed as weighting methods and only post-VSN is used as a variance stabilization method as it performs best, also only combinations with 2 to 6 molecules are used.
For the filtered combinations, the weighting methods seem quite similar, with Median performing best overall, with the lowest average score for the various normalization molecules and the highest scored for the pure random data (Figure 4.24).
For the filtered combinations, the difference between the various molecules got bigger, with phenylalanine now showing the smallest variance overall, and cis-urocanic acid performing the best overall. Also the best combinations of the pure random molecules never reach the same minimum scores as the other molecules which shows that the method is working, as random values do not get good scores. Also there is a clear difference between the selected molecules, which mostly derive from the skin and the features which derive from sweat. Also most random selected features show a similar average value then the selected features, derived from the skin, except one that performs exactly the same as the the linear contamination features, indicating that features could be classified into bioactive and contamination features with this approach if needed (Figure 4.24, Appendix Figure 5.22 & Figure 5.23).

The best combinations for the wine study can be represented as a molecule network again, now displaying only the filtered combinations: the post-VSN stabilization method, and the non-weighted, Median, and Rank2 weighted combinations. When including all tested datasets (selected molecules, randomly chosen features, linear sweat features, linear contamination features, and random values), and only including combinations that are at most 10% worse than the best found combination, it shows two clusters: the selected molecules and the randomly chosen features, with only the Median weighting method remaining in this selection, highlighting it as the best weighting method. When further selecting to include only the combinations worse than 5% of the best combination, only randomly selected features remain (Figure 4.25).
If selecting only the selected molecules and examining the combinations where scores are 10% and 5%, it shows that the best combinations consistently include glutamic acid and tyrosine, and sometimes include glycine, alongside other molecules that typically form groups, such as tryptophan with creatinine, uracil and cis-urocanic acid, or 3-methylglutaric acid, uric acid, hypoxanthine, and xanthine, or S-Adenosylmethionine. Therefore, there appears to be no definitive optimal combination or molecule for a universal normalization, but rather groups of molecule classes with different properties. The common ground among all these molecules is that they are relatively small and possess good to moderate solubility while being biologically active in some metabolic way (Figure 4.25).
The best combinations of the random molecules also demonstrate a variety of solubilities ranging from high to moderate and exhibit diverse structures, including small peptides, acids, and aromatic groups. However, it cannot be determined if some of these may be contaminants, as most do not originate from human metabolism but could still be exogenous molecules from the diet (Figure 4.25).

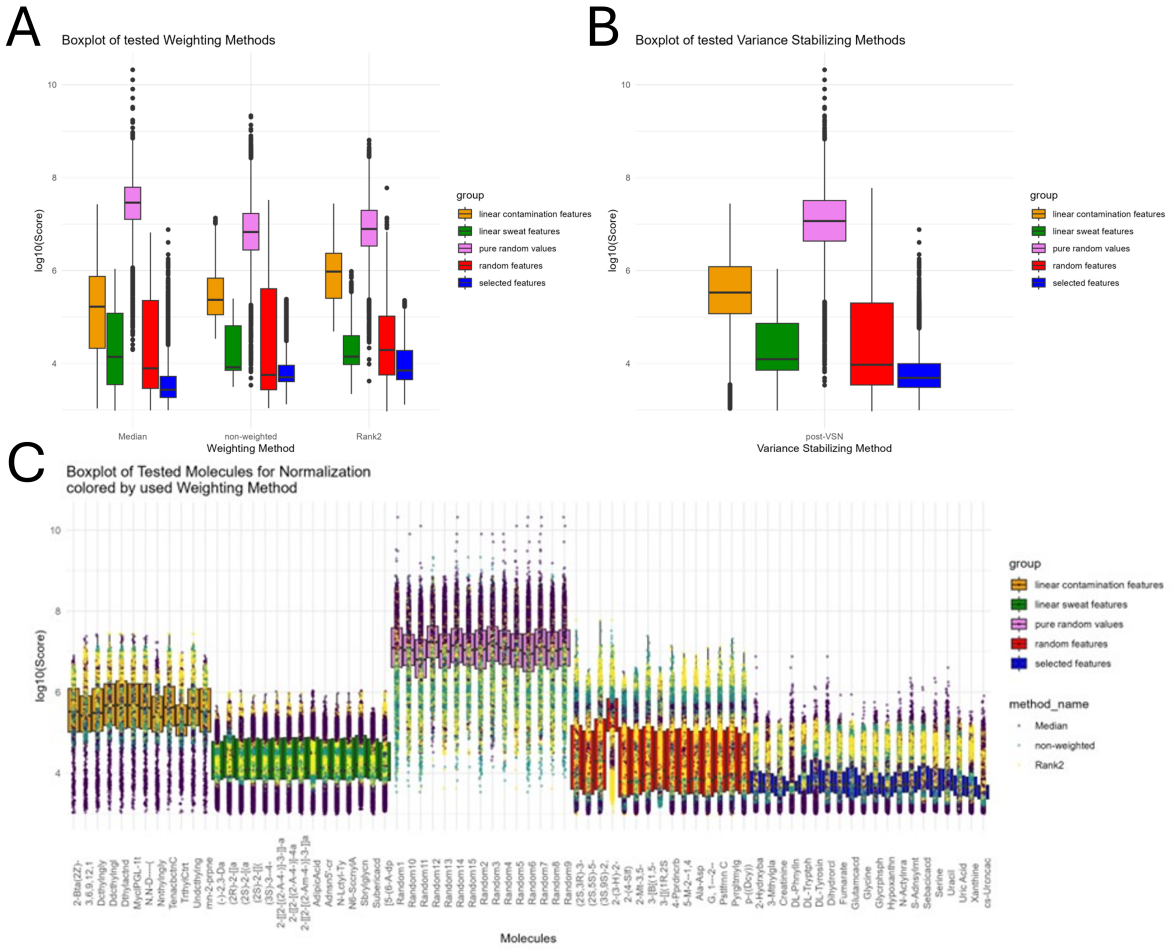

Figure 4.24 – Complete overview of all combinatorial combinations for all the filtered calculations from the wine study, illustrated using boxplots. The 20 selected molecules are in blue (selected features), the 15 random molecules are in red (random features), the 15 linear sweat features are in green (linear sweat features), and the 11 linear common contamination samples are in orange (linear contamination features), and the 15 purely random values are in violet (pure random values). A) Overview of tested weighting methods, B) Overview of the tested variance-stabilizing method, C) Overview of tested normalization molecules, colored by weighting methods.

The most effective normalization strategies are consistently found to rely on a core set of stable molecules, complemented by various bioactive small molecules with moderate to high solubility. In the wine study, the highest-performing combinations consistently involve the use of post-VSN variance stabilization alongside the Median weighting method.

Among the selected molecules, the top normalization combinations offer similar improvements, including slightly enhanced curve fitting, improved clustering, reduced standard deviation for the corr_factors, and a modest reduction in the number of significant features detected. These optimal groups typically feature a stable core of molecules with varying additional components, such as "glutamic acid + tyrosine + tryptophan + cis-urocanic acid + creatinine + uracil," "tyrosine + glutamic acid + 3-methylglutaric acid + uric acid + hypoxanthine + xanthine," or "glutamic acid + tyrosine + S-adenosylmethionine + glycine."

A similar pattern is observed for the highest-ranking combinations involving linear sweat molecules. While some of these demonstrate slightly poorer curve fit scores, they then are associated with an increased number of significant features. Here as well, a stable core, primarily lactoyl-tyrosine and adenosine 5'-carboxamide, is observed, with two distinct groups of supplementary molecules forming complete normalization sets.

This outcome is biologically plausible, as many of these molecules are central to primary metabolism and subject to tight regulatory control. This likely enables them to effectively compensate for sample matrix variability and technical variation. It should also be noted that, within each dataset, the identified normalization groups span a wide range of retention times and molecular classes, suggesting broad representativity among the selected features.

The molecules from both the selected and linear sweat features were further filtered by retaining only those appearing in the top combinations, ultimately resulting in 10 selected features and 11 linear sweat features (see Table 5.13). These represent compounds derived from skin extract and sweat, and could provide advantageous normalization combinations. As such, they were also examined using the wine study data with the combinatorial brute-force approach. For this analysis, only post-VSN stabilization and Median weighting were utilized, as these methods previously demonstrated the best performance. Combinations containing up to eight different molecules were evaluated.

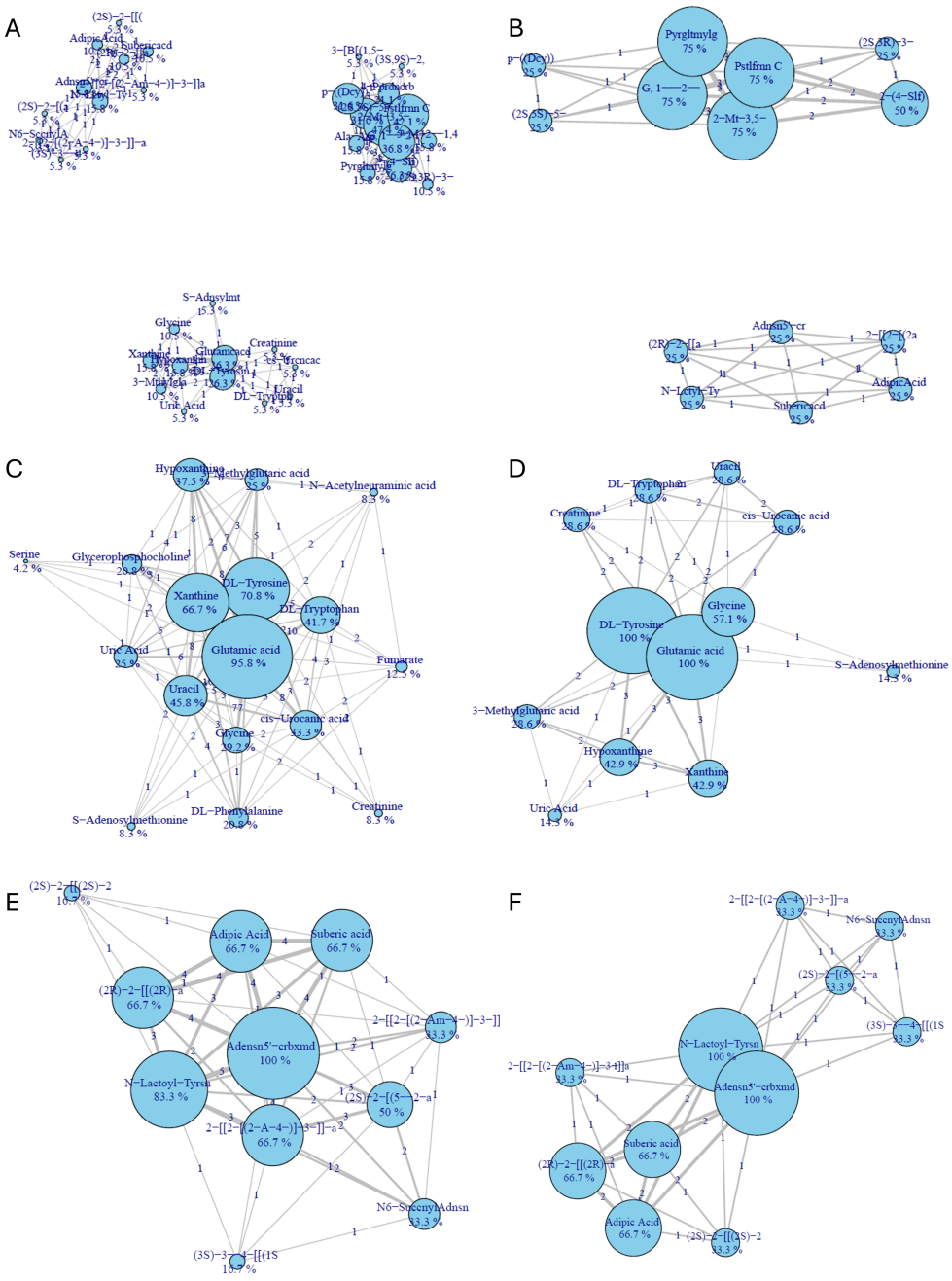

Figure 4.25 – Co-occurrence networks of all the sampled molecule groups and the filtered methods, exploring the best normalization combinations of the wine study using a brute-force approach. A) Top combinations with a score only 10% bigger than the best found combination, B) Top combinations with a score only 5% bigger than the best found combination, C) Top combinations of of the selected molecule combinations with a score only 10% bigger than the best found combination, D) Top combinations of of the selected molecule combinations with a score only 5% bigger than the best found combination, E) Top combinations of of the linear sweat molecule combinations with a score only 10% bigger than the best found combination, F) Top combinations of of the linear sweat molecule combinations with a score only 5% bigger than the best found combination.

Distinct patterns emerged for the different molecules. Most linear sweat features exhibited similar performance, with comparable average scores but high variance. In contrast, the selected molecules displayed both lower average scores and lower variance. Notably, uracil performed worse than other selected molecules, aligning more closely with the majority of sweat features, whereas adipic acid's performance was similar to that of the selected features. These findings suggest which molecules might be most effective within normalization combinations. The curve score largely mirrored these results, with only slight differences observed in the minimal scores.

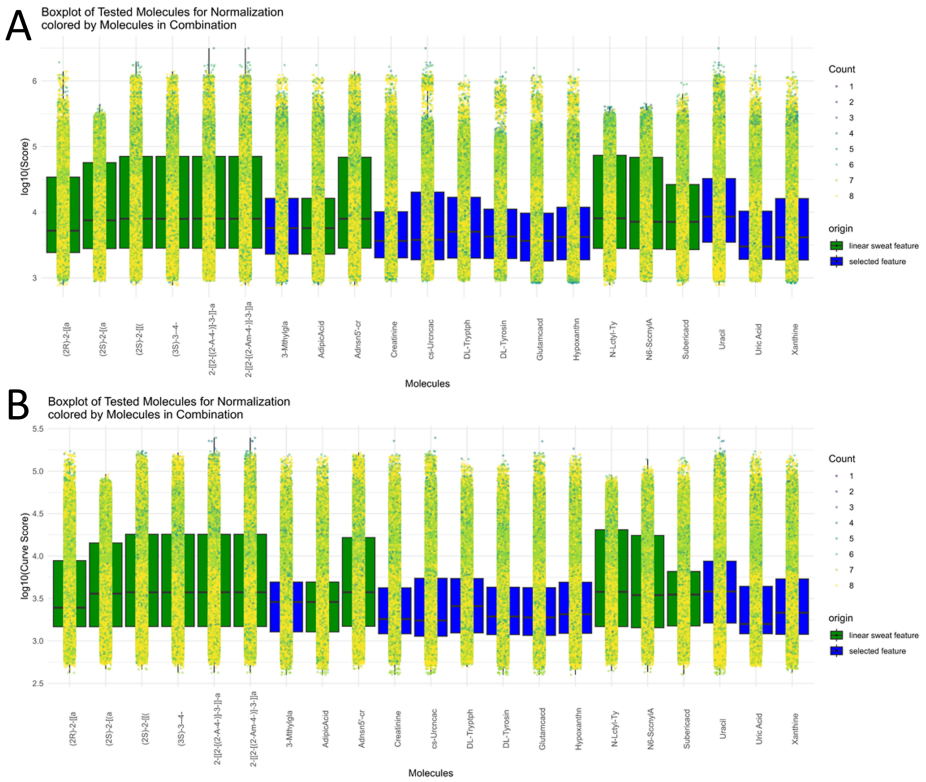

Figure 4.26 – Complete overview of all combinatorial combinations for all the calculations from the wine study, illustrated using boxplots. The 10 best selected molecules are in blue (selected features), and the 11 best linear sweat features are in green (linear sweat features). A) Overview of tested normalization molecules, colored by weighting methods, B) Overview of tested normalization molecules, scored by curve score, colored by weighting methods.

When examining the molecule networks within the best-performing combinations, certain selected features, such as glutamic acid, xanthine, and hypoxanthine, consistently contributed to strong performance, confirming earlier results. Interestingly, among combinations containing eight molecules, those composed predominantly of sweat features achieved the highest total scores. However, with respect to the curve score, selected molecules yielded better results within the combinations. The superior performance of sweat feature combinations in the total score is attributable to an increase in the number of significant features after normalization, whereas selected features did not alter this number. Furthermore, in combinations containing seven or fewer molecules, the top-performing sets generally consisted of five molecules—including the stable core of glutamic

acid, xanthine, and hypoxanthine. For combinations of up to eight molecules, additional selected molecules such as creatinine, tyrosine, uracil, and cis-urocanic acid frequently appeared in the most successful combinations.

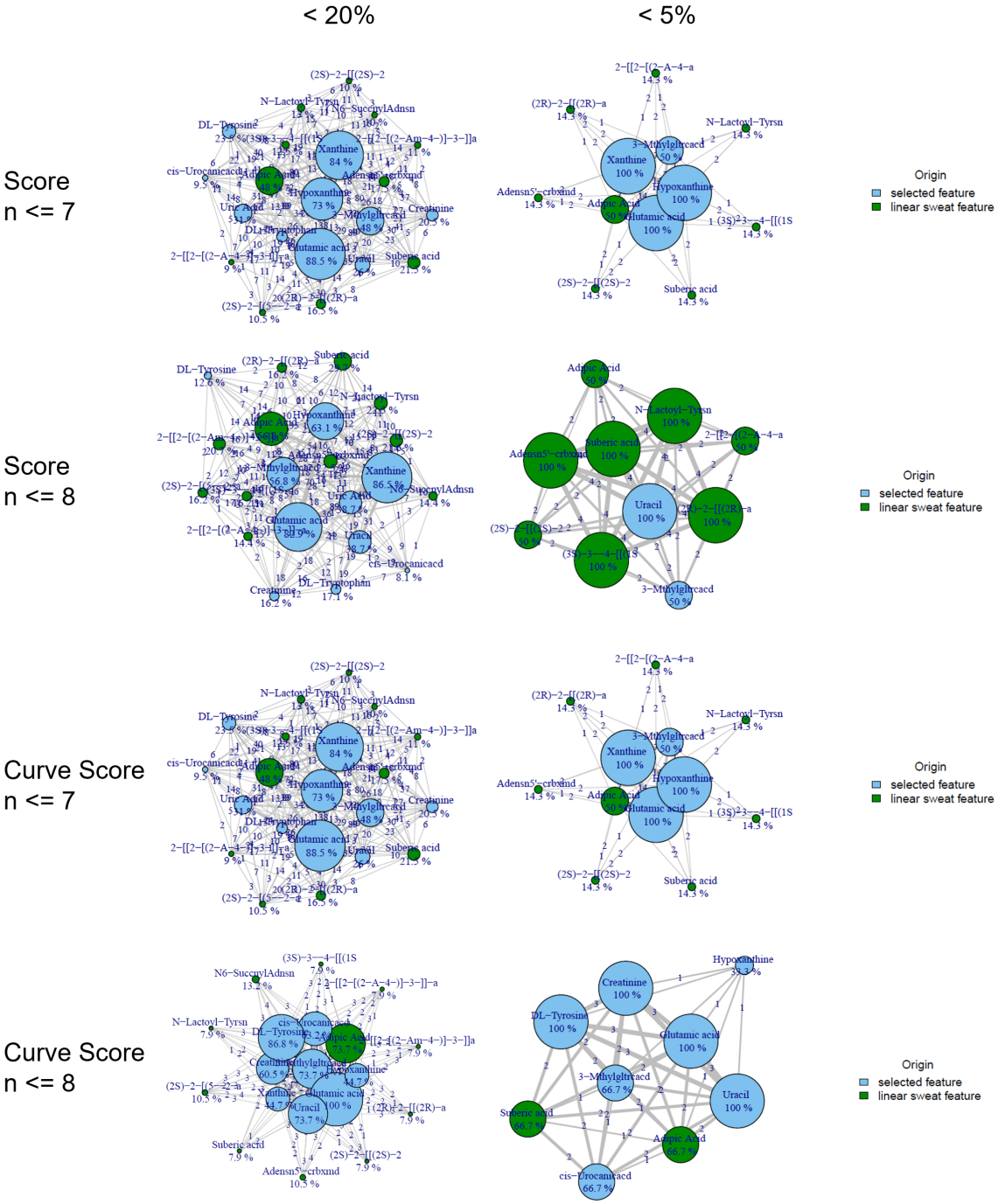

Figure 4.27 – Co-occurrence networks of the 10 best selected molecules in blue (selected features), and the 11 best linear sweat features in green (linear sweat features), exploring the best normalization combinations of the wine study using a brute-force approach. Showing various different variations, like the top combinations with up to 7 or 8 molecules with either a score or curve score only 20% or 5% bigger than the best found combination.

5 | Conclusion and Outlook

Developing a robust and transferable normalization method for finger sweat metabolomics has revealed both the potential and complexity of this non-invasive biofluid. What appears, at first, as a simple matrix is in fact a complex interplay of biological variability, sampling artifacts, and matrix effects, all superimposed on a chemical landscape shaped by the dynamic interaction of sweat and skin constituents. While it gradually unravels throughout this thesis, it does so sometimes alongside the thesis itself and other times through the latest experiments related to this biological matrix, there are still many unknowns.

With all the insights gained from this thesis and the discussion with the Gerner group, I propose a hypothesis that aims to describe the finger sweat matrix more comprehensively to better understand our method. Some challenges arise from the composition of the matrix and the origin of its features, derived from active sweat and dermal skin, which have different underlying kinetics. Other challenges stem from the LC-MS method, including differences in ionization among various features and issues like ion suppression.

The total abundance of features (TA) is composed of a specific ratio between the occurrence of features derived from sweat at a particular concentration (C_{sweat}) and from the skin (C_{skin}). These features may originate entirely from one source or lie somewhere on a spectrum between the two, illustrated by a matrix that depicts the ratios. Furthermore, there is an ionization efficiency (I_{eff}) for each feature, which incorporates competitive interactions among various co-eluting features. Additionally, specific error terms can not be ignored ($e_{\text{sweat}}, e_{\text{skin}}$). The sweat volume ($V_{\text{sweat}}$) solely affects the features derived from sweat. However, there exists an overarching parameter that controls the total sample amount (U_{sample}). This includes sampling conditions, such as the type of paper and method used, the sampling duration, and various unknown factors like applied pressure and interpersonal differences.

$$\mathrm{TA} = \left[\left(\begin{pmatrix} 1 \\ 0.97 \\ 0.5 \\ \vdots \\ 0 \end{pmatrix} \odot \mathrm{I}_{\text{eff}} \cdot C_{\text{sweat}} + e_{\text{sweat}} \right) \cdot V_{\text{sweat}} + \left(\begin{pmatrix} 0 \\ 0.03 \\ 0.5 \\ \vdots \\ 1 \end{pmatrix} \odot \mathrm{I}_{\text{eff}} \cdot C_{\text{skin}} + e_{\text{skin}} \right) \right] \cdot U_{\text{sample}} \tag{5.1}$$

The hypothesis itself is simplified again, as a more detailed hypothesis for the total abundance of features (TA) acknowledges that these parameters are interdependent. The ratio between sweat- and skin-derived molecules is a function of sweat volume (V_{sweat}), which itself varies with sampling duration, method, individual physiology, and other conditions included in U_{sample}. The ionization efficiency for each molecule (I_{eff}) is likewise a dynamic quantity, depending not only on the molecule's identity and the LC-MS method, but also on the concentrations of all co-eluting species, leading to competitive ionization and ion suppression effects. Because of these dependencies, a full description of TA requires a system of coupled and possibly differential equations, reflecting how the variables influence each other during sampling and analysis.

Here, g_1 and g_2 are functions that describe the kinetics of sweat-derived and skin-derived concentrations, respectively, depending on sampling rate, sweat volume, sample collection techniques, intrinsic skin properties, and potential contamination on the skin. The function h characterizes the ionization efficiency, incorporating the effects of the totoal concentrations $[C]$ of all co-eluting molecules, as well as the technical settings of the LC-MS method. Finally, f integrates these variables—including the ratios of feature origins, ionization efficiency, sweat volume, and sampling parameters—into an overall model for the total abundance of features (TA). This function f therefore expresses that the measured signal is not simply a direct sum of its parts but emerges from a complex and interdependent system.

$$\begin{aligned}
\frac{dC_{\text{sweat}}}{dt} &= g_1(\text{sampling rate}, V_{\text{sweat}}, U_{\text{sample}}, \ldots) \\
\frac{dC_{\text{skin}}}{dt} &= g_2(\text{skin properties}, U_{\text{sample}}, \text{potential contaminations}, \ldots) \\
\text{I}_{\text{eff}} &= h([C], \text{method}) \\
\text{TA} &= f(\text{ratios}, \text{I}_{\text{eff}}, V_{\text{sweat}}, U_{\text{sample}}, \ldots)
\end{aligned} \tag{5.2}$$

To rigorously test how robust and transferable different normalization strategies are, multiple datasets were used, varying in experimental setup, measurement technology, and biological background, including several studies on caffeine and wine and samples from a wide variety of individuals. The main goal was to see which normalization methods allow reliable comparisons between and within people, regardless of these differences.

To develop a robust normalization approach for finger sweat samples, this thesis began with a comprehensive list of 66 candidate molecules, selecting and refining them based on consistent detection and low susceptibility to external contamination. This filtering was crucial for establishing normalization approaches on a dependable molecular foundation.

The selected molecules underwent various filtering steps and ultimately generated satisfactory combinations. However, it proved challenging to determine which combinations performed best, as several different combinations exhibited similar performances.

Further exploration of molecules thought to be the main contributors to sweat did not show superior performance compared to others. This highlights the complexity of sweat analysis and the need for a multi-faceted approach that includes a variety of molecules.

Initial attempts to use single molecules or unoptimized combinations quickly demonstrated their limitations. No single compound, even those biologically plausible, could consistently correct for unknown sweat volumes or standardize data between samples and studies. Instead, it became evident that effective normalization requires tailored combinations of molecules combined with an appropriate weighting strategy. Among the tested approaches, median weighting of selected metabolites proved most reliable, while the Log2 method was too aggressive—dampening signals to the point that even random data sometimes appeared "normalized." The Sqrt method performed better but still did not match the consistency and interpretability of the Median method.

Variance stabilization methods such as PQN and VSN were systematically evaluated for their efficacy in stabilizing variance across samples and studies. While these methods do enhance reproducibility and robustness—especially when applied after normalization—they provided limited improvement to pharmacokinetic curve fitting. This underscores that their primary value lies in supporting consistency across experiments rather than in drastically improving within-study normalization or data structure.

Bayesian optimization was applied to efficiently explore a vast parameter space, as testing every possible combination of molecules directly would have been computationally intensive and impractical. By modeling the search process, Bayesian optimization identified promising molecular combinations, streamlining the process of optimizing results. However, a combinatorial brute-force approach, where every possible inclusion or exclusion of molecules was explicitly tested, demonstrated that exhaustive computation can be crucial for comprehensive insight. This was necessary because the optimization task involved discrete choices, a molecule is either included in a combination or not, while Bayesian optimization operates in a continuous search space. This mismatch resulted in a landscape with sharp transitions, where the optimization score could abruptly change and produces broad plateaus of duplicate solutions. Thus, while Bayesian optimization accelerated the search at first, after the molecules were strictly filtered, the finding of the next step was computationally more expensive than just calculating every combination itself.

An important point is that not all features may be normalized using the same strategy. Different methods might be needed depending on the origin of the molecule in the sweat. This origin could be from the dermal extract or the active sweat, or both in varying ratios. Additionally, there is a challenge regarding feature linearity, and non-linear features likely require different methods than linear ones. However, all of this is not yet well understood and needs to be studied in greater depth in the future.

Overall, the results show that there isn't a single "best" molecule or combination for normalizing finger sweat data—rather, the best approach seems to be a group of small, biologically active, and fairly soluble molecules, often including amino acids like glutamic acid and tyrosine, or other bioactive substances in the sweat like lactoyl-tyrosine and adenosine 5'-carboxamide. Strategies such as post-VSN stabilization and Median weighting helped consistently improve results, regardless of the exact combination. There's also a clear difference between bioactive molecules sourced and contaminations, as well as a

slight difference between molecules originating mainly from the skin compared to those from sweat, and this distinction could be helpful in future analyses, perhaps even allowing to classify better where features come from.

In conclusion, while a universal normalization method remains elusive, this thesis examines various finger sweat datasets and studies, proposing the Median weighting method and post-VSN variance stabilization method for future normalization strategies, as these were the most effective in several studies. Glutamic acid with xanthine and hypoxanthine provide a solid foundation for a normalization combination, supported by different molecules or molecular groups that can enhance the combination's performance and robustness.

Additionally, the thesis provides an overview of what to expect from future measurements. The results indicate that the computational method could potentially classify features based on their origin, whether as dermal extracts, from active sweat, or from contamination. Furthermore, it demonstrates that the whole finger sweat method has improved over time, showing poorer results and higher variability in older studies, but providing an excellent basis for the raw results in the latest studies, which often require minimal improvement. Features that exhibit noisy time course data typically have low intensity and show peak integration issues, necessitating even more stringent filters in the future to eliminate those noisy peaks. The normalization combinations still need to prove their transferability to other datasets and require further testing in the latest studies. Moreover, the origins of the features and their linearity need further understanding, as this knowledge could be advantageous since different features may require different strategies.

Bibliography

[1] L. Niu, C. Dang, L. Li, N. Guo, Y. Xu, X. Li, Q. Xu, L. Cheng, L. Zhang, L. Liu, Next-generation sequencing-based identification of EGFR and NOTCH2 complementary mutations in non-small cell lung cancer, *Oncology Letters*, 2021, *22*, 594, DOI 10.3892/ol.2021.12855.

[2] M. L. Dalurzo, A. Avilés-Salas, F. A. Soares, Y. Hou, Y. Li, A. Stroganova, B. Öz, A. Abdillah, H. Wan, Y.-L. Choi, Testing for EGFR mutations and ALK rearrangements in advanced non-small-cell lung cancer: considerations for countries in emerging markets, *OncoTargets and therapy*, 2021, *14*, 4671–4692, DOI 10.2147/OTT.S313669.

[3] A. Pandey, S. P. Gupta, Personalized medicine: a comprehensive review, *Oriental Journal of Chemistry*, 2024, *40*, 933–944, DOI 10.13005/ojc/400403.

[4] S. G. Waghmare, A. N. Z. Khannam, Individualized medicine: revolutionizing healthcare with tailored therapies, *EPRA International Journal of Research & Development*, 2024, *9*, 18–20, DOI 10.36713/epra17655.

[5] T. Bardakjian, P. Gonzalez-Alegre in Handbook of Clinical Neurology, *Vol. 147*, Elsevier, **2018**, pp. 93–102.

[6] M. Dalamaga, Clinical metabolomics: Useful insights, perspectives and challenges, *Metabolism Open*, 2024, *22*, 100290, DOI 10.1016/j.metop.2024.100290.

[7] D. K. Trivedi, K. A. Hollywood, R. Goodacre, Metabolomics for the masses: the future of metabolomics in a personalized world, *New Horizons in Translational Medicine*, 2017, *3*, 294–305, DOI 10.1016/j.nhtm.2017.06.001.

[8] D. Manjusha, V. Prashant, R. Shrirang, Role of metabolomics in advancing precision medicine and personalized nutrition: a systematic review of clinical applications and future prospects, *International Journal of Recent Innovations in Medicine and Clinical Research*, 2024, *6*, 70–75, DOI 10.18231/j.ijrimcr.2024.053.

[9] H. O. Doğan, Metabolomics: a review of liquid chromatography mass spectrometry-based methods and clinical applications, *Turkish Journal of Biochemistry*, 2024, *49*, 1–14, DOI 10.1515/tjb-2023-0095.

[10] K. Shanmugam, An overview of systems biology & metabolomics, *Oncology Treatment Discovery*, 2024, *2*, 37–48, DOI 10.26689/otd.v2i2.6934.

[11] J. Sarkar, R. Singh, S. Chandel, Understanding LC/MS-based metabolomics: a detailed reference for natural product analysis, *PROTEOMICS – Clinical Applications*, 2025, *19*, e202400048, DOI 10.1002/prca.202400048.

[12] R. Chaleckis, I. Meister, P. Zhang, C. E. Wheelock, Challenges, progress and promises of metabolite annotation for LC–MS-based metabolomics, *Current Opinion in Biotechnology*, 2019, *55*, 44–50, DOI 10.1016/j.copbio.2018.07.010.

[13] B. Venkatesh, T. J. Morgan, J. Cohen, Interstitium: the next diagnostic and therapeutic platform in critical illness, *Critical Care Medicine*, 2010, *38*, 630–636, DOI 10.1097/CCM.0b013e3181f24406.

[14] H. Wiig, O. Tenstad, P. O. Iversen, R. Kalluri, R. Bjerkvig, Interstitial fluid: the overlooked component of the tumor microenvironment?, *Fibrogenesis & Tissue Repair*, 2010, *3*, 1–11, DOI 10.1186/1755-1536-3-12.

[15] H. Wiig, M. A. Swartz, Interstitial fluid and lymph formation and transport: physiological regulation and roles in inflammation and cancer, *Physiological Reviews*, 2012, *92*, 1005–1060, DOI 10.1152/physrev.00037.2011.

[16] S. Kim, M. S. Lee, H. S. Yang, J. H. Jung, Enhanced extraction of skin interstitial fluid using a 3D printed device enabling tilted microneedle penetration, *Scientific Reports*, 2021, *11*, 14018, DOI 10.1038/s41598-021-93235-3.

[17] R. H. Stewart, A modern view of the interstitial space in health and disease, *Frontiers in Veterinary Science*, 2020, *7*, 609583, DOI 10.3389/fvets.2020.609583.

[18] N. Theise, Evidence for continuity of interstitial spaces across tissue and organ boundaries in humans, *The FASEB Journal*, 2022, *36*, 666, DOI 10.1096/fasebj.2022.36.S1.0I666.

[19] L. B. Baker, A. S. Wolfe, Physiological mechanisms determining eccrine sweat composition, *European Journal of Applied Physiology*, 2020, *120*, 719–752, DOI 10.1007/s00421-020-04323-7.

[20] J. N. Hussain, N. Mantri, M. M. Cohen, Working up a good sweat – the challenges of standardising sweat collection for metabolomics analysis, *The Clinical Biochemist Reviews*, 2017, *38*, 13–34.

[21] B. A. Katchman, M. Zhu, J. Blain Christen, K. S. Anderson, Eccrine sweat as a biofluid for profiling immune biomarkers, *PROTEOMICS – Clinical Applications*, 2018, *12*, 1800010, DOI 10.1002/prca.201800010.

[22] B. Burat, A. Reynaerts, D. Baiwir, M. Fléron, G. Eppe, T. Leal, G. Mazzucchelli, Characterization of the human eccrine sweat proteome—a focus on the biological variability of individual sweat protein profiles, *International Journal of Molecular Sciences*, 2021, *22*, 10871, DOI 10.3390/ijms221910871.

[23] J. Brunmair, M. Gotsmy, L. Niederstaetter, B. Neuditschko, A. Bileck, A. Slany, M. L. Feuerstein, C. Langbauer, L. Janker, J. Zanghellini, S. M. Meier-Menches, C. Gerner, Finger sweat analysis enables short interval metabolic biomonitoring in humans, *Nature Communications*, 2021, *12*, 5993, DOI 10.1038/s41467-021-26245-4.

[24] M. Bolliger, D. Wasinger, J. Brunmair, G. Hagn, M. Wolf, K. Preindl, B. Reiter, A. Bileck, C. Gerner, F. Fitzal, S. M. Meier-Menches, Mass spectrometry-based analysis of eccrine sweat supports predictive, preventive and personalised medicine in a cohort of breast cancer patients in austria, *EPMA Journal*, 2025, 1–18, DOI 10.1007/s13167-025-00396-6.

[25] E. Marasco, K. Ricanek, H. Le, We are also metabolites: towards understanding the composition of sweat on fingertips via hyperspectral imaging, *Digital*, 2023, *3*, 137–145, DOI 10.3390/digital3020010.

[26] M. Harker, H. Coulson, I. Fairweather, D. Taylor, C. A. Daykin, Study of metabolite composition of eccrine sweat from healthy male and female human subjects by 1H NMR spectroscopy, *Metabolomics*, 2006, *2*, 105–112, DOI 10.1007/s11306-006-0024-4.

[27] K. Kuwayama, K. Tsujikawa, H. Miyaguchi, T. Kanamori, Y. T. Iwata, H. Inoue, Time-course measurements of caffeine and its metabolites extracted from fingertips after coffee intake: a preliminary study for the detection of drugs from fingerprints, *Analytical and Bioanalytical Chemistry*, 2013, *405*, 3945–3952, DOI 10.1007/s00216-012-6569-3.

[28] K. Longman, O. W. Akkerman, S. Ghimire, M. S. Bolhuis, M. A. Chambers, M. G. G. Sturkenboom, M. J. Bailey, Measurement of isoniazid in tuberculosis patients using finger sweat with creatinine normalisation: a controlled administration study, *International Journal of Antimicrobial Agents*, 2024, *64*, 107231, DOI 10.1016/j.ijantimicag.2024.107231.

[29] W. Gao, S. Emaminejad, H. Y. Y. Nyein, S. Challa, K. Chen, A. Peck, H. M. Fahad, H. Ota, H. Shiraki, D. Kiriya, D.-H. Lien, G. A. Brooks, R. W. Davis, A. Javey, Fully integrated wearable sensor arrays for multiplexed in situ perspiration analysis, *Nature*, 2016, *529*, 509–514, DOI 10.1038/nature16521.

[30] N. Mishra, N. T. Garland, K. A. Hewett, M. Shamsi, M. D. Dickey, A. J. Bandodkar, A soft wearable microfluidic patch with finger-actuated pumps and valves for on-demand, longitudinal, and multianalyte sweat sensing, *ACS Sensors*, 2022, *7*, 3169–3180, DOI 10.1021/acssensors.2c01669.

[31] S. R. S. Pour, D. Calabria, A. Emamiamin, E. Lazzarini, A. Pace, M. Guardigli, M. Zangheri, M. Mirasoli, Microfluidic-based non-invasive wearable biosensors for real-time monitoring of sweat biomarkers, *Biosensors*, 2024, *14*, 1–20, DOI 10.3390/bios14010029.

[32] B. Zhong, X. Qin, H. Xu, L. Liu, L. Li, Z. Li, L. Cao, Z. Lou, J. A. Jackman, N.-J. Cho, L. Wang, Interindividual- and blood-correlated sweat phenylalanine multimodal analytical biochips for tracking exercise metabolism, *Nature Communications*, 2024, *15*, 624, DOI 10.1038/s41467-024-44751-z.

[33] V. Jain, M. Ochoa, H. Jiang, R. Rahimi, B. Ziaie, A mass-customizable dermal patch with discrete colorimetric indicators for personalized sweat rate quantification, *Microsystems & Nanoengineering*, 2019, *5*, 1–12, DOI 10.1038/s41378-019-0067-0.

[34] A. Mena-Bravo, M. D. Luque de Castro, Sweat: A sample with limited present applications and promising future in metabolomics, *Journal of Pharmaceutical and Biomedical Analysis*, 2014, *90*, 139–147, DOI 10.1016/j.jpba.2013.10.048.

[35] J. P. Trollmann, MA thesis, University of Vienna, Vienna, **2025**.

[36] I. Branco, A. Choupina, Bioinformatics: new tools and applications in life science and personalized medicine, *Applied Microbiology and Biotechnology*, 2021, *105*, 937–951, DOI 10.1007/s00253-020-11056-2.

[37] M. Chen, R. Hofestädt, J. Taubert, Integrative bioinformatics: history and future, *Journal of Integrative Bioinformatics*, 2019, *16*, 20192001, DOI 10.1515/jib-2019-2001.

[38] T. Behl, I. Kaur, A. Sehgal, S. Singh, S. Bhatia, A. Al-Harrasi, G. Zengin, E. E. Babes, C. Brisc, M. Stoicescu, M. M. Toma, C. Sava, S. G. Bungau, Bioinformatics accelerates the major tetrad: a real boost for the pharmaceutical industry, *International Journal of Molecular Sciences*, 2021, *22*, 6184, DOI 10.3390/ijms22126184.

[39] E. J. Parker, K. C. Billane, N. Austen, A. Cotton, R. M. George, D. Hopkins, J. A. Lake, J. K. Pitman, J. N. Prout, H. J. Walker, A. Williams, D. D. Cameron, Untangling the Complexities of Processing and Analysis for Untargeted LC-MS Data Using Open-Source Tools, *Metabolites*, 2023, *13*, 463, DOI 10.3390/metabo13040463.

[40] I. Binanto, H. L. Hendric Spits Warnars, N. F. Sianipar, B. S. Abbas in 2019 6th International Conference on Information Technology, Computer and Electrical Engineering (ICITACEE), **2019**, pp. 1–5.

[41] J. Sun, Y. Xia, Pretreating and normalizing metabolomics data for statistical analysis, *Genes & Diseases*, 2024, *11*, 100979, DOI 10.1016/j.gendis.2023.04.018.

[42] Y. Wu, L. Li, Sample normalization methods in quantitative metabolomics, *Journal of Chromatography A*, 2016, *1430*, 80–95, DOI 10.1016/j.chroma.2015.12.007.

[43] R. Di Guida, J. Engel, J. W. Allwood, R. J. M. Weber, M. R. Jones, U. Sommer, M. R. Viant, W. B. Dunn, Non-targeted UHPLC-MS metabolomic data processing methods: a comparative investigation of normalisation, missing value imputation, transformation and scaling, *Metabolomics*, 2016, *12*, 93, DOI 10.1007/s11306-016-1030-9.

[44] C. Brunius, L. Shi, R. Landberg, Large-scale untargeted LC-MS metabolomics data correction using between-batch feature alignment and cluster-based within-batch signal intensity drift correction, *Metabolomics*, 2016, *12*, 173, DOI 10.1007/s11306-016-1124-4.

[45] ProteoWizard technical documentation: msconvert, https://proteowizard.sourceforge.io/tools/msconvert.html.

[46] M. C. Chambers, B. Maclean, R. Burke, D. Amodei, D. L. Ruderman, S. Neumann, L. Gatto, B. Fischer, B. Pratt, J. Egertson, K. Hoff, D. Kessner, N. Tasman, N. Shulman, B. Frewen, T. A. Baker, M.-Y. Brusniak, C. Paulse, D. Creasy, L. Flashner, K. Kani, C. Moulding, S. L. Seymour, L. M. Nuwaysir, B. Lefebvre, F. Kuhlmann, J. Roark, P. Rainer, S. Detlev, T. Hemenway, A. Huhmer, J. Langridge, B. Connolly, T. Chadick, K. Holly, J. Eckels, E. W. Deutsch, R. L. Moritz, J. E. Katz, D. B. Agus, M. MacCoss, D. L. Tabb, P. Mallick, A cross-platform toolkit for mass spectrometry and proteomics, *Nature Biotechnology*, 2012, *30*, 918–920, DOI 10.1038/nbt.2377.

[47] mzmine, https://github.com/mzmine.

[48] SIRIUS, https://github.com/sirius-ms.

[49] SIRIUS | Lehrstuhl Bioinformatik Jena, https://bio.informatik.uni-jena.de/software/sirius/.

[50] R. Schmid, S. Heuckeroth, A. Korf, A. Smirnov, O. Myers, T. S. Dyrlund, R. Bushuiev, K. J. Murray, N. Hoffmann, M. Lu, A. Sarvepalli, Z. Zhang, M. Fleischauer, K. Dührkop, M. Wesner, S. J. Hoogstra, E. Rudt, O. Mokshyna, C. Brungs, K. Ponomarov, L. Mutabdžija, T. Damiani, C. J. Pudney, M. Earll, P. O. Helmer, T. R. Fallon, T. Schulze, A. Rivas-Ubach, A. Bilbao, H. Richter, L.-F. Nothias, M. Wang, M. Orešič, J.-K. Weng, S. Böcker, A. Jeibmann, H. Hayen, U. Karst, P. C. Dorrestein, D. Petras, X. Du, T. Pluskal, Integrative analysis of multimodal mass spectrometry data in MZmine 3, *Nature Biotechnology*, 2023, *41*, 447–449, DOI 10.1038/s41587-023-01690-2.

[51] K. Dührkop, M. Fleischauer, M. Ludwig, A. A. Aksenov, A. V. Melnik, M. Meusel, P. C. Dorrestein, J. Rousu, S. Böcker, SIRIUS 4: a rapid tool for turning tandem mass spectra into metabolite structure information, *Nature Methods*, 2019, *16*, 299–302, DOI 10.1038/s41592-019-0344-8.

[52] K. Dührkop, K. Scheubert, S. Böcker, Molecular formula identification with SIRIUS, *Metabolites*, 2013, *3*, 506–516, DOI 10.3390/metabo3020506.

[53] M. E. Ritchie, B. Phipson, D. Wu, Y. Hu, C. W. Law, W. Shi, G. K. Smyth, Limma powers differential expression analyses for rna-sequencing and microarray studies, *Nucleic Acids Research*, 2015, *43*, e47, DOI 10.1093/nar/gkv007.

[54] limma, http://bioconductor.org/packages/limma/.

[55] D. Chicco, F. Cumbo, C. Angione, Ten quick tips for avoiding pitfalls in multi-omics data integration analyses, *PLOS Computational Biology*, 2023, *19*, e1011224, DOI 10.1371/journal.pcbi.1011224.

[56] R. K. Azad, V. Shulaev, Metabolomics technology and bioinformatics for precision medicine, *Briefings in Bioinformatics*, 2019, *20*, 1957–1971, DOI 10.1093/bib/bbx170.

[57] M. Gotsmy, J. Brunmair, C. Büschl, C. Gerner, J. Zanghellini, Probabilistic quotient's work and pharmacokinetics' contribution: countering size effect in metabolic time series measurements, *BMC Bioinformatics*, 2022, *23*, 379, DOI 10.1186/s12859-022-04918-1.

[58] P. Filzmoser, B. Walczak, What can go wrong at the data normalization step for identification of biomarkers?, *Journal of Chromatography A*, 2014, *1362*, 194–205, DOI 10.1016/j.chroma.2014.08.050.

[59] B. Low, Y. Wang, T. Zhao, H. Yu, T. Huan, Closing the knowledge gap of post-acquisition sample normalization in untargeted metabolomics, *ACS Measurement Science Au*, 2024, *4*, 702–711, DOI 10.1021/acsmeasuresciau.4c00047.

[60] F. Dieterle, A. Ross, G. Schlotterbeck, H. Senn, Probabilistic quotient normalization as robust method to account for dilution of complex biological mixtures. Application in 1H NMR metabonomics, *Analytical Chemistry*, 2006, *78*, 4281–4290, DOI 10.1021/ac051632c.

[61] J. E. Wulff, M. W. Mitchell, A comparison of various normalization methods for LC/MS metabolomics data, *Advances in Bioscience and Biotechnology*, 2018, *9*, 339–351, DOI 10.4236/abb.2018.98022.

[62] M. Wang, L. Jiang, R. Jian, J. Y. Chan, Q. Liu, M. P. Snyder, H. Tang, RobNorm: model-based robust normalization method for labeled quantitative mass spectrometry proteomics data, *Bioinformatics*, 2021, *37*, 815–821, DOI 10.1093/bioinformatics/btaa904.

[63] H.-W. Uh, L. Klarić, I. Ugrina, G. Lauc, A. K. Smilde, J. J. Houwing-Duistermaat, Choosing proper normalization is essential for discovery of sparse glycan biomarkers, *Molecular Omics*, 2020, *16*, 231–242, DOI 10.1039/C9MO00174C.

[64] W. Huber, A. Von Heydebreck, H. Sültmann, A. Poustka, M. Vingron, Variance stabilization applied to microarray data calibration and to the quantification of differential expression, *Bioinformatics*, 2002, *18*, 96–104, DOI 10.1093/bioinformatics/18.suppl_1.S96.

[65] W. Huber, A. v. Heydebreck, H. Sueltmann, A. Poustka, M. Vingron, Parameter estimation for the calibration and variance stabilization of microarray data, *Statistical Applications in Genetics and Molecular Biology*, 2003, *2*, 3, DOI 10.2202/1544-6115.1008.

[66] Introduction to vsn, 2024, https://bioconductor.org/packages/devel/bioc/vignettes/vsn/inst/doc/A-vsn.html.

[67] D. Singh, B. Singh, Investigating the impact of data normalization on classification performance, *Applied Soft Computing*, 2020, *97*, 105524, DOI 10.1016/j.asoc.2019.105524.

[68] M. Weiss, Is the one-compartment model with first order absorption a useful approximation?, *Pharmaceutical Research*, 2023, *40*, 2147–2153, DOI 10.1007/s11095-023-03582-1.

[69] E. R. Garrett, Simplified methods for the evaluation of the parameters of the time course of plasma concentration in the one-compartment body model with first-order invasion and first-order drug elimination including methods for ascertaining when such rate constants are equal, *Journal of Pharmacokinetics and Biopharmaceutics*, 1993, *21*, 689–734, DOI 10.1007/BF01113501.

[70] E. R. Garrett, The bateman function revisited: a critical reevaluation of the quantitative expressions to characterize concentrations in the one compartment body model as a function of time with first-order invasion and first-order elimination | journal of pharmacokinetics and pharmacodynamics, *Journal of Pharmacokinetics and Biopharmaceutics*, 1994, *22*, 103–128.

[71] E. Roanes-Lozano, A. González-Bermejo, E. Roanes-Macías, J. Cabezas, An application of computer algebra to pharmacokinetics: the bateman equation, *SIAM Review*, 2006, *48*, 133–146, DOI 10.1137/050634074.

[72] M. Savva, X. Yuan, A reevaluation of prazosin pharmacokinetics in a two-compartment model, the apparent volume of distribution and comparative simulations in the one-compartment model, *Journal of Biosciences and Medicines*, 2022, *10*, 108–140, DOI 10.4236/jbm.2022.101010.

[73] S. Mortensen, A. Jonsdottir, 'Introduction to PK/PD modelling - with focus on PK and stochastic differential equations', en, Technical Report, Technical University of Denmark, **2008**.

[74] R. G. Hahn, R. O. Dull, A slow-exchange interstitial fluid compartment in volunteers and anesthetized patients: kinetic analysis and physiology, *Anesthesia & Analgesia*, 2024, *139*, 339, DOI 10.1213/ANE.0000000000006767.

[75] A tutorial on bayesian optimization, 2018, http://arxiv.org/abs/1807.02811.

[76] J. Snoek, H. Larochelle, R. P. Adams in Advances in Neural Information Processing Systems, *Vol. 25*, Curran Associates, Inc., **2012**.

[77] R. Roussel, A. L. Edelen, T. Boltz, D. Kennedy, Z. Zhang, F. Ji, X. Huang, D. Ratner, A. S. Garcia, C. Xu, J. Kaiser, A. F. Pousa, A. Eichler, J. O. Lübsen, N. M. Isenberg, Y. Gao, N. Kuklev, J. Martinez, B. Mustapha, V. Kain, C. Mayes, W. Lin, S. M. Liuzzo, J. St. John, M. J. V. Streeter, R. Lehe, W. Neiswanger, Bayesian optimization algorithms for accelerator physics, *Physical Review Accelerators and Beams*, 2024, *27*, 084801, DOI 10.1103/PhysRevAccelBeams.27.084801.

[78] L. B. Sheiner, S. L. Beal, Bayesian individualization of pharmacokinetics: simple implementation and comparison with non-bayesian methods, *Journal of Pharmaceutical Sciences*, 1982, *71*, 1344–1348, DOI 10.1002/jps.2600711209.

[79] bayesOpt function - RDocumentation, https://www.rdocumentation.org/packages/ParBayesianOptimization/versions/1.2.6/topics/bayesOpt.

[80] Y. Zhang, S. Fan, G. Wohlgemuth, O. Fiehn, Denoising autoencoder normalization for large-scale untargeted metabolomics by gas chromatography–mass spectrometry, *Metabolites*, 2023, *13*, 944, DOI 10.3390/metabo13080944.

[81] B. Bruszel, E. Tóth-Molnár, T. Janáky, Z. Szabó, Sources of variance in human tear proteomic samples: statistical evaluation, quality control, normalization, and biological insight, *International Journal of Molecular Sciences*, 2024, *25*, 1559, DOI 10.3390/ijms25031559.

[82] F. Brix, T. Demetrowitsch, J. Jensen-Kroll, H. Zacharias, S. Szymczak, M. Laudes, S. Schreiber, K. Schwarz, Evaluating the effect of data merging and post-acquisition normalization on statistical analysis of untargeted high-resolution mass spectrometry based urinary metabolomics data, *Analytical Chemistry*, 2024, *96*, 33–40, DOI 10.1021/acs.analchem.3c01380.

[83] H. Ghosson, Y. Guitton, A. Ben Jrad, C. Patil, D. Raviglione, M.-V. Salvia, C. Bertrand, Electrospray ionization and heterogeneous matrix effects in liquid chromatography/mass spectrometry based meta-metabolomics: A biomarker or a suppressed ion?, *Rapid Communications in Mass Spectrometry*, 2021, *35*, e8977, DOI 10.1002/rcm.8977.

[84] P. Sekula, O.-N. Goek, L. Quaye, C. Barrios, A. S. Levey, W. Römisch-Margl, C. Menni, I. Yet, C. Gieger, L. A. Inker, J. Adamski, W. Gronwald, T. Illig, K. Dettmer, J. Krumsiek, P. J. Oefner, A. M. Valdes, C. Meisinger, J. Coresh, T. D. Spector, R. P. Mohney, K. Suhre, G. Kastenmüller, A. Köttgen, A metabolome-wide association study of kidney function and disease in the general population, *Journal of the American Society of Nephrology*, 2016, *27*, 1175, DOI 10.1681/ASN.2014111099.

[85] P. H. Hart, M. Norval, The multiple roles of urocanic acid in health and disease, *The Journal of investigative dermatology*, 2021, *141*, 496–502, DOI 10.1016/j.jid.2020.07.017.

[86] Kosmetik-Produkte, https://kosmetikanalyse.org/kosmetik-produkte.

List of Figures

List of Tables

Appendix

Molecule Evaluation and General Data Overview

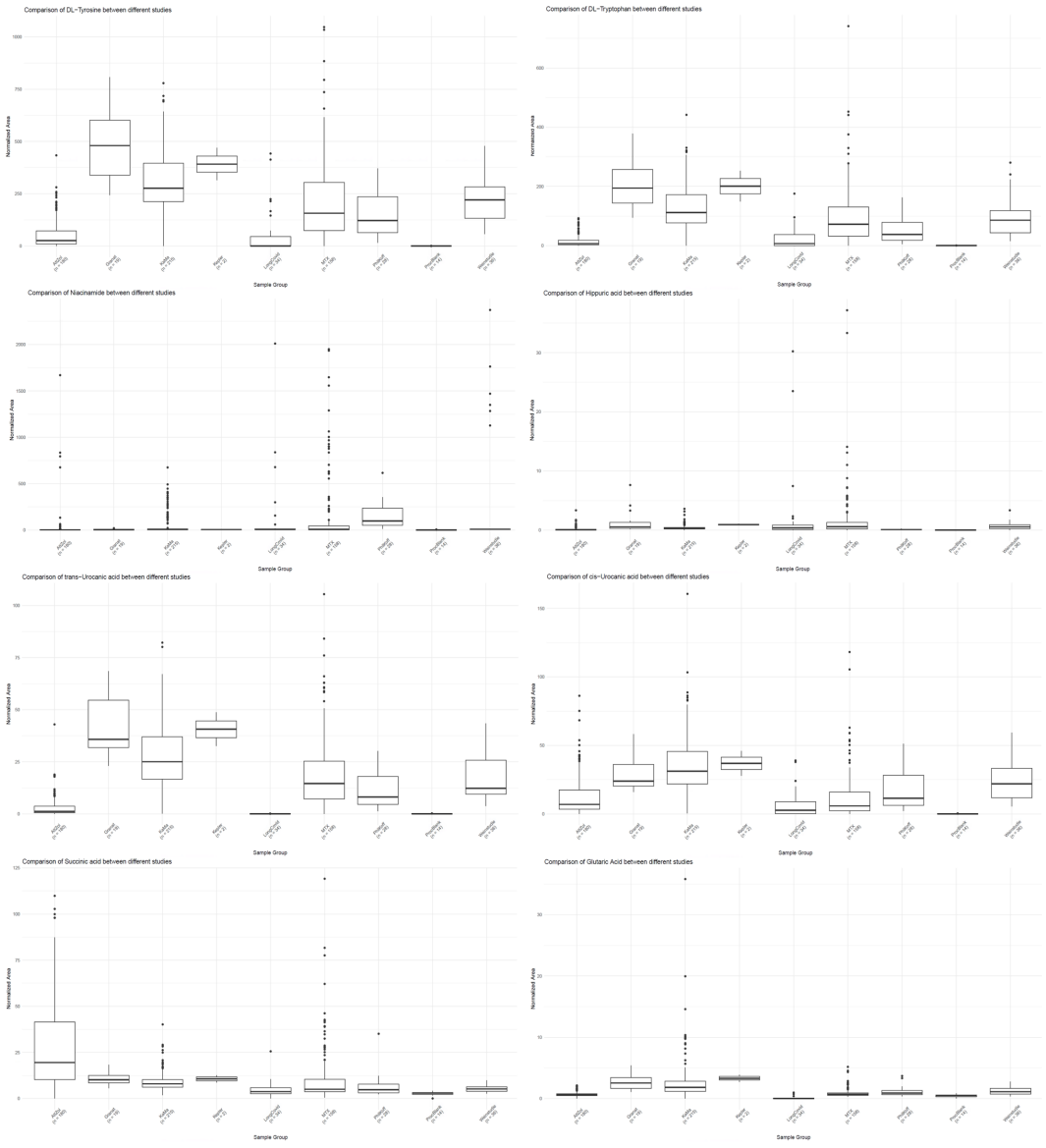

Figure 5.1 – Comparison of the caffeine-D9 normalized abundance of the selected molecules over various studies, Part 1.

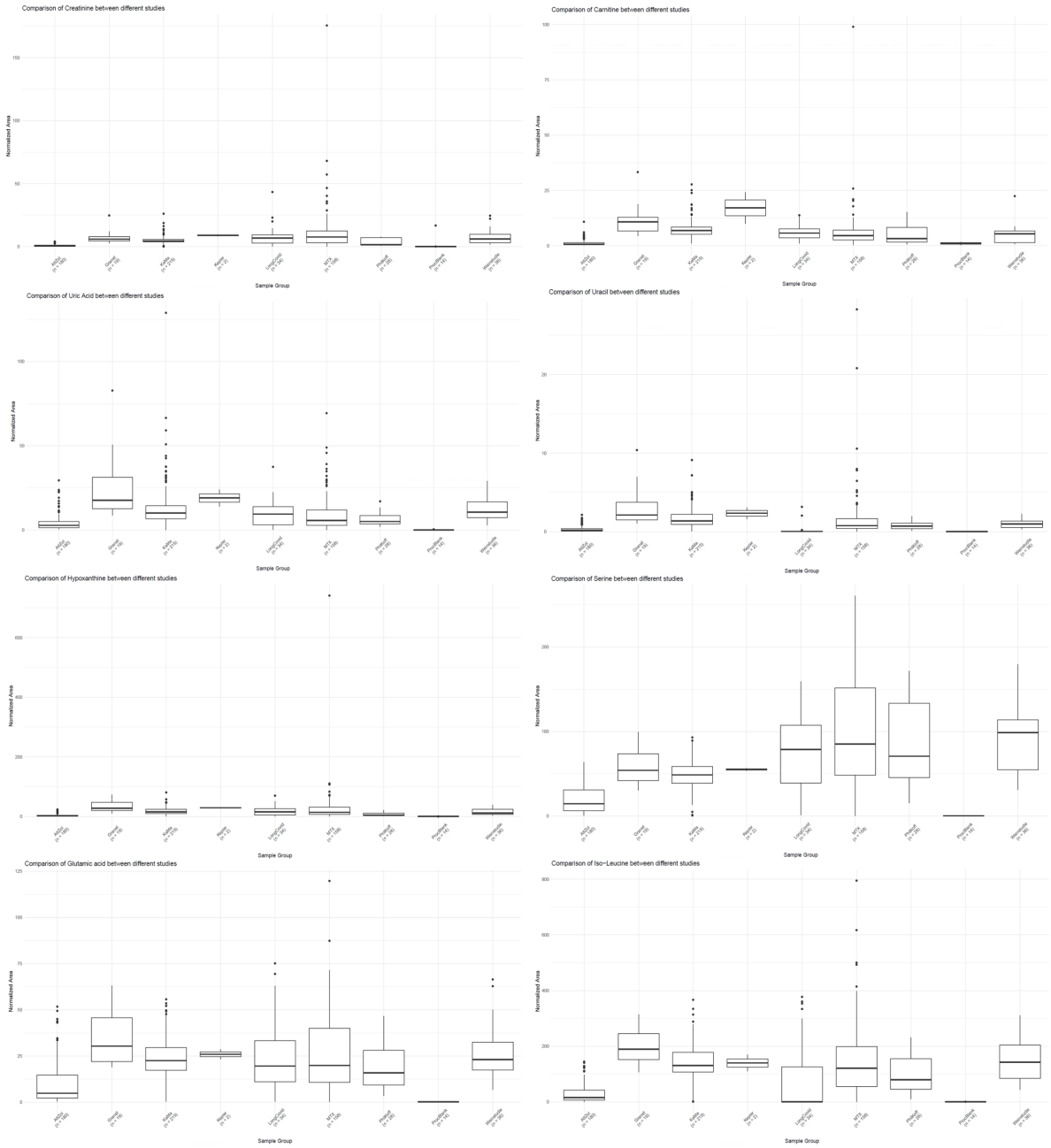

Figure 5.2 – Comparison of the caffeine-D9 normalized abundance of the selected molecules over various studies, Part 2.

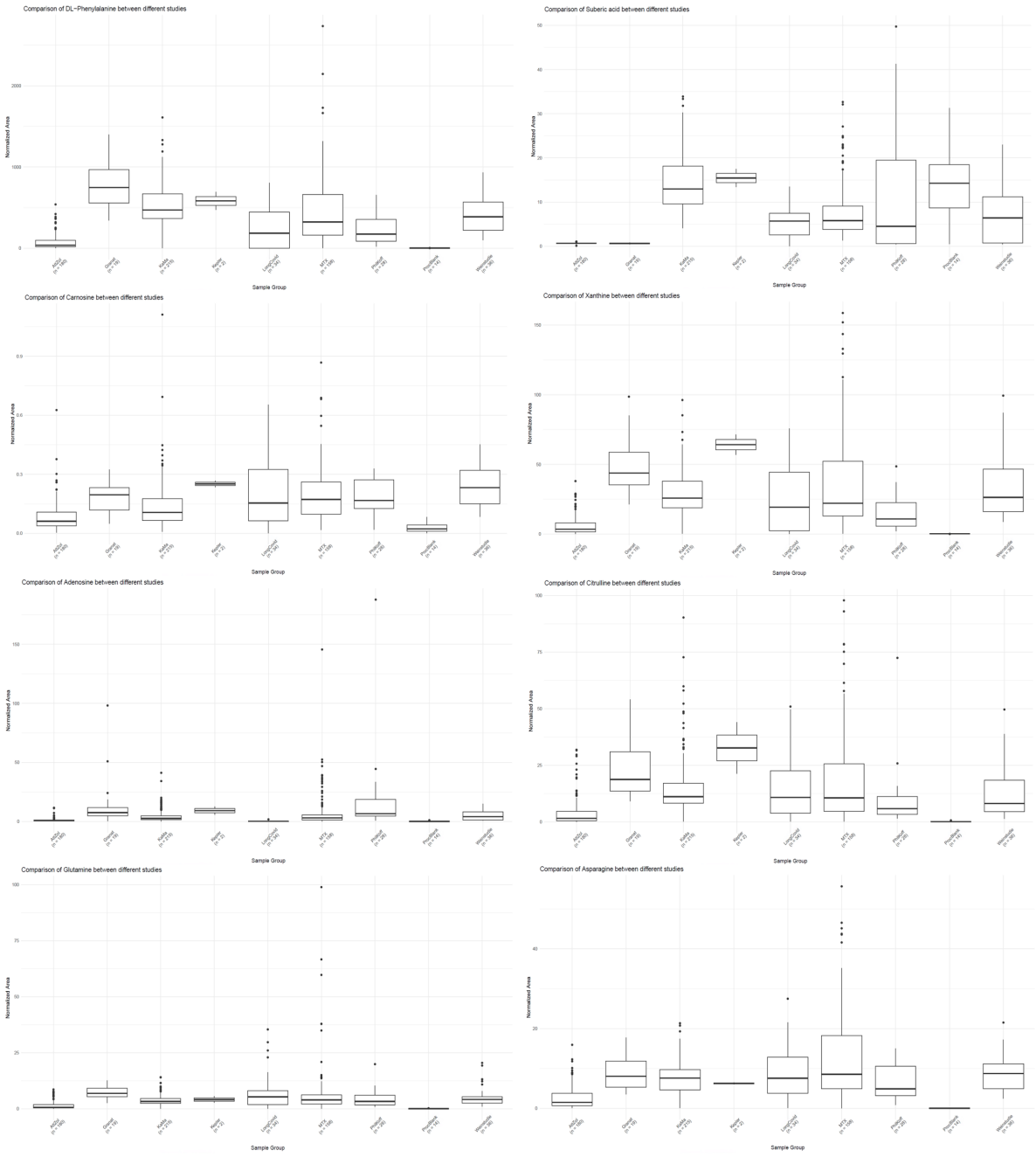

Figure 5.3 – Comparison of the caffeine-D9 normalized abundance of the selected molecules over various studies, Part 3.

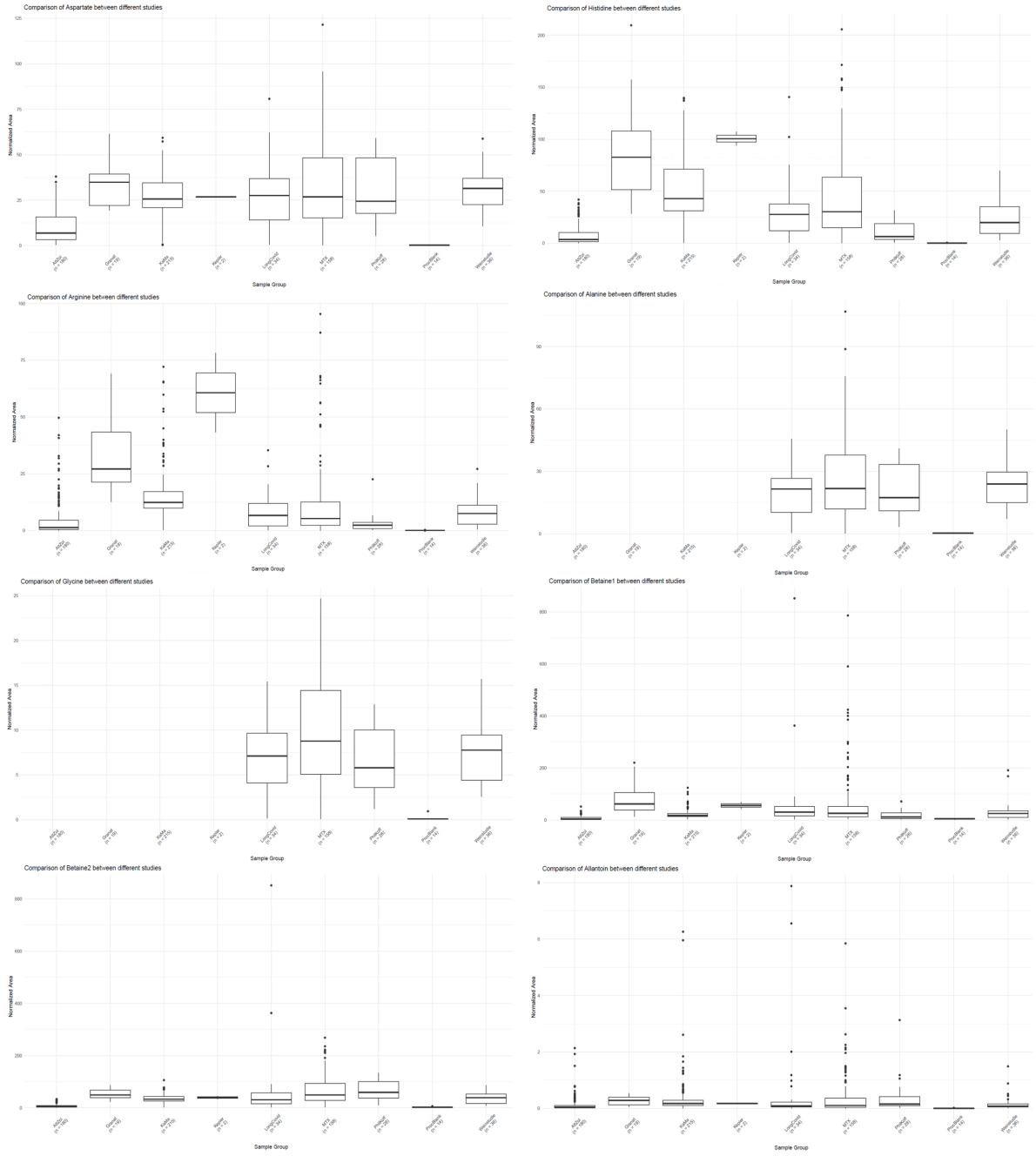

Figure 5.4 – Comparison of the caffeine-D9 normalized abundance of the selected molecules over various studies, Part 4.

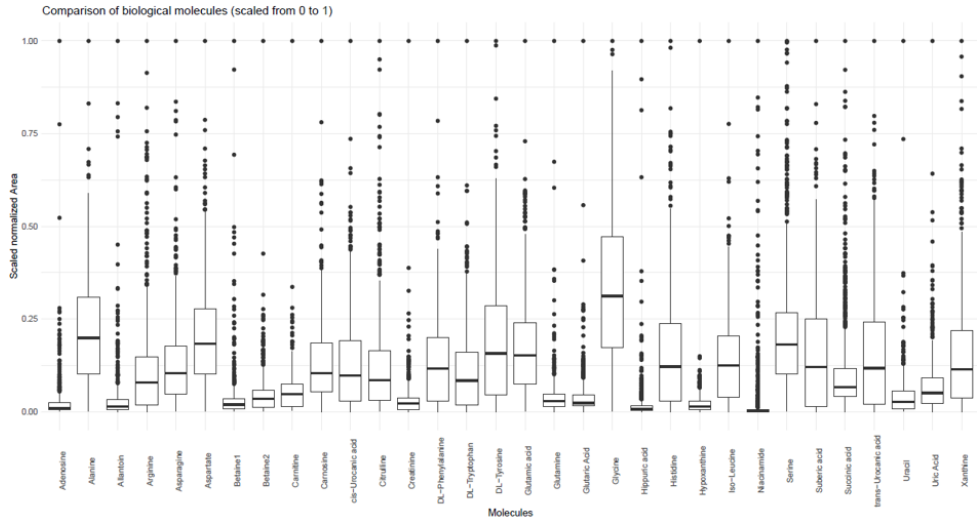

Figure 5.5 – Comparison of the selected molecules over all experiments, scaled between 1 and 0.

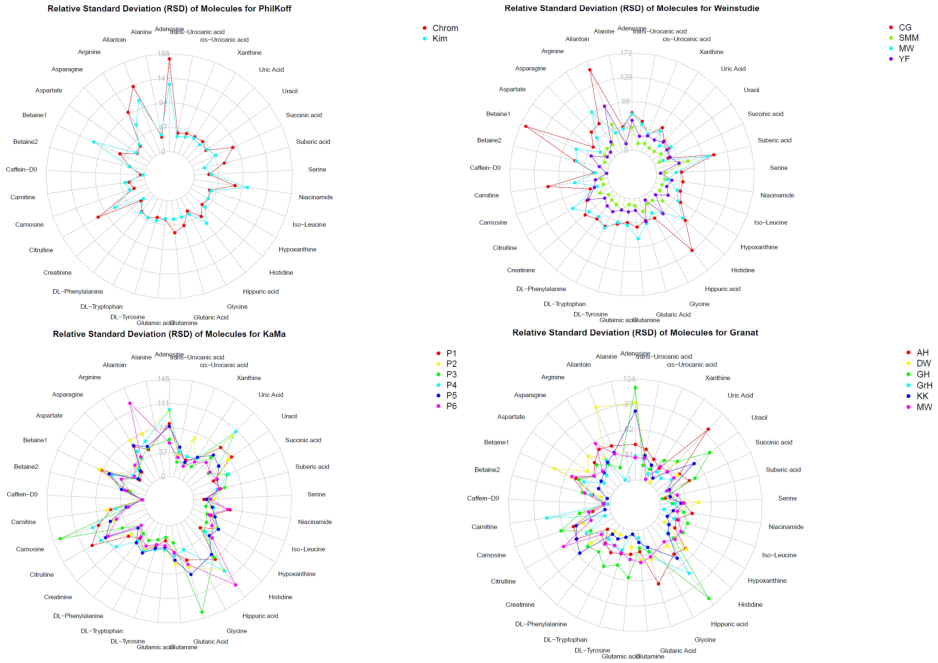

Figure 5.6 – Comparison of the RSD of the selected molecules over the individuals of various studies.

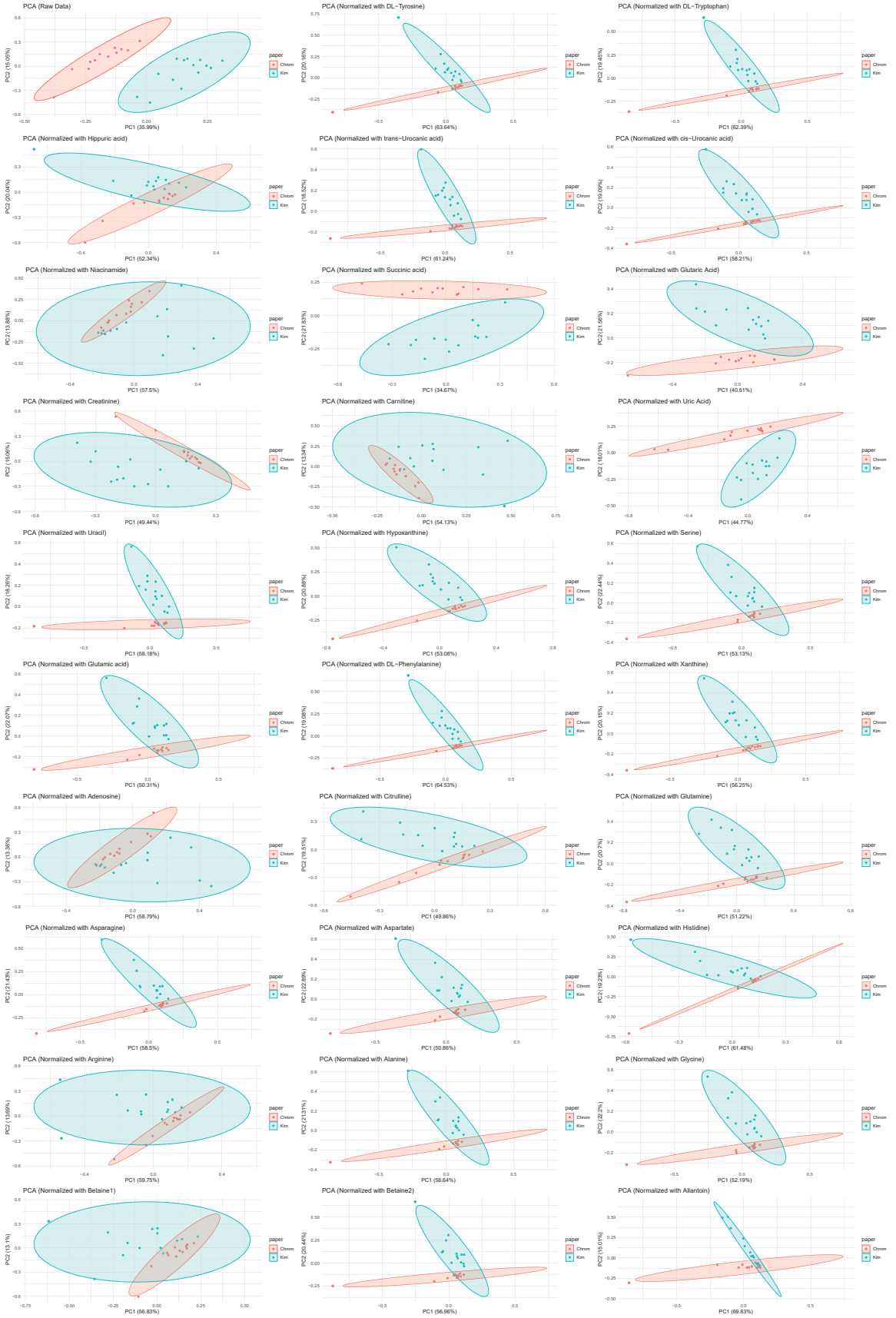

Figure 5.7 – PCA of caffeine data measured with 2 different papers, Kimtech (Kim) and Chromatography (Chrom) paper. PCA's are shown raw and normalized with different molecules.

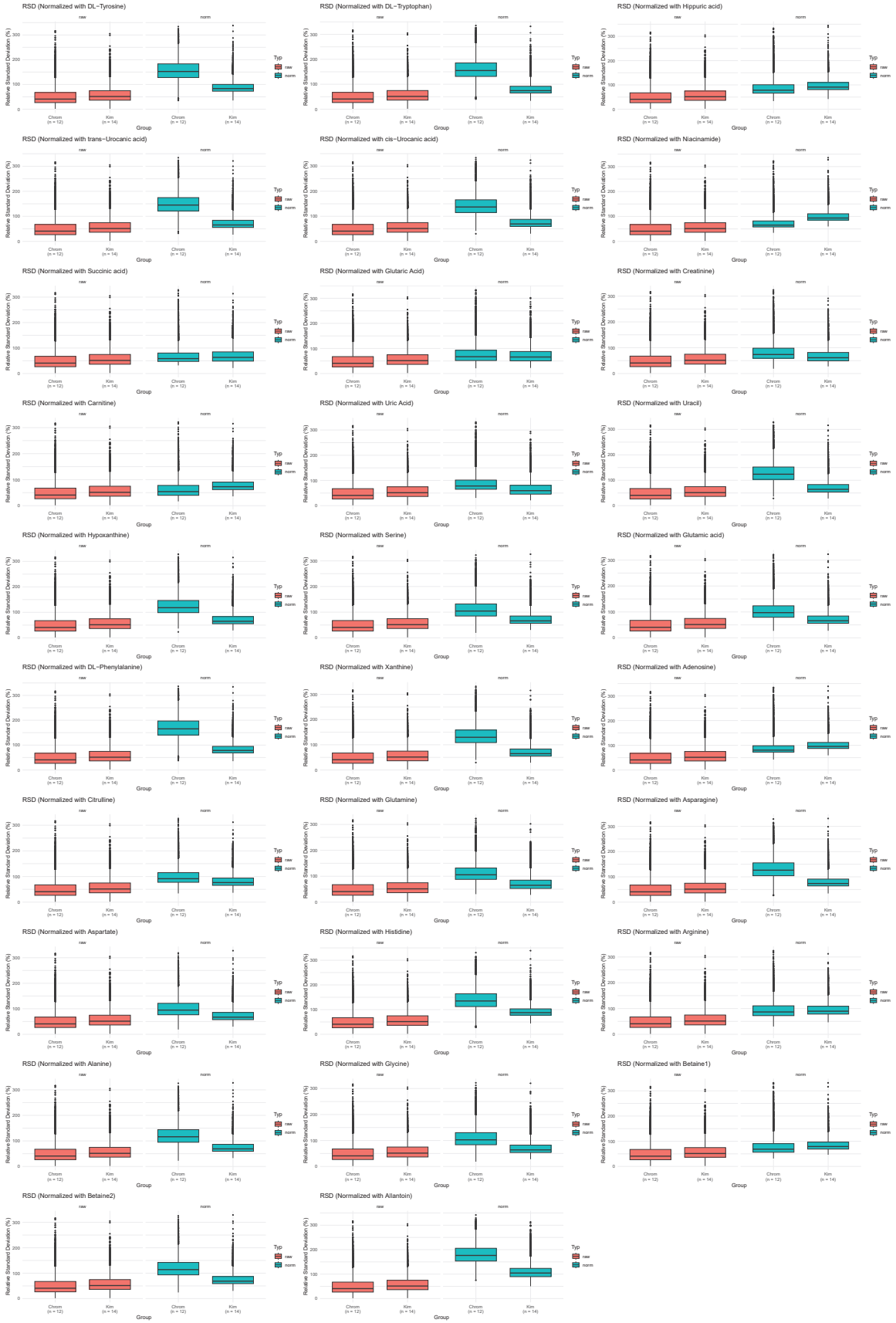

Figure 5.8 – RSD of caffeine data measured with 2 different papers, Kimtech (Kim) and Chromatography (Chrom) paper. RSD's are shown raw and normalized with different molecules.

Figure 5.9 – Normalization of pharmacokinetic caffeine curves with selected biological molecules of a caffeine study of and from Philipp.

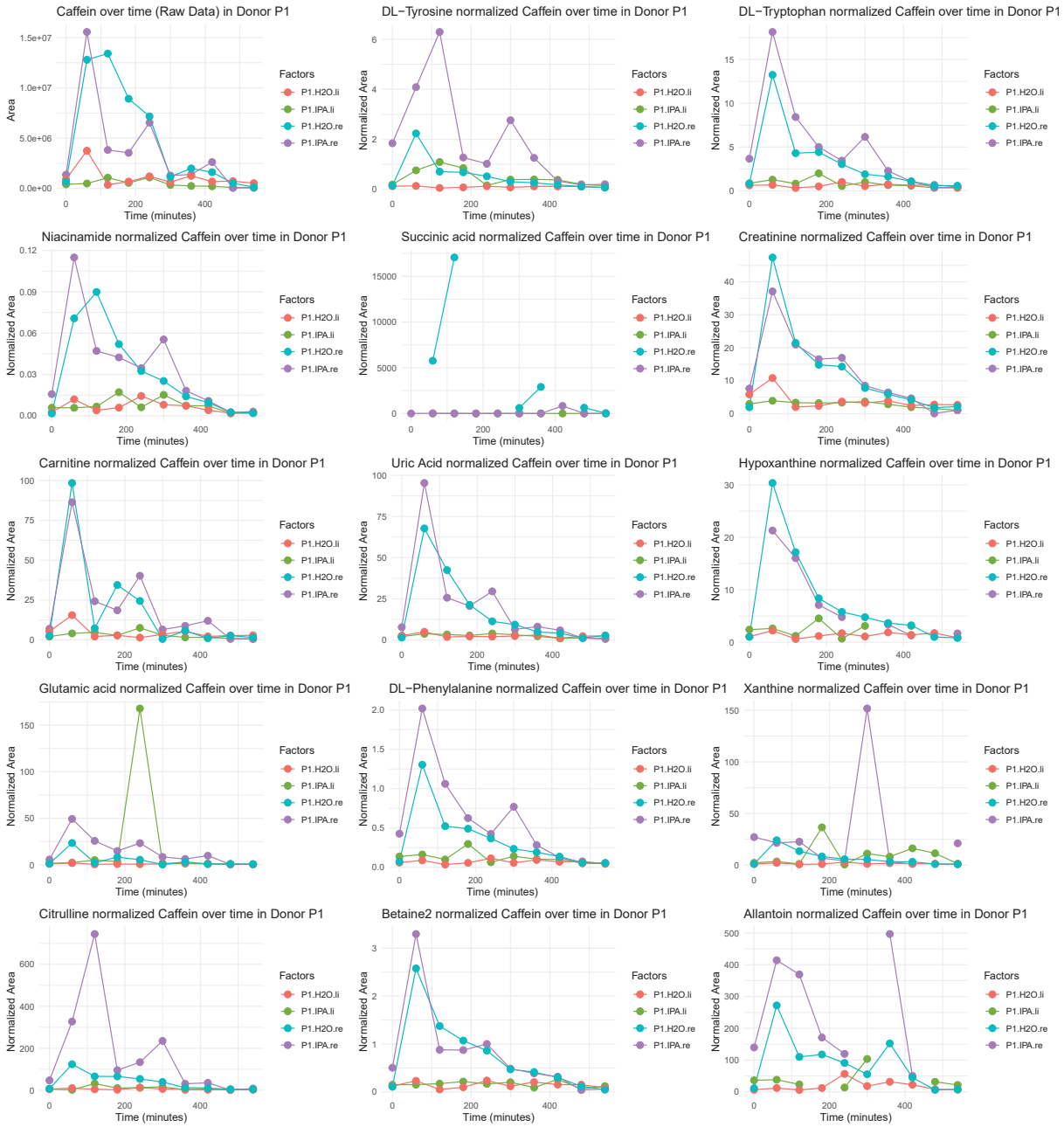

Figure 5.10 – Normalization of pharmacokinetic caffeine curves with selected biological molecules of a caffeine study from Simon.

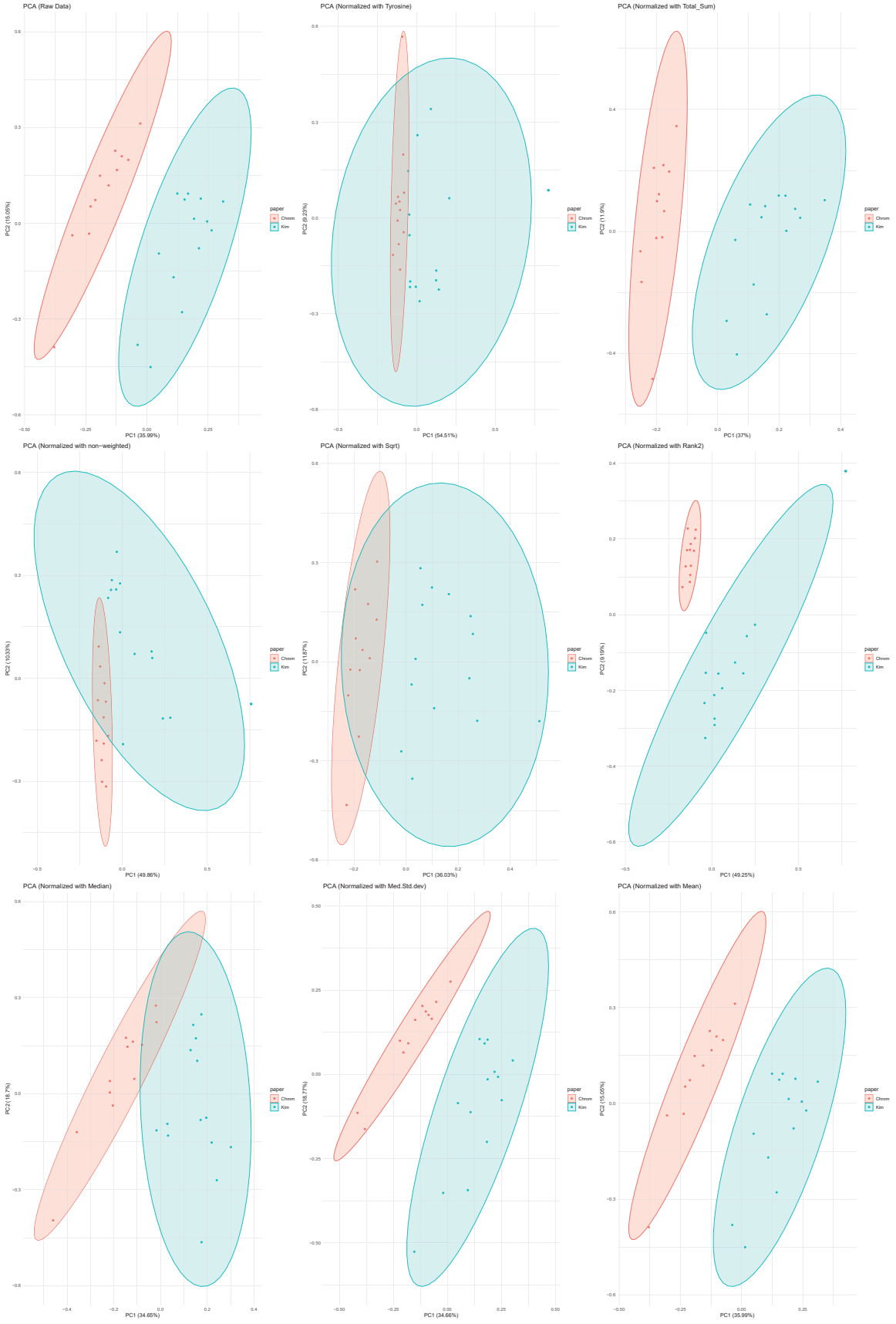

Figure 5.11 – PCA of caffeine data measured with 2 different papers, Kimtech (Kim) and Chromatography (Chrom) paper. PCA's are shown raw and normalized with different (weighting) methods. Total Sum uses a sum of all features of the sample, non-weighted uses the sum of the 32 shown molecules, the other methods are names how the 32 molecules are weighted before they are summed up.

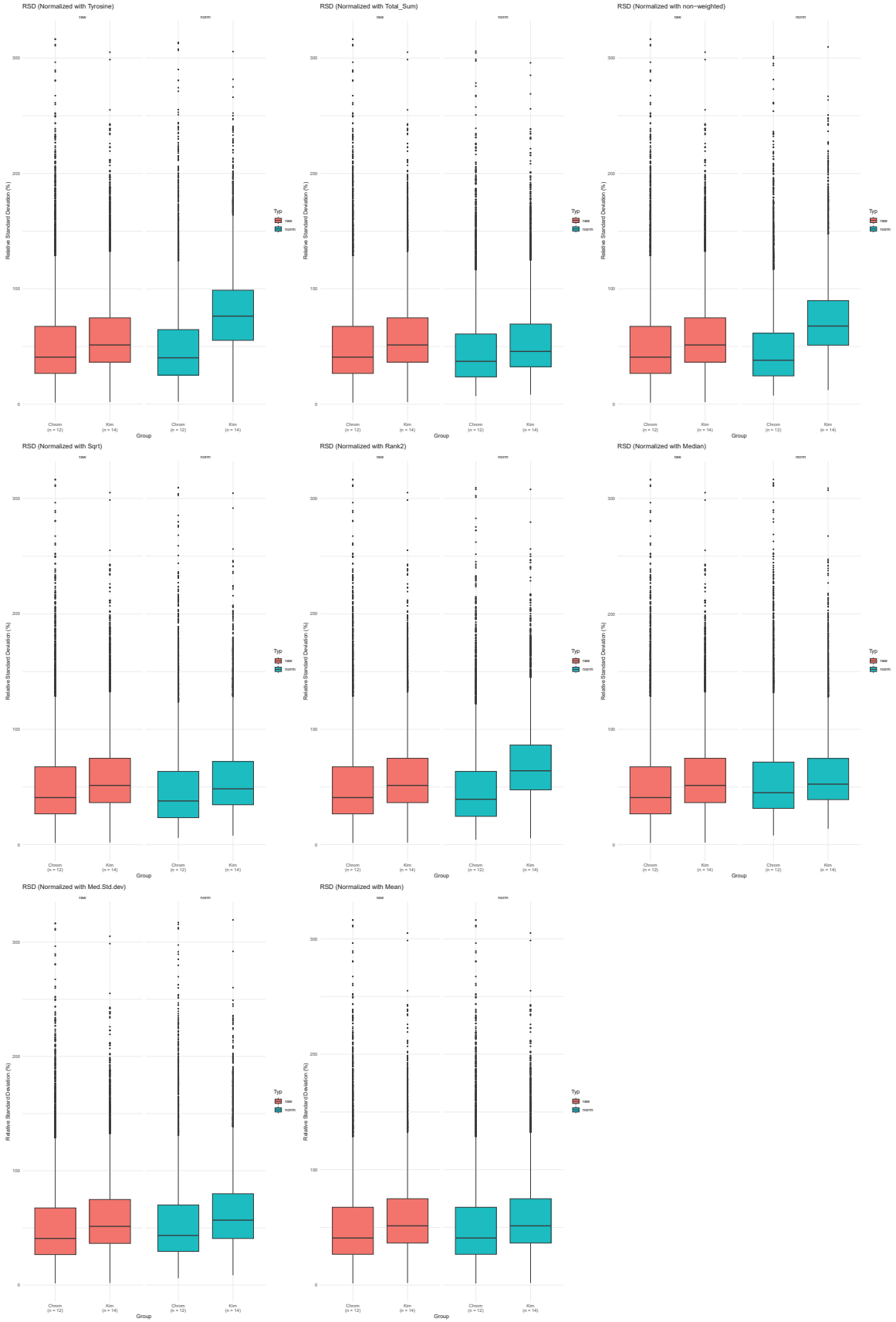

Figure 5.12 – RSD of caffeine data measured with 2 different papers, Kimtech (Kim) and Chromatography (Chrom) paper. RSD's are shown raw and normalized with different (weighting) methods. Total Sum uses a sum of all features of the sample, non-weighted uses the sum of the 32 shown molecules, the other methods are names how the 32 molecules are weighted before they are summed up.

Table 5.1 – Filtered list of molecules with the LC-MS properties used in Simon study normalization calculations.

Molecule Name	**Molecular Formula**	**Precursor Adduct**	**Explicit Retention Time**
DL-Tyrosine	$C_9H_{11}NO_3$	[M+H]+	1.15
DL-Tryptophan	$C_{11}H_{12}N_2O_2$	[M+H]+	2.28
Hippuric acid	$C_9H_9NO_3$	[M-H]-	2.46
trans-Urocanic acid	$C_6H_6N_2O_2$	[M-H]-	0.75
cis-Urocanic acid	$C_6H_6N_2O_2$	[M-H]-	0.83
cis-Urocanic acid	$C_6H_6N_2O_2$	[M-H]-	0.99
Succinic acid	$C_4H_6O_4$	[M-H]-	0.84
Creatinine	$C_4H_7N_3O$	[M+H]+	0.34
Carnitine	$C_7H_{15}NO_3$	[M+H]+	0.33
Uric Acid	$C_5H_4N_4O_3$	[M+H]+	0.85
Uracil	$C_4H_4N_2O_2$	[M+H]+	1.13
Hypoxanthine	$C_5H_4N_4O$	[M+H]+	0.89
Glutamic acid	$C_5H_9NO_4$	[M+H]+	0.31
Iso-Leucine1	$C_6H_{13}NO_2$	[M+H]+	0.87
Iso-Leucine2	$C_6H_{13}NO_2$	[M+H]+	0.94
DL-Phenylalanine	$C_9H_{11}NO_2$	[M+H]+	1.7
Xanthine	$C_5H_4N_4O_2$	[M+H]+	1.15
Adenosine	$C_{10}H_{13}N_5O_4$	[M+H]+	1.45
Citrulline	$C_6H_{13}N_3O_3$	[M+H]+	0.32

Table 5.2 – Filtered list of molecules with the LC-MS properties used in Philipp study normalization calculations.

Molecule Name	**Molecular Formula**	**Precursor Adduct**	**Explicit Retention Time**
DL-Tyrosine	$C_9H_{11}NO_3$	[M+H]+	0.88
DL-Tryptophan	$C_{11}H_{12}N_2O_2$	[M+H]+	2.36
Hippuric acid	$C_9H_9NO_3$	[M-H]-	2.97
trans-Urocanic acid	$C_6H_6N_2O_2$	[M-H]-	0.54
cis-Urocanic acid	$C_6H_6N_2O_2$	[M-H]-	0.66
Succinic acid	$C_4H_6O_4$	[M-H]-	0.93
Glutaric Acid	$C_5H_8O_4$	[M-H]-	1.5
Creatinine	$C_4H_7N_3O$	[M+H]+	0.44
Carnitine	$C_7H_{15}NO_3$	[M+H]+	0.43
Uric Acid	$C_5H_4N_4O_3$	[M+H]+	0.77
Uracil	$C_4H_4N_2O_2$	[M+H]+	0.98
Hypoxanthine	$C_5H_4N_4O$	[M+H]+	0.79
Glutamic acid	$C_5H_9NO_4$	[M+H]+	0.45
Iso-Leucine	$C_6H_{13}NO_2$	[M+H]+	0.85
DL-Phenylalanine	$C_9H_{11}NO_2$	[M+H]+	1.6
Carnosine	$C_9H_{14}N_4O_3$	[M+H]+	4.32
Xanthine	$C_5H_4N_4O_2$	[M+H]+	0.94
Adenosine	$C_{10}H_{13}N_5O_4$	[M+H]+	1.1
Citrulline	$C_6H_{13}N_3O_3$	[M+H]+	0.45
Glutamine	$C_5H_{10}N_2O_3$	[M+H]+	0.44
Asparagine	$C_4H_8N_2O_3$	[M+H]+	0.44
Aspartate	$C_4H_7NO_4$	[M+H]+	0.44
Histidine	$C_6H_9N_3O_2$	[M+H]+	0.44
Alanine	$C_3H_7NO_2$	[M+H]+	0.44

Table 5.3 – Filtered list of molecules with the LC-MS properties used in Julia study normalization calculations.

Molecule Name	**Molecular Formula**	**Precursor Adduct**	**Explicit Retention Time**
DL-Tyrosine	$C_9H_{11}NO_3$	[M+H]+	0.93
DL-Tryptophan	$C_{11}H_{12}N_2O_2$	[M+H]+	2.2
Hippuric acid	$C_9H_9NO_3$	[M-H]-	2.97
trans-Urocanic acid	$C_6H_6N_2O_2$	[M-H]-	0.56
cis-Urocanic acid	$C_6H_6N_2O_2$	[M-H]-	0.74
Succinic acid	$C_4H_6O_4$	[M-H]-	0.94
Glutaric Acid	$C_5H_8O_4$	[M-H]-	1.42
Creatinine	$C_4H_7N_3O$	[M+H]+	0.39
Carnitine	$C_7H_{15}NO_3$	[M+H]+	0.39
Uric Acid	$C_5H_4N_4O_3$	[M+H]+	0.78
Hypoxanthine	$C_5H_4N_4O$	[M+H]+	0.79
Glutamic acid	$C_5H_9NO_4$	[M+H]+	0.4
Iso-Leucine	$C_6H_{13}NO_2$	[M+H]+	0.96
DL-Phenylalanine	$C_9H_{11}NO_2$	[M+H]+	1.53
Xanthine	$C_5H_4N_4O_2$	[M+H]+	0.97
Adenosine	$C_{10}H_{13}N_5O_4$	[M+H]+	1.12
Citrulline	$C_6H_{13}N_3O_3$	[M+H]+	0.41
Glutamine	$C_5H_{10}N_2O_3$	[M+H]+	0.39
Asparagine	$C_4H_8N_2O_3$	[M+H]+	0.39
Aspartate	$C_4H_7NO_4$	[M+H]+	0.39
Histidine	$C_6H_9N_3O_2$	[M+H]+	0.36

Figure 5.13 – Comparison of weighting strategies for the molecule combinations used to normalize pharmacokinetic caffeine curves with selected biological molecules. A) Caffeine study of and from Philipp, B) Caffeine study from Simon.

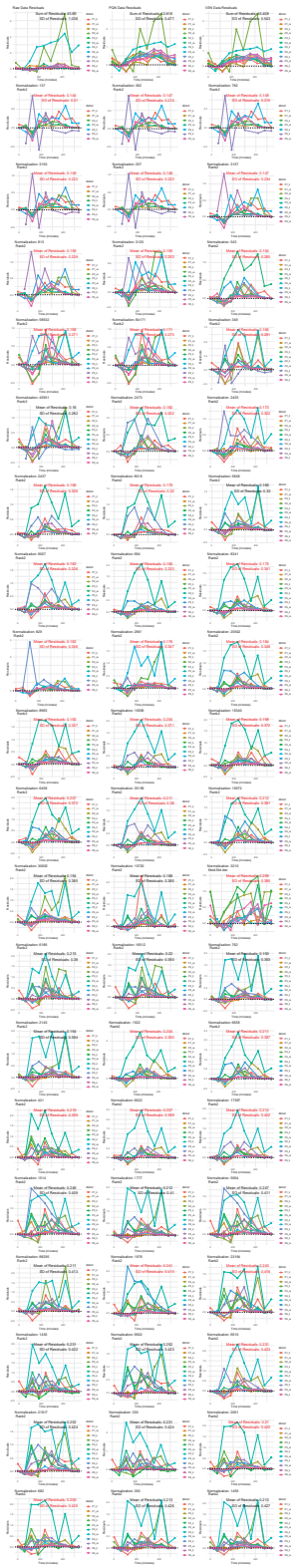

Figure 5.14 – Comparison of the residuals for each sample regarding the top normalization combinations in the Simon caffeine study, tested on all donors alongside the raw data and the PQN and VSN stabilized data for comparison.

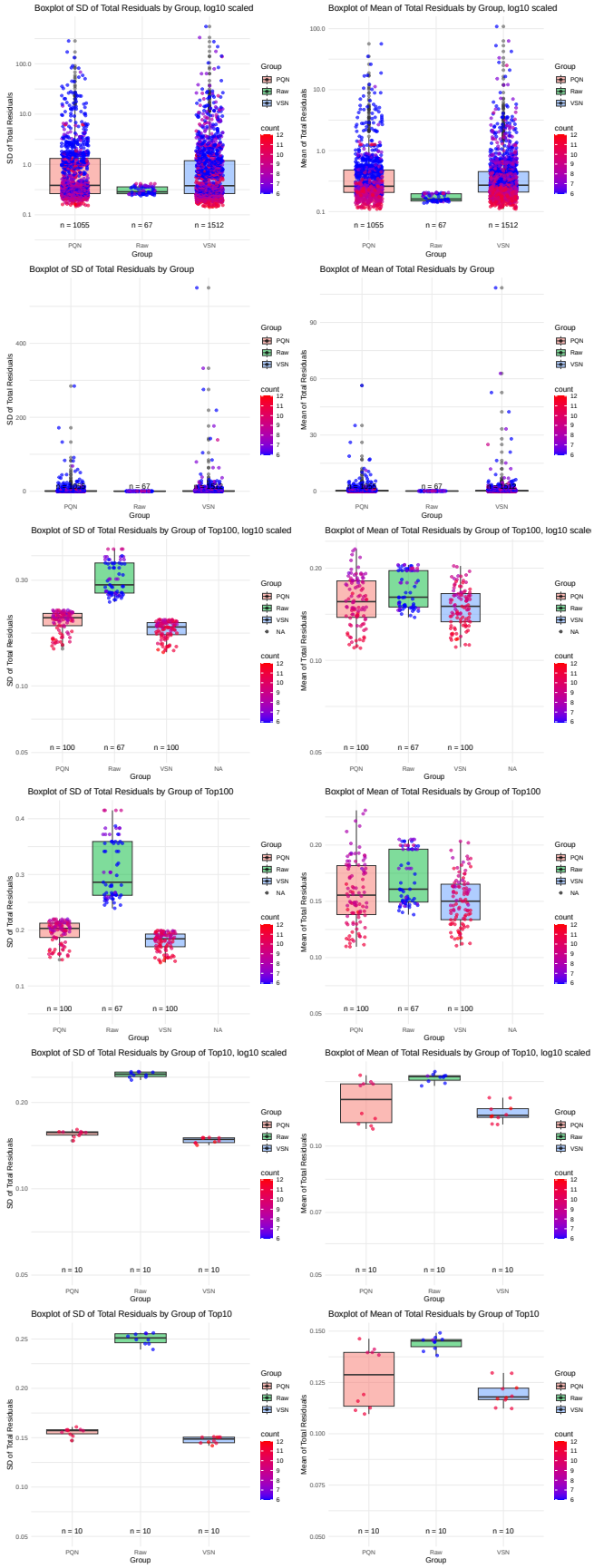

Figure 5.15 – Overview of the standard deviation of the residuals for all donors concerning the top 10000 normalization combinations that can normalize 6 or more of the 12 different donors in the Simon caffeine study, using boxplots.

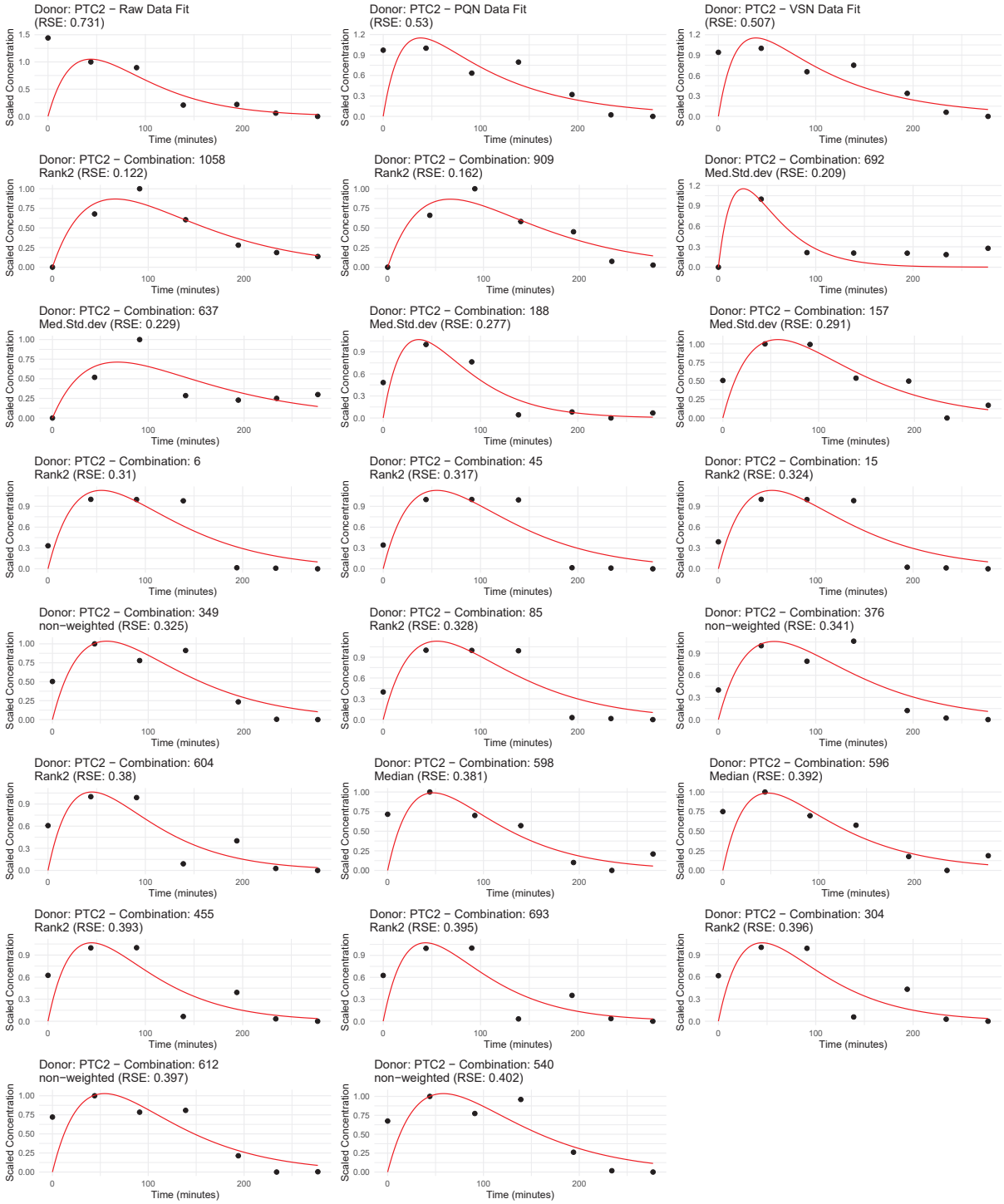

Figure 5.16 – Overview of top normalization combinations for the Philipp caffeine study for donor PTC2.

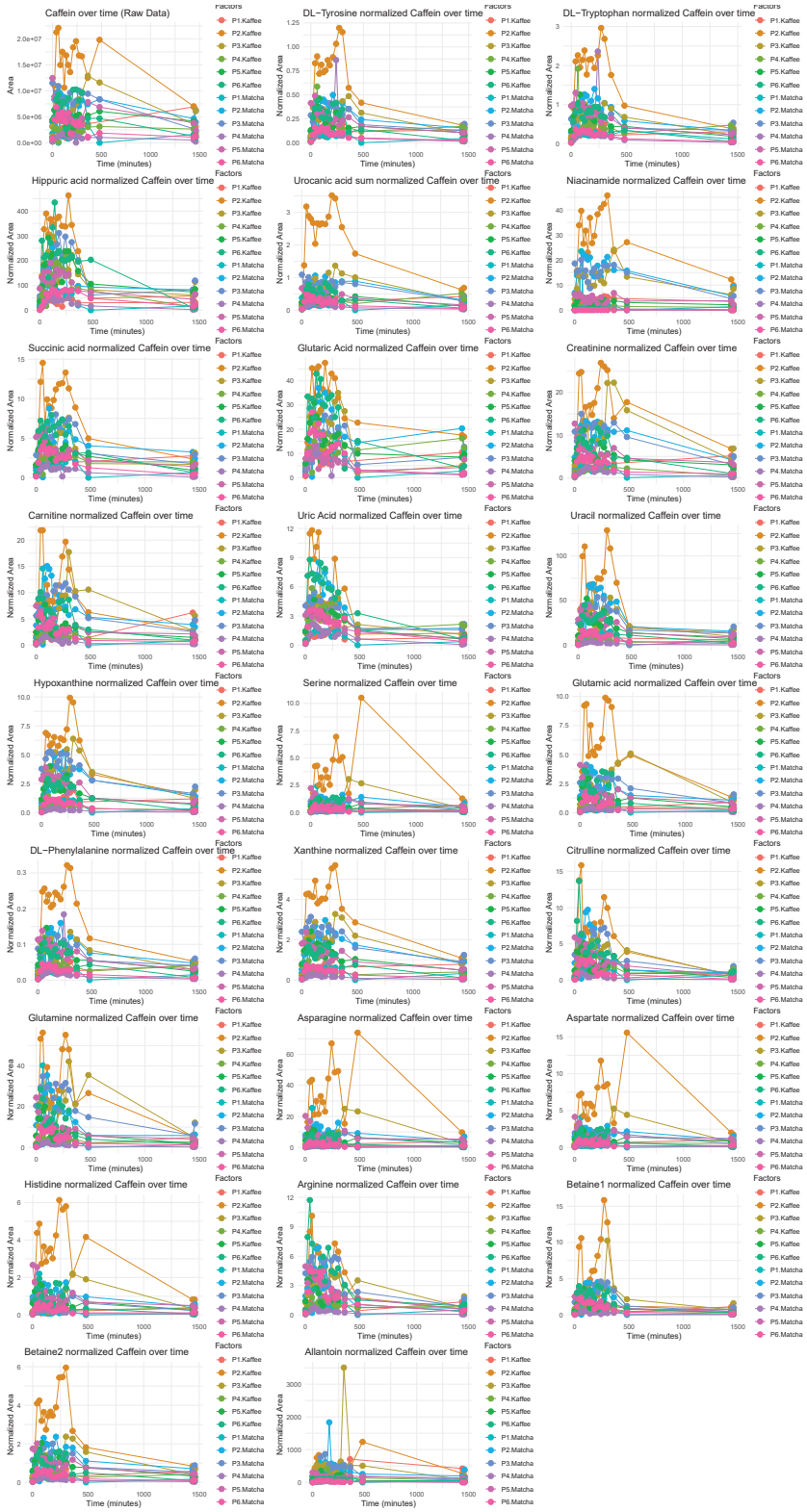

Figure 5.17 – Overview of data points normalized with the different normalization molecules tested on the Samra coffee matcha study.

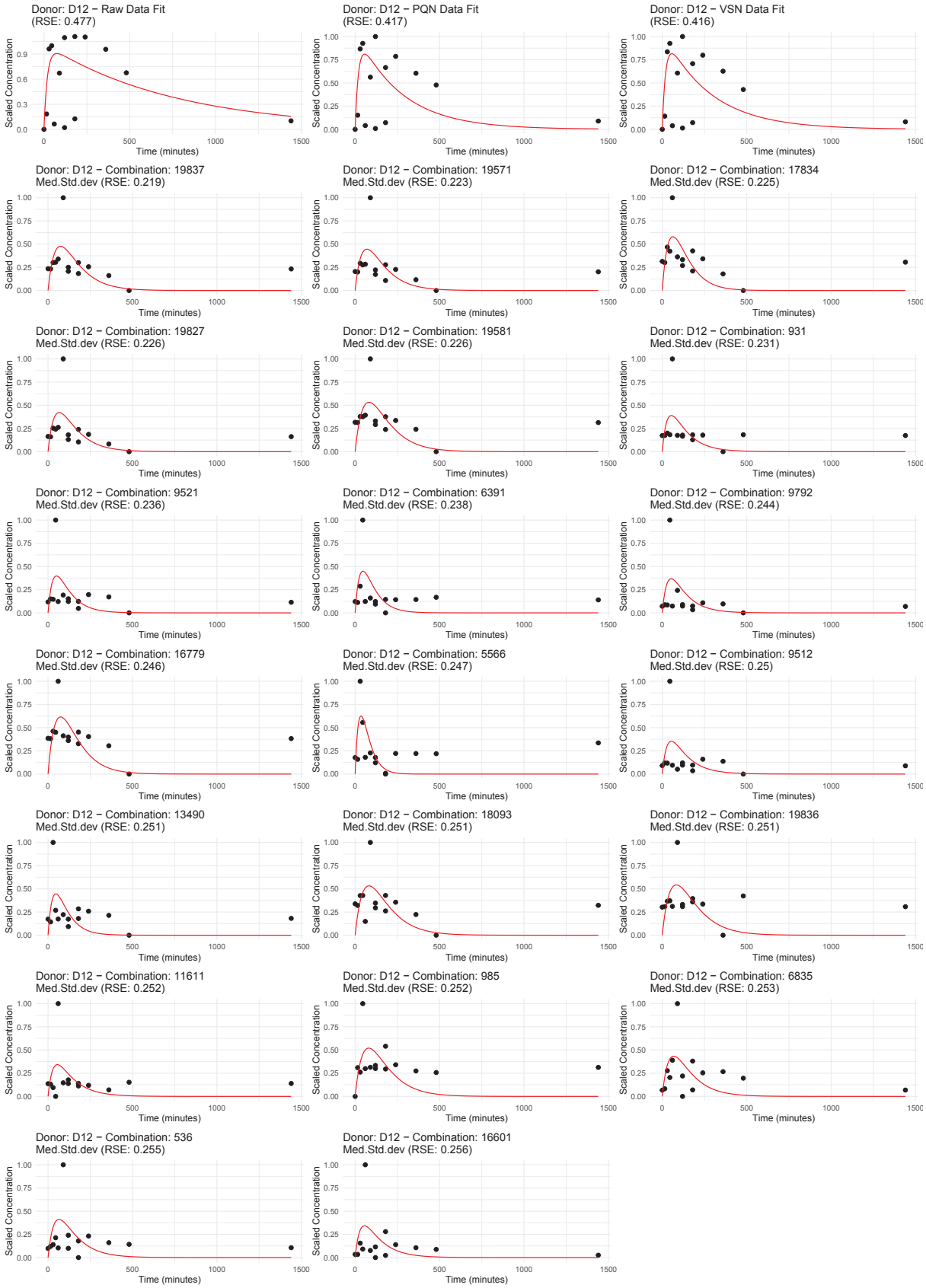

Figure 5.18 – Overview of data points normalized with the different normalization molecules tested on the Julia coffee matcha study for donor D12.

Table 5.4 – Filtered list of molecules with the LC-MS properties used in the Bayesian optimization approach with the combined caffeine studies of Simon, Philipp and Julia.

Molecule Name	**Molecular Formula**	**Precursor Adduct**	**Explicit Retention Time Philipp**	**Explicit Retention Time Simon**	**Explicit Retention Time Julia**
DL-Tyrosine	$C_9H_{11}NO_3$	[M+H]+	0.88	1.15	0.9
DL-Tryptophan	$C_{11}H_{12}N_2O_2$	[M+H]+	2.28	2.2	2.15
trans-Urocanic acid	$C_6H_6N_2O_2$	[M-H]-	0.54	0.75	0.56
cis-Urocanic acid	$C_6H_6N_2O_2$	[M-H]-	0.66	0.83	0.74
Succinic acid	$C_4H_6O_4$	[M-H]-	0.93	0.84	0.94
Creatinine	$C_4H_7N_3O$	[M+H]+	0.44	0.34	0.39
Uric Acid	$C_5H_4N_4O_3$	[M+H]+	0.77	0.85	0.75
Hypoxanthine	$C_5H_4N_4O$	[M+H]+	0.79	0.89	0.76
Glutamic acid	$C_5H_9NO_4$	[M+H]+	0.45	0.31	0.4
DL-Phenylalanine	$C_9H_{11}NO_2$	[M+H]+	1.7	1.53	1.5
Xanthine	$C_5H_4N_4O_2$	[M+H]+	0.94	1.15	0.9
Citrulline	$C_6H_{13}N_3O_3$	[M+H]+	0.45	0.32	0.41

Table 5.5 – Transition list of wine and potato molecules with the LC-MS properties used in the Bayesian optimization approach for the wine study.

Molecule Name	**Molecular Formula**	**Precursor Adduct**	**m/z**	**Explicit Retention Time**	**Notes**
Ethyl gallate	$C_9H_{10}O_5$	$[M-H]^-$	197.0455	3.43	Wine
Tetraethyl pyrophosphite	$C_8H_{20}O_5P_2$	$[M+Na]^+$	281.0682	1.083	Wine
Succinic anhydride	$C_4H_4O_3$	$[M+H]^+$	101.0233	2.93	Wine
[(2R,3S,4S,5R,6S)-6-(3,5-dihydroxyphenoxy)-3,4-dihydroxy-5-(3,4,5-trihydroxybenzoyl)oxyoxan-2-yl]methyl 3,4,5-trihydroxybenzoate	$C_{26}H_{24}O_{16}$	$[M-H]^-$	591.103	1.98	Wine
Itaconic acid	$C_5H_6O_4$	$[M-H]^-$	129.0193	2.77	Wine
Tryptanthrin	$C_{15}H_8N_2O_2$	$[M+H]^+$	283.0259	2.71	Potato
3,7-Dihydro-1-butyl-7-(5,6-dihydroxyhexyl)-3-methyl-1H-purine-2,6-dione	$C_{16}H_{26}N_4O_4$	$[M+Na]^+$	361.1828	4.069	Potato

Table 5.6 – Filtered list of molecules with the LC-MS properties used in the Bayesian optimization approach for the beginning of the calculations of the wine study.

Molecule Name	**Molecular Formula**	**Precursor Adduct**	**Explicit Retention Time**
DL-Tyrosine	$C_9H_{11}NO_3$	[M+H]+	0.88
DL-Tryptophan	$C_{11}H_{12}N_2O_2$	[M+H]+	2.3
cis-Urocanic acid	$C_6H_6N_2O_2$	[M-H]-	0.76
Creatinine	$C_4H_7N_3O$	[M+H]+	0.43
Uric Acid	$C_5H_4N_4O_3$	[M+H]+	0.77
Hypoxanthine	$C_5H_4N_4O$	[M+H]+	0.79
Glutamic acid	$C_5H_9NO_4$	[M+H]+	0.43
DL-Phenylalanine	$C_9H_{11}NO_2$	[M+H]+	1.56
Xanthine	$C_5H_4N_4O_2$	[M+H]+	0.92
Uracil	$C_4H_4N_2O_2$	[M+H]+	0.65
Propionylcarnitine	$C_{10}H_{19}NO_4$	[M+H]+	0.86
Glycerophosphocholine	$C_8H_{20}NO_6P$	[M+H]+	0.43
N-Acetylneuraminic acid	$C_{11}H_{19}NO_9$	[M-H]-	0.58

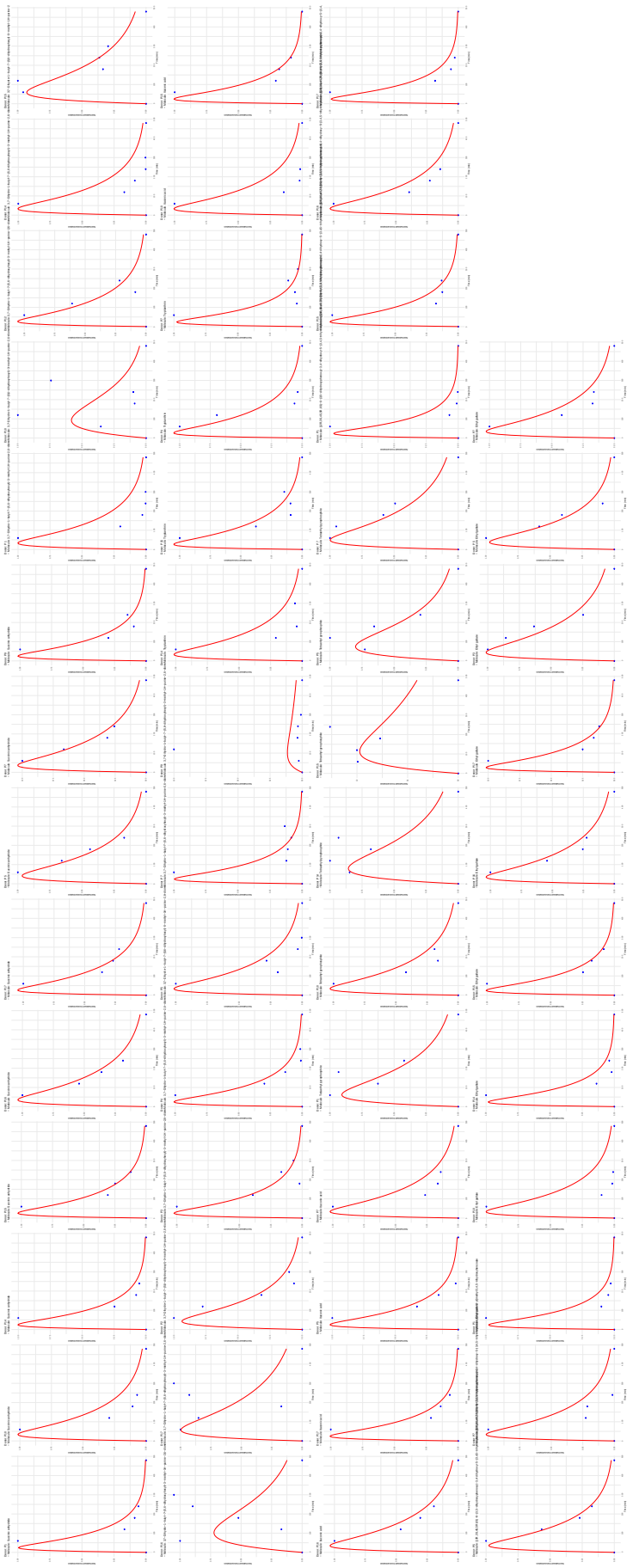

Figure 5.19 – Overview of normalized wine study data with fitted curves using a one-compartment model for all donors and molecules.

Table 5.7 – Transition list of adjusted wine and potato molecules with the LC-MS properties used in the Bayesian optimization approach for the wine study.

Molecule Name	m/z	Explicit Retention Time	Notes
Ethyl gallate	197.0455	3.43	Wine
Gallic acid	169.0142	1.26	Wine
Succinic anhydride	101.0233	2.93	Wine
[(2R,3S,4S,5R,6S)-6-(3,5-dihydroxyphenoxy)-3,4-dihydroxy-5-(3,4,5-trihydroxybenzoyl)oxyoxan-2-yl]methyl 3,4,5-trihydroxybenzoate	591.103	1.98	Wine
Itaconic acid	129.0193	2.77	Wine
Tryptanthrin	283.0259	2.71	Potato

Table 5.8 – Filtered and updated list of molecules with the LC-MS properties used in the Bayesian optimization approach for the beginning of the calculations of the wine study.

Molecule Name	Molecular Formula	Precursor Adduct	Explicit Retention Time
DL-Tyrosine	$C_9H_{11}NO_3$	[M+H]+	0.88
DL-Tryptophan	$C_{11}H_{12}N_2O_2$	[M+H]+	2.3
cis-Urocanic acid	$C_6H_6N_2O_2$	[M-H]-	0.76
Creatinine	$C_4H_7N_3O$	[M+H]+	0.43
Uric Acid	$C_5H_4N_4O_3$	[M+H]+	0.77
Hypoxanthine	$C_5H_4N_4O$	[M+H]+	0.79
Glutamic acid	$C_5H_9NO_4$	[M+H]+	0.43
DL-Phenylalanine	$C_9H_{11}NO_2$	[M+H]+	1.56
Xanthine	$C_5H_4N_4O_2$	[M+H]+	0.92
Uracil	$C_4H_4N_2O_2$	[M+H]+	0.65
Propionylcarnitine	$C_{10}H_{19}NO_4$	[M+H]+	0.86
Glycerophosphocholine	$C_8H_{20}NO_6P$	[M+H]+	0.43
N-Acetylneuraminic acid	$C_{11}H_{19}NO_9$	[M-H]-	0.58
Citrate	$C_6H_8O_7$	[M-H]-	0.84
Fumarate	$C_4H_4O_4$	[M-H]-	0.42

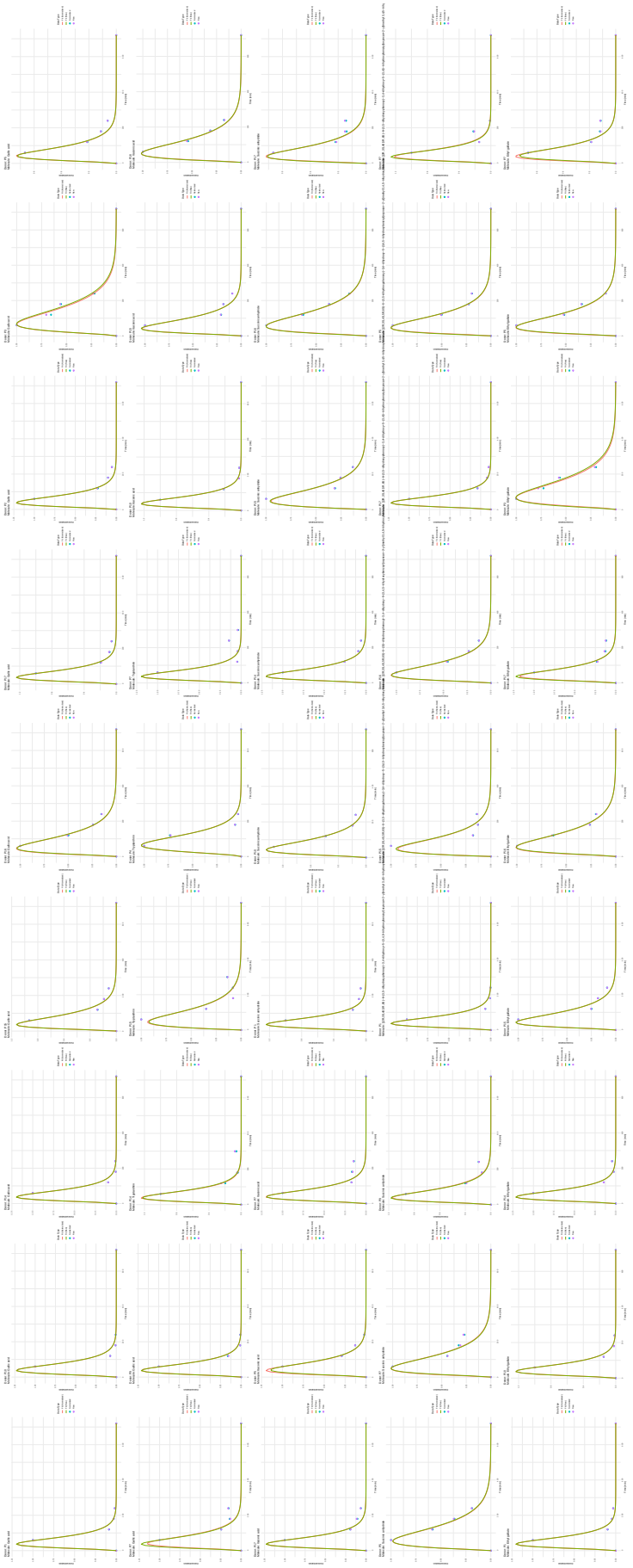

Figure 5.20 – Overview of normalized wine study data with fitted curves using a two-compartment model for all donors and molecules.

Table 5.9 – Filtered and updated list of molecules with the LC-MS properties used in the Bruteforce approach for the broader calculations of the wine study.

Molecule Name	**Molecular Formula**	**Precursor Adduct**	**Explicit Retention Time**
DL-Tyrosine	$C_9H_{11}NO_3$	[M+H]+	0.88
DL-Tryptophan	$C_{11}H_{12}N_2O_2$	[M+H]+	2.3
cis-Urocanic acid	$C_6H_6N_2O_2$	[M-H]-	0.76
Creatinine	$C_4H_7N_3O$	[M+H]+	0.43
Uric Acid	$C_5H_4N_4O_3$	[M+H]+	0.78
Hypoxanthine	$C_5H_4N_4O$	[M+H]+	0.79
Glutamic acid	$C_5H_9NO_4$	[M+H]+	0.43
DL-Phenylalanine	$C_9H_{11}NO_2$	[M+H]-	1.56
Xanthine	$C_5H_4N_4O_2$	[M+H]-	0.92
Uracil	$C_4H_4N_2O_2$	[M+H]+	0.66
Glycerophosphocholine	$C_8H_{20}NO_6P$	[M+H]+	0.43
N-Acetylneuraminic acid	$C_{11}H_{19}NO_9$	[M-H]-	0.58
Fumarate	$C_4H_4O_4$	[M-H]-	0.42
S-Adenosylmethionine	$C_{15}H_{22}N_6O_5S$	[M+H]+	4.33
2-Hydroxybutyric acid	$C_4H_8O_3$	[M-H]-	0.44
3-Methylglutaric acid	$C_6H_{10}O_4$	[M-H]-	2.41
Dihydrouracil	$C_4H_6N_2O_2$	[M+H]+	0.92
Sebacic acid	$C_{10}H_{18}O_4$	[M-H]-	4.7
Glycine	$C_2H_5NO_2$	[M+H]+	0.42
Serine	$C_3H_7NO_3$	[M+H]+	0.42

Table 5.10 – Comprehensive list of the randomly chosen molecules with the LC-MS properties used in the Bruteforce approach for the broader calculations of the wine study.

Molecule Name	**Molecular Formula**	**m/z**	**Precursor Adduct**	**Explicit Retention Time**	**Abbreviation**
3-[[[(1R,2S,4S)-1,2,4a,5-tetramethyl-2,3,4,7,8a-hexahydronaphthalen-1-yl]methyl]-2,5-dihydroxycyclohexa-2,5-diene-1,4-dione	$C_{21}H_{28}O_4$	345.2033	[M+H]+	4.8628	3-[[[(1R,2S
Pyroglutamyl glutamylllysine	$C_{16}H_{26}N_4O_7$	387.1877	[M+H]+	1.2487	Pyrgltmylgl
(2S,3R)-3-methyl-2-[[(2S)-3-methyl-2-[(3-oxo-2,4-dihydroquinoxaline-1-carbonyl) amino]butanoyl]amino] pentanoate	$C_{20}H_{28}N_4O_5$	405.2116	[M+H]+	3.4975	(2S,3R)-3
5-Methyl-2-cyclohexene-1,4-dione	$C_7H_8O_2$	125.0596	[M-H]-	3.1384	5-M-2-1,4
4-Piperidinecarboxamide	$C_6H_{12}N_2O$	129.1022	[M+H]+	2.7795	4-Pprdncbrb
Pestalafuranone C	$C_{11}H_{16}O_3$	219.0991	[M-H]-	3.7865	PestlfnrnnC
(2S,5S)-5-carboxyethyl proline	$C_8H_{13}N_4O_4$	186.0771	[M+H]+	2.1105	(2S,5S)-5-p
Ala-Asp	$C_7H_{12}N_2O_5$	203.0673	[M-H]-	0.6428	Ala-Asp
2-(4-Sulfophenyl)butyric acid	$C_{10}H_{12}O_5$	243.0328	[M-H]-	4.2688	2-(4-Sf)
2-Methyl-3,5-dinitrobenzoic acid	$C_8H_6N_2O_6$	260.9912	[M-H]-	3.1373	2-Mt-3,5-a
2-(3-Hydroxydodecanoylamino)-2-deoxyglucose	$C_{18}H_{35}NO_7$	376.2338	[M+H]+	3.8281	2-(3-H-g)
Guanidinet, 1-tert-butyl-2-methoxy-3-(3-pyridyl)-	$C_{11}H_{16}O_3$	245.1359	[M+H]+	3.4522	1-t-b-2-
p-[(Dicyanomethyl)azo] benzenesulfonic acid	$C_9H_6N_4O_3S$	251.0239	[M-H]-	1.5648	p-[(Dcy)
3-[Bis(1,5-dimethylpyrazol-3-yl)methyl] amino]propan-1-ol	$C_{15}H_{25}N_5O$	314.1939	[M+H]+	3.8635	3-[B(1,5-
(3S,9S)-2,8-dioxo-N-propan-2-yl-1,7,11-triazatricyclo[7.4.0.$0^{3,7}$] tridecane-11-carboxamide	$C_{14}H_{22}N_4O_3$	317.1571	[M+H]+	3.2781	(3S,9S)-2,

Table 5.11 – Comprehensive list of the molecules with good linearity and appearing in finger sweat with their LC-MS properties used in the Bruteforce approach for the updated calculations of the wine study.

Molecule Name	Molecular Formula	m/z	Precursor Adduct	Explicit Retention Time	Abbreviation
[5-(6-Aminopurin-9-yl)-3,4-dihydroxyoxolan-2-yl]methyl dihydrogen phosphate	$C_{10}H_{14}N_5O_7P$	348.0705	[M+H]+	0.7742	[5-(6-A-9-)-3dp
(2R)-2-[[(2R)-5-oxopyrrolidine-2-carbonyl]amino]butanedioic acid	$C_9H_{12}N_2O_6$	243.0622	[M-H]-	0.8635	(2R)-2-[[(2R)-a
(2S)-2-[[(5-oxopyrrolidin-2-yl)formamido]pentanedioic acid	$C_{10}H_{14}N_2O_6$	239.0672	[M-H]-	1.1126	(2S)-2-[[(5–2-a
2-[[2-[(2-Amino-4-carboxybutanoyl)amino]-3-methylbutanoyl]amino]butanedioic acid	$C_{14}H_{23}N_3O_8$	362.1562	[M+H]+	1.4368	2-[[2-[(2-Am-4-)]-3-]Ja
2-[[2-[(2-Amino-4-carboxybutanoyl)amino]-3-carbopropanoyl]amino]-3-methylpentanoic acid	$C_{15}H_{25}N_3O_8$	376.1717	[M+H]+	1.8725	2-[[2-[(2-A-4-)]-3-]]-a
(2S)-2-[[(2S)-2-azaniumyl-3-((1H-indol-3-yl)propanoyl)amino]] butanedioate	$C_{15}H_{17}N_3O_5$	320.1243	[M+H]+	1.9078	(2S)-2-[[(2S)-2
2-[[2-[(2-Amino-4-carboxybutanoyl)amino]-4-carbopropanoyl]amino]-3-methylpentanoic acid	$C_{16}H_{27}N_3O_8$	390.1877	[M+H]+	2.3604	2-[[2-[(2-A-4-)]-4a
Adipic Acid	$C_6H_{10}O_4$	145.0506	[M-H]-	2.4019	Adipic Acid
N6-Succinyl Adenosine	$C_{14}H_{17}N_5O_8$	384.1152	[M+H]+	2.4698	N6 Succnyl_Adnsn
(3S)-3-azaniumyl-4-[[(1S)-1-carboxylato-2-[(1H-indol-3-yl)ethyl]amino]-4-oxobutanoate	$C_{15}H_{17}N_3O_5$	320.124	[M+H]+	2.6744	(3S)-3–4-[[(1S
N-Lactoyl-Tyrosine	$C_{12}H_{15}NO_5$	254.1025	[M+H]+	2.998	N-Lactoyl-Tyrsn
Adenosine 5'-carboxamide	$C_{10}H_{12}N_6O_4$	239.0931	[M+H]+	3.0085	Adensn5'-crbxmd
Suberylglycine	$C_{10}H_{17}NO_5$	230.1033	[M-H]-	3.1476	Suberylglycine
(-)-2,3-Dimethylbutane-1,2,3-tricarboxylic acid	$C_9H_{14}O_6$	217.0718	[M-H]-	3.5586	(-)-2,3-D-1,2,a
Suberic acid	$C_8H_{14}O_4$	157.0859	[M+H]+	3.7528	Suberic acid

Table 5.12 – Comprehensive list of the molecules with good linearity and appearing as common contamination's in finger sweat samples with their LC-MS properties used in the Bruteforce approach for the updated calculations of the wine study.

Molecule Name	**Molecular Formula**	**m/z**	**Precursor Adduct**	**Explicit Retention Time**	**Abbreviation**
3,6,9,12,15,18,21-Heptaoxatricosane-1,23-diol	$C_{16}H_{34}O_9$	371.2275	[M+H]+	3.3803	3,6,9,12,1
Nonaethylene glycol	$C_{18}H_{38}O_{10}$	415.2537	[M+H]+	3.5385	Nnthylngly
Decaethylene glycol	$C_{20}H_{42}O_{11}$	476.3062	$[M+NH_4]+$	3.6776	Dcthylngly
Undecaethylene glycol	$C_{22}H_{46}O_{12}$	520.3323	$[M+NH_4]+$	3.8020	Undcthylng
Dodecaethylene glycol	$C_{24}H_{50}O_{13}$	564.3586	$[M+NH_4]+$	3.9113	Ddcthylngl
Mycobacterium leprae PGL-1 trisaccharide	$C_{23}H_{42}O_{14}$	543.2620	[M+H]+	3.8013	MyclPGL-1t
Tenacibactin C	$C_{23}H_{42}N_4O_8$	541.2618	[M+K]+	3.8018	TenacbctnC
N,N-Dimethyl-beta-ethyl-beta-(phenylmethyl)-1H-imidazole-1-ethanamine	$C_{16}H_{23}N_3$	296.1517	[M+K]+	3.9140	N,N-D—-(
Diethyl acetonedicarboxylate	$C_9H_{14}O_5$	203.0914	[M+H]+	4.5131	Dthylactnd
Triethyl Citrate	$C_{12}H_{20}O_7$	299.1098	[M+Na]+	4.5141	TrthylCtrt
2-Butenedioic acid (2Z)-,mono-2-propenyl ester	$C_7H_8O_4$	157.0494	[M+H]+	4.5187	2-Ba(2Z)-e

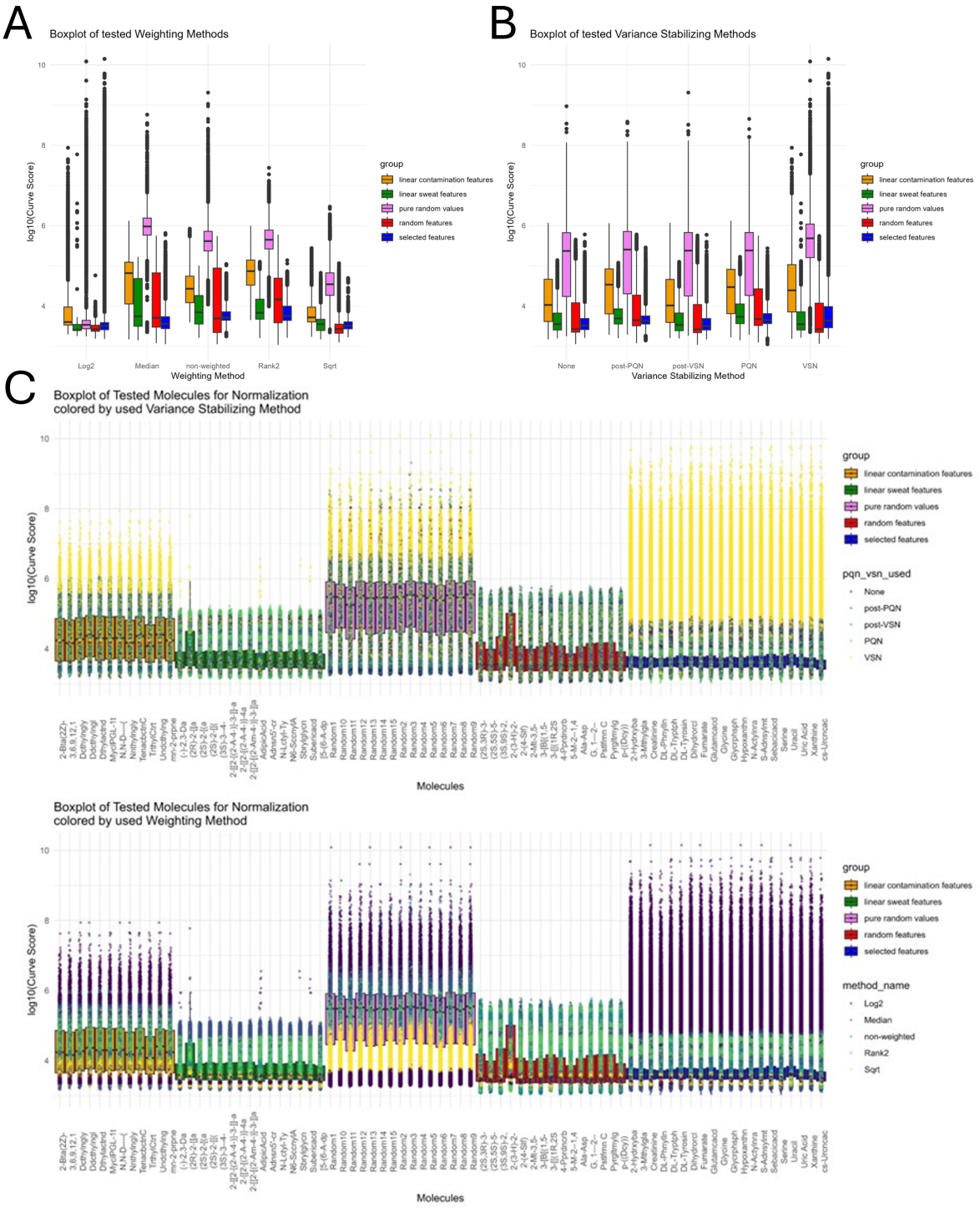

Figure 5.21 – Complete overview of all combinatorial combinations for all the different performed calculations from the wine study, compared by curve score, illustrated using boxplots. The 20 selected molecules are in blue (selected features), the 15 random molecules are in red (random features), the 15 linear sweat features are in green (linear sweat features), and the 11 linear common contamination samples are in orange (linear contamination features), and the 15 purely random values are in violet (pure random values). A) Overview of tested weighting methods, B) Overview of tested variance-stabilizing methods, C) Overview of tested normalization molecules, colored by variance-stabilizing methods, D) Overview of tested normalization molecules, colored by weighting methods.

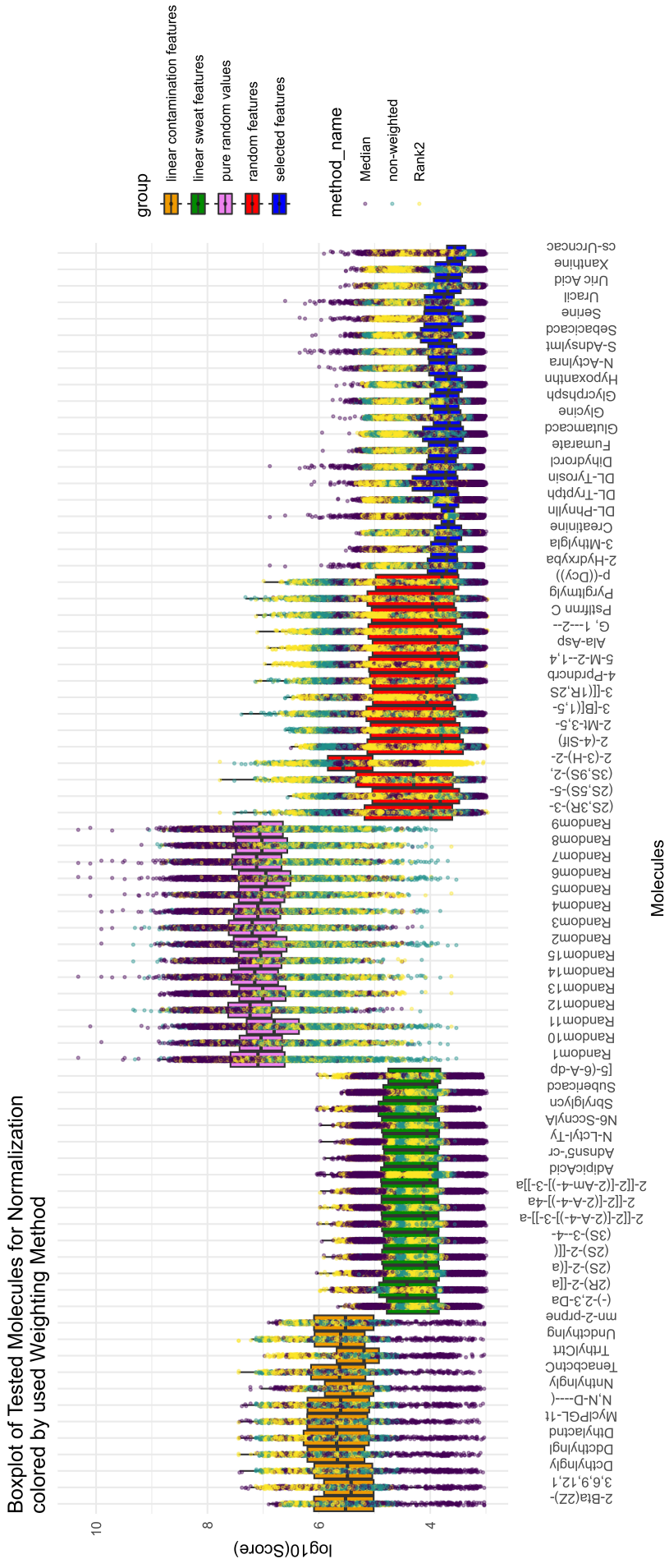

Figure 5.22 – Complete overview of all filtered combinatorial combinations for all the different performed calculations from the wine study, compared by curve score, illustrated using boxplots, colored by variance-stabilizing methods. The 20 selected molecules are in blue (selected features), the 15 random molecules are in red (random features), the 15 linear sweat features are in green (linear sweat features), and the 11 linear common contamination samples are in orange (linear contamination features), and the 15 purely random values are in violet (pure random values).

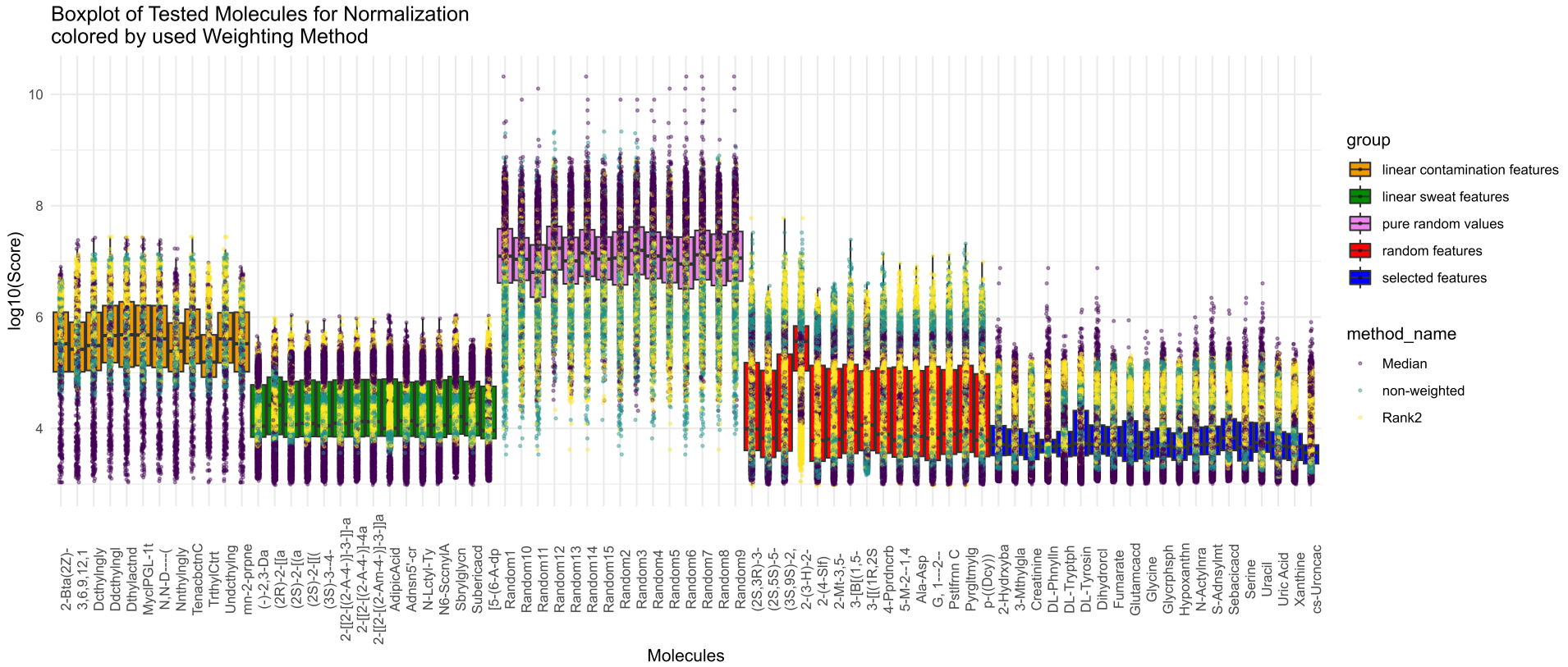

Figure 5.23 – Complete overview of all filtered combinatorial combinations for all the different performed calculations from the wine study, compared by curve score, illustrated using boxplots, colored by variance-stabilizing methods. The 20 selected molecules are in blue (selected features), the 15 random molecules are in red (random features), the 15 linear sweat features are in green (linear sweat features), and the 11 linear common contamination samples are in orange (linear contamination features), and the 15 purely random values are in violet (pure random values).

Table 5.13 – Comprehensive list of the molecules with good linearity and appearing in finger sweat with their LC-MS properties used in the Bruteforce approach for the updated calculations of the wine study.

Molecule Name	Molecular Formula	m/z	Precursor Adduct	Explicit Retention Time	Abbreviation
(2R)-2-[[(2R)-5-oxopyrrolidine-2-carbonyl]amino]butanedioic acid	$C_9H_{12}N_2O_6$	243.0622	[M-H]-	0.8635	(2R)-2-[[(2R)-a
(2S)-2-[[(5-oxopyrrolidin-2-yl)formamido]pentanedioic acid	$C_{10}H_{14}N_2O_6$	239.0672	[M-H]-	1.1126	(2S)-2-[[(5–2-a
2-[[2-[(2-Amino-4-carboxybutanoyl)amino]-3-methylbutanoyl]amino]butanedioic acid	$C_{14}H_{23}N_3O_8$	362.1562	[M+H]+	1.4368	2-[[2-[(2-Am-4-)]-3-]Ja
2-[[2-[(2-Amino-4-carboxybutanoyl)amino]-3-carbopropanoyl]amino]-3-methylpentanoic acid	$C_{15}H_{25}N_3O_8$	376.1717	[M+H]+	1.8725	2-[[2-[(2-A-4-)]-3-]]-a
(2S)-2-[[(2S)-2-azaniumyl-3-((1H-indol-3-yl)propanoyl)amino]] butanedioate	$C_{15}H_{17}N_3O_5$	320.1243	[M+H]+	1.9078	(2S)-2-[[(2S)-2
Adipic Acid	$C_6H_{10}O_4$	145.0506	[M-H]-	2.4019	Adipic Acid
N6-Succinyl Adenosine	$C_{14}H_{17}N_5O_8$	384.1152	[M+H]+	2.4698	N6 Succnyl_Adnsn
(3S)-3-azaniumyl-4-[[(1S)-1-carboxylato-2-[(1H-indol-3-yl)ethyl]amino]-4-oxobutanoate	$C_{15}H_{17}N_3O_5$	320.124	[M+H]+	2.6744	(3S)-3–4-[[(1S
N-Lactoyl-Tyrosine	$C_{12}H_{15}NO_5$	254.1025	[M+H]+	2.998	N-Lactoyl-Tyrsn
Adenosine 5'-carboxamide	$C_{10}H_{12}N_6O_4$	239.0931	[M+H]+	3.0085	Adensn5'-crbxmd
Suberic acid	$C_8H_{14}O_4$	157.0859	[M+H]+	3.7528	Suberic acid
DL-Tyrosine	$C_9H_{11}NO_3$	182.08104	[M+H]+	0.88	DL-Tyrosine
DL-Tryptophan	$C_{11}H_{12}N_2O_2$	205.09706	[M+H]+	2.3	DL-Tryptophan
cis-Urocanic acid	$C_6H_6N_2O_2$	137.03561	[M-H]-	0.76	cis-Urocanicacd
Creatinine	$C_4H_7N_3O$	114.06616	[M+H]+	0.43	Creatinine
Uric Acid	$C_5H_4N_4O_3$	169.03556	[M+H]+	0.78	Uric Acid
Hypoxanthine	$C_5H_4N_4O$	137.04574	[M+H]+	0.79	Hypoxanthine
Glutamic acid	$C_5H_9NO_4$	148.0604	[M+H]+	0.43	Glutamic acid
Xanthine	$C_5H_4N_4O_2$	151.02611	[M+H]-	0.92	Xanthine
Uracil	$C_4H_4N_2O_2$	113.03451	[M+H]+	0.66	Uracil
3-Methylglutaric acid	$C_6H_{10}O_4$	145.05057	[M-H]-	2.41	3-Mthylgltrcacd